A BIOMECHANICAL ANALYSIS OF SEATING STRESSES BASED UPON WHEELCHAIR PROPULSION

by

Justin Michael Pedersen

A thesis submitted to the faculty of
The University of Utah
in partial fulfillment of the requirements for the degree of

Master of Science

Department of Mechanical Engineering

The University of Utah

May 2013

The University of Utah Graduate School

STATEMENT OF THESIS APPROVAL

The thesis of **Justin Michael Pedersen**

has been approved by the following supervisory committee members:

Donald Bloswick	, Co-Chair	**13-Feb-2013** Date Approved
Andrew Merryweather	, Co-Chair	**13-Feb-2013** Date Approved
Stacy Bamberg	, Member	**13-Feb-2013** Date Approved

and by **Tim Ameel** , Chair of

the Department of **Mechanical Engineering**

and by Donna M. White, Interim Dean of The Graduate School.

ABSTRACT

This thesis aims to measure the difference in seated normal and shear stresses based upon different types of wheelchair propulsion types. Previous studies have measured biomechanical influence of wheelchair propulsion at the upper extremities. This study intends to measure the biomechanical differences at the seating surface where wheelchair users are vulnerable to deep tissue and skin breakdowns. Pressure ulcers have been studied to form based upon a number of factors, specifically: too much pressure, friction, shear, and heat/moisture buildup. However, very little research has been performed measuring seating stresses *in vivo* based upon wheelchair propulsion.

Multiple metrics were used to measure the normal and shear stresses in 10 ambulatory subjects (5 male and 5 female). To measure normal pressure, pressure mapping was used. To measure the shear stresses, a Molten Predia was used to measure shear. Two dramatically different wheelchair cushions were used: an air adjustable cushion and an HR-42 Foam block of similar size. Two different types of manual wheelchair propulsion were used: the traditional hand-rim wheelchair and the developmental lever-arm wheelchair.

It was hypothesized that the combination of the lever-arm wheelchair and the properly adjusted air cushion would significantly reduce the normal pressure and shear stresses associated with chair propulsion. The data showed a significant

difference for the normal pressure for 9 of the 10 subjects in favor of the air cushion over the foam cushion. However, the shear data did not show a significant difference for a reduction of shear for any configuration of testing.

TABLE OF CONTENTS

LIST OF FIGURES

LIST OF TABLES

BACKGROUND

Wheelchairs are designed to provide support and mobility for persons who are not able to do so under their own power. Because of this, the duration of wheelchair use is often prolonged periods of time. This necessitates the use of cushions to help provide comfort and protection against pressure ulcers. This breakdown of skin or underlying tissues occurs most commonly when sustained mechanical loads are subjected over a period of time, particularly common in persons who must remain in a bed or a wheelchair for long periods of time. Four main factors lead to the occurrence of pressure ulcers: normal pressure, shear stress, surface friction, and the accumulation of heat and moisture (Bader, Bouten, Colin, & Oomens, 2005; Ferrarin, Andreoni, & Pedotti, 2000; Minkel, 2000; Reuler & Cooney, 1981). The majority of wheelchair users are spinal cord injury (SCI) individuals who do not have sensation at the cushion interface (Reuler & Cooney, 1981). This presents a problem as SCI individuals are not able to identify when dangerous amounts of pressure or stress are applied to critical areas, whereas an able-bodied individual would simply shift positions due to discomfort. Cushions attempt to distribute the seating pressure over as much of the surface as possible, which in turn decreases the normal pressure. A common way to distribute pressure better is to contour the cushion surface, which increases the surface area and provides stability to the cushion such that the user is secured in place (Bader et al., 2005; Brienza, Geyer, Karg, & Jan, 2001; Brienza & Karg, 1998).

The idea that a pressure threshold exists for the creation of pressure ulcers is highly debated within the industry. Many theoretical and studies involving animals have suggested that the risk of pressure ulcers is a function of time and load (Armstrong, 1985; Brienza, Karg, Geyer, Kelsey, & Trefler, 2001; Edwards & Marks, 1995; Manorama, Baek, Vorro, Sikorskii, & Bush, 2010; Sacks, 1989). Over a 2-hour period, it is theorized that a pressure range of 60-80 mmHg (8.0-10.6 kPa) would be sufficient to cause pressure ulceration (Armstrong, 1985; Reuler & Cooney, 1981; Stekelenburg et al., 2007).

When diagnosing pressure ulcers, friction at the seating surface is commonly found to be the source because the skin traditionally shows signs of irritation or inflammation. However, the influence of shear stress is typically a hidden factor, as it is not commonly identified at the skin surface. While friction induces shear and results in ischemia, the presence of shear is less distinguishable than friction because shear usually causes deep tissue pressure ulcers (Hanson, Langemo, Anderson, Thompson, & Hunter, 2010; Sanders, Goldstein, & Leotta, 1995). The influence of deep tissue shear under prolonged load can limit blood flow through capillaries where diffusion of oxygen and metabolites to the cell are reduced or blocked (Hendrik & Goossens, 1994; Manorama et al., 2010; Stekelenburg et al., 2007). Over time, shearing force can cause extensive dissection or tearing within the tissue, located in the plane of the greatest concentration of shear (Reichel, 1958). The reason for this is the addition of shear reduces the amount of normal pressure required to cause a breakdown of the skin (Doughty et al., 2006; Gilsdorf, Patterson, Fisher, & Appel, 1990; Hanson et al., 2010; Ohura, Takahashi, & Ohura, 2008; Reichel, 1958; Sanders et al., 1995).

Much research has been performed as to the performance of wheelchair cushions with respect to the four major pressure ulcer influences. However, very little research has been performed to measure the effect of wheelchair propulsion on wheelchair cushion stresses seen by the user, particularly with respect to various forms of propulsion. Traditional manual wheelchairs require significant use of the upper body, exposing the user to upper-body musculoskeletal disorders (Aissaoui, Arabi, Lacoste, Zalzal, & Dansereay, 2002; Bloswick, Erickson, Browns, Howell, & Mecham, 2003; Boninger, Baldwin, Cooper, Koontz, & Chan, 2000; Chaffin, Andersson, & Martin, 2006). Raphael et al. undertook a study to measure the biomechanical difference between four wheelchair propulsion types, two of which will be used in this study (Raphael, Merryweather, Butler, & Bloswick, 2011). The two wheelchairs used in this study are the traditional hand-rim propelled chair and the lever-arm propelled chair, which incorporates a rowing motion, putting the wrists in a more neutral position. Using the lever-arm wheelchair design, Raphael et al. measured a 14% decrease in moment about the shoulder, a 67% decrease in moment about the elbow, and a 92% decrease in moment about the wrist (Raphael et al., 2011).

This study aims to investigate the normal pressure distribution and shear stress accumulation for two different manual wheelchair propulsion methods and two different wheelchair cushions: the traditional hand-rim method and the lever-arm propulsion method, with a polyurethane foam cushion and an air adjustable cushion. Additionally, this study investigates the effects of different forms of cushions, particularly a basic foam cushion and an air adjustable cushion, on these manual wheelchairs to identify the

effectiveness of cushion influence to reduce the pressure and increase the comfort of the user. Below is a list of the hypotheses for the study:

H_1: The air adjustable cushion will result in greater pressure distribution than the foam cushion.

H_2: The air adjustable cushion will result in less shear stress than the foam cushion.

H_3: The lever-arm wheelchair propulsion method will result in less shear stress than the wheel-rim propulsion method.

H_4: The combination of lever-arm wheelchair propulsion and air adjustable cushion will produce less shear stress than the combination of wheel-rim wheelchair propulsion and the form cushion.

METHODS

Test Subject Participants

Five male and five female test subjects were enlisted for this study, all between the ages of 18 to 65. Gilsdorf et al. undertook a study that measured approximately a 10% difference in pressure on critical boney structures. This is due to various levels of muscle atrophy for long-term wheelchair users as opposed to larger muscle mass for able bodied individuals (Gilsdorf, Patterson, & Fisher, 1991). For purposes of comparative differences between testing configurations, able-bodied individuals were used for this study. All subjects were of good health and could fit comfortably on the cushions without tissue interference from the wheelchairs. After reviewing and signing a University-Approved Informed Consent Document, subjects changed into tight fitting shorts (81% polyester and 19% elastane), shown in Figure 1. Three different sizes of tight fitting shorts were used: small, medium, and large. The shorts were laundered between each subject. Anthropometric data was gathered for each participant and is shown in Table 1. The test subject order was randomized to reduce any test effect. The order of testing is shown in Table 1.

Cushion Descriptions

Two cushions were used for testing: an open-celled polyurethane HR42 foam of size 10cm x 41cm x 41cm and an air-adjustable cushion of similar size. The function of

the air-adjustable cushion is to distribute air over the cushion to reduce areas of increased pressure, particularly boney structures such as the ischial tuberosities, sacrum, and the greater trochanters. The same cover stretchable cover, consisting of Nylon Lycra, was used for both cushions. The Foam and Air-adjustable cushions can be seen in Figure 2 and Figure 3, respectively.

Wheelchair Descriptions

Two wheelchair propulsion methods were included in the testing: (1) the wheel-rim wheelchair: a sling Everest and Jennings capable of fitting a 44cm wide cushion, shown in Figure 4; and (2) the lever-arm wheelchair: a custom-made lever-arm propulsion chair, constructed by the University of Utah Ergonomics and Safety Laboratory. The lever-arm chair was modified from a wheel-rim wheelchair, as shown in Figure 5. The armrests were removed to allow clearance for lever actuation. Lever arms extend from the front of each side of the chair, attached to a caliper and rotor assembly. The rotors are fixed to a sprocket, which actuates a bicycle chain to a sprocket on the rear wheel, as shown in Figure 6. The left or right side lever controls the corresponding wheel, allowing forward or reverse movement of each wheel, independent of the other. A similar wheelchair design is currently available to consumers: the WIJIT ("WIJIT: Move at the Speed of Life,"). The concept behind both designs is similar; however, the levers are concentric with the axle of the wheel on the WIJIT.

The participants were allowed time to familiarize themselves with the two types of wheelchairs. Many of the subjects struggled with the lever-arm chair at first, but were able to maneuver the chair satisfactorily after a few minutes of practice. Once the

subjects were able to demonstrate their capabilities to run the courses in both wheelchairs, testing began.

Pressure Map Calibration and Validation

The XSensor X2 Pressure Map was calibrated prior to testing as per the XSensor guide to map calibration. This process involves calibration of a low and high value, calibrating the range from 0 to 200 mmHg. The calibration was then validated using 4.5 kg and 22.7 kg weights by placing each weight on the map for 120 seconds at a time, recording the pressure displayed by the map. The values were within the allowable 10% range of the actual weight in both cases. The pressure map calibration was accepted. Only one calibration was performed over the course of testing.

Cushion Adjustment Method

The traditional method for adjusting air adjustable cushions is to have a physical therapist use their hand to palpate the subject at the ischial tuberosities. The purpose of this is to identify a 13mm to 25mm gap under the "sitting bones" to ensure that the ischial tuberosities are not resting on the hard surface below the cushions. The cushion manufacturer identified a gap of 13-25mm between the ischial tuberosities and the bottom of the cushion as the optimal pressure distribution over the seating surface. This is a variable process as each physical therapist has different size fingers and different feel for what a proper gap is at the ischial tuberosities. Additionally, the physical therapist may endure excessive stresses in the wrists and fingers while palpating the sit bones of larger sized individuals.

Another method was developed for this study to reduce the variability of cushion adjustment from physical therapist palpation, producing a repeatable and quantitative adjustment method for the cushion. A physical therapist was not used in the adjustment of the air cushion. Instead, a developmental adjustment method, which measures the height offset at the iliac crest, was performed and validated using pressure mapping. The air cushion was completely deflated and the pressure map was set on the top surface of the cushion. The testing subject then sat on the deflated cushion, displaying areas of high pressure (usually at the IT's). The cushion adjustment instructions state that the cushion should be inflated such that there is 13-25mm offset of cushion between the user and the flat surface of the wheelchair. To achieve the 13-25mm offset, the pressure map was used to inflate the cushion until the IT's were starting to lift off the surface, this was seen by a decrease in pressure at the IT's. This is illustrated in Figure 7 for a representative subject. The pressure map was used to identify the point at which the IT's were transitioning off the bottom out point and was measured as the datum point. The testing subject was explained the location of the iliac crest and was then asked to identify the top of their right iliac crest. A bubble level was used to translate the height of the iliac crest to a ruler to measure the height from the floor to the point at the iliac crest. The cushion was then inflated to 19mm higher than the datum point. Note: 19mm is the ideal adjustment offset, but the range of 13-25mm is suggested for customization for the individual, as per the manufacturer instructions. The testing subject was allowed to sit on the cushion for 120 seconds while the pressure map recorded the pressure distribution. This is illustrated on Figure 8 for a representative subject. The testing subject was asked if they felt comfortable in the cushion after the adjustment; every testing subject said the

cushion was comfortable for them. As a third check, the pressure distribution was monitored with the pressure map to verify the cushion was redistributing the pressure over the surface while not producing any high pressure points. At this point, the cushion was considered adjusted for the individual testing subject. No repeatability cushion adjustment methods were tested after the first adjustment.

This method worked well for able-bodied individuals with no visual signs of obliquities from the pressure map output. However, for robustness of study, it is recommended that the left and right side of the iliac crest be measured for offset. This would identify if one side has a smaller gap. The iliac crest was picked as a relatively fixed location within the skeletal system. Originally it was suspected that the greater trochanter could be used. However, it was identified the greater trochanter produced some rotation when air was applied to the cushion, producing inaccurate measurement of cushion adjustment offset.

Pressure Mapping

The wheel-rim propulsion wheelchair was adjusted as needed for the testing subject. The only major adjustment was raising or lowering the foot rests. A cushion was secured in place with Velcro tabs to the bottom of the cover and top of the sling of the chair. The pressure map was placed on the cushion. The testing subject then sat on the cushion in a comfortable upright posture. Any wrinkles were smoothed out in the pressure map, if needed. The test subject sat on the cushion for 120 seconds before standing up to unload the cushion, as shown in Figure 9. This gave the cushion time to accept the user. The testing subject was removed from the cushion for 120 seconds, allowing the cushion to recover form the previous loading. Each testing subject

performed five loading periods for each cushion, with 120 seconds allowed between each loading period for cushion recovery. The order was randomized to eliminate test effect.

Shear Sensor Validation

To measure shear at the cushion seating surface interface, a Predia sensor was used. The sensor is from the Molten Corporation out of Hiroshima, Japan. See Figure 10. The Predia measures shear in the forward and backward direction. A LabView program was created to record the data at 100 Hz. To validate the measurement and logging capabilities, a fixture was constructed to achieve a 30° angle. A smoothed piece of Teflon sheet of a low coefficient of friction was placed on the 30° inclined plane with a cutout that the Predia sensor could fit into, as shown in Figure 11. The Sensor was adhered into the cutout using aggressive double-sided adhesive; as shown in Figure 12. 2.0 kg and 7.0kg masses whereas placed over the sensor adhered to the sensor with aggressive two-sided adhesive. Calculating the lateral load on the sensor and comparing it with the measured shear loads produced a calibration curve. The calibration was only performed once. A validation was performed at the start and finish of each test subject. The validation process included the same fixture as shown in Figure 11, but only one mass (2.4kg) was used to measure the shear.

Shear Measurement

In the Akins et al. study, the Predia sensor was placed anterior of the ischial tuberosity location to mount the sensor on a flat section rather than on the boney prominence of the ischial tuberosities. This method was followed to compare bench testing data to human subject data (Akins, Karg, & Brienza, 2011). For the Predia sensor

placement, the subject was asked to sit on the lever-arm wheelchair and, using their left hand, identify the left ischial tuberosity. The subjects were asked to leave a finger located at the ishcial tuberosity while they stood up. The Predia sensor was positioned 10cm on center anterior (in the orientation of the seated subject) of the left ischial tuberosity. The subject was then asked to compress the Predia sensor against the skintight shorts. The Predia sensor was oriented such that the direction of positive shear was facing in the anterior direction (to the seated subject). Aggressive two-sided adhesive held the Predia in place, though special care had to be taken during testing to maintain the sensor in place.

In a previous study of wheelchair propulsion by Bloswick et al., a series of obstacle courses were set up to analyze the biomechanical stresses of wheelchair propulsion (Bloswick et al., 2003). Based upon initial pilot testing, it was identified that the course shown in Figure 13 produced the largest amount of repeatable shear. The obstacle course was setup for maneuvering the two wheelchairs. The course required the test subjects to complete a three-point turn by starting at the right side of the course (as shown in Figure 13), and then inverted the course and the test subjects performed the same three-point turn by starting on the left side (as shown in Figure 14). The testing subjects were asked to maneuver the chairs at a comfortable pace and perform a complete stop before progressing to the next portion of the course. The course was divided into four segments: 1. Start of the course (from complete stop), 2. Full stop after turn before backing up, 3. Full stop after backing up, and 4. Full stop after turn to end trial. Prior to the start of a trial, subjects were asked to perform a pressure relief lift. The pressure relief lift was incorporated to reduce any test effect of built up shear from previous trials

or positioning. The pressure relief lift was performed by having the subjects lift themselves straight up using the frame or armrests of the chair, as shown in Figure 15.

A LabView circuit was created to log the data from the Predia shear sensor. A voltage trigger was used to identify key locations in the shear data, ie locations 1-4 of Figure 13 and Figure 14. The test operator actuated a circuit that trigger a voltage spike at the time of each of the four testing segments for the three-point turn, as shown in Figure 16. A small amount of voltage could be seen in the test data while the trigger was compressed, allowing ease of the test operator to identify key locations of the testing for data analysis. The Predia sensor is rated at 60 Hz; however, initial testing indicated missing peaks in the data as observed from visual inspection of the Predia sensor during testing. The LabView VI logged the data at 100 Hz and the square waves of the Predia were filtered.

The two cushions, with the two wheelchair propulsion types, and the two courses were tested in a random order to produce 16 testing configurations, as shown in Table 2. Each configuration was tested at three trials each, with a pressure relief lift between each trial.

Figure 1 – Test subject wearing tight fitting short, experimenting with lever-arm wheelchair prior to testing.

Table 1 – Test subject anthropometric data displayed by subject order.

	Gender	Age	Height (cm)	Body Weight (kg)	Seated Hip Width (cm)	BMI
Subject 1	Male	24	190.5	99.8	43.2	27.5
Subject 2	Male	25	185.4	79.4	35.6	23.1
Subject 3	Female	33	172.7	63.5	40.6	21.3
Subject 4	Male	26	185.4	70.3	35.6	20.5
Subject 5	Female	24	157.5	54.4	35.6	21.9
Subject 6	Female	29	175.3	77.1	43.2	25.1
Subject 7	Male	56	188.0	104.3	43.2	29.5
Subject 8	Female	51	172.7	57.2	38.1	19.2
Subject 9	Male	51	180.3	77.1	38.1	23.7
Subject 10	Female	27	175.3	64.4	38.1	21.0
Average		34.6	178.3	74.8	39.1	23.3
Male Average		36.4	185.9	86.2	39.1	24.9
Female Average		32.8	170.7	63.3	39.1	21.7

Figure 2 – Foam cushion with cover.

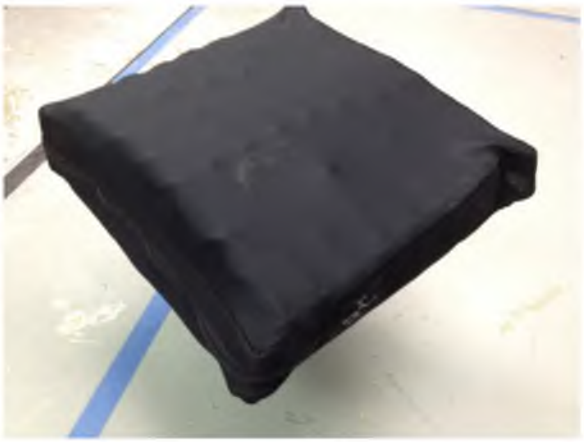

Figure 3 – Air-adjustable cushion with cover.

Figure 4 – Traditional wheel-rim propulsion wheelchair with sling seat and footrests.

Figure 5 – Lever-arm wheelchair. Levers were attached with braking levers to actuate the chain and propel the wheel. The lever controls the corresponding wheel independently.

Figure 6 – Chain activation assembly. The calipers are compressed upon the rotor when the brake is applied from the hand lever. Upon application of brake, the lever is clamped to the rotor, rotating the wheel forward or backward.

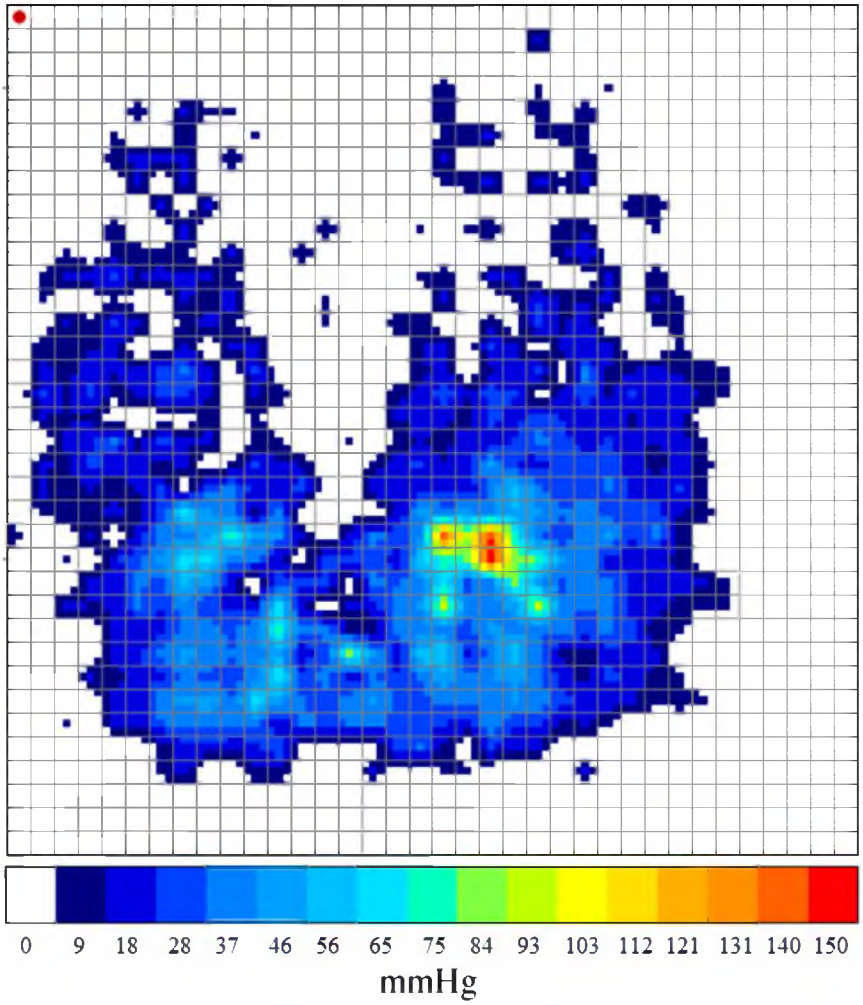

Figure 7 – Air cushion deflated, preadjustment. Note the areas of high pressure located at the right ischial tuberosity.

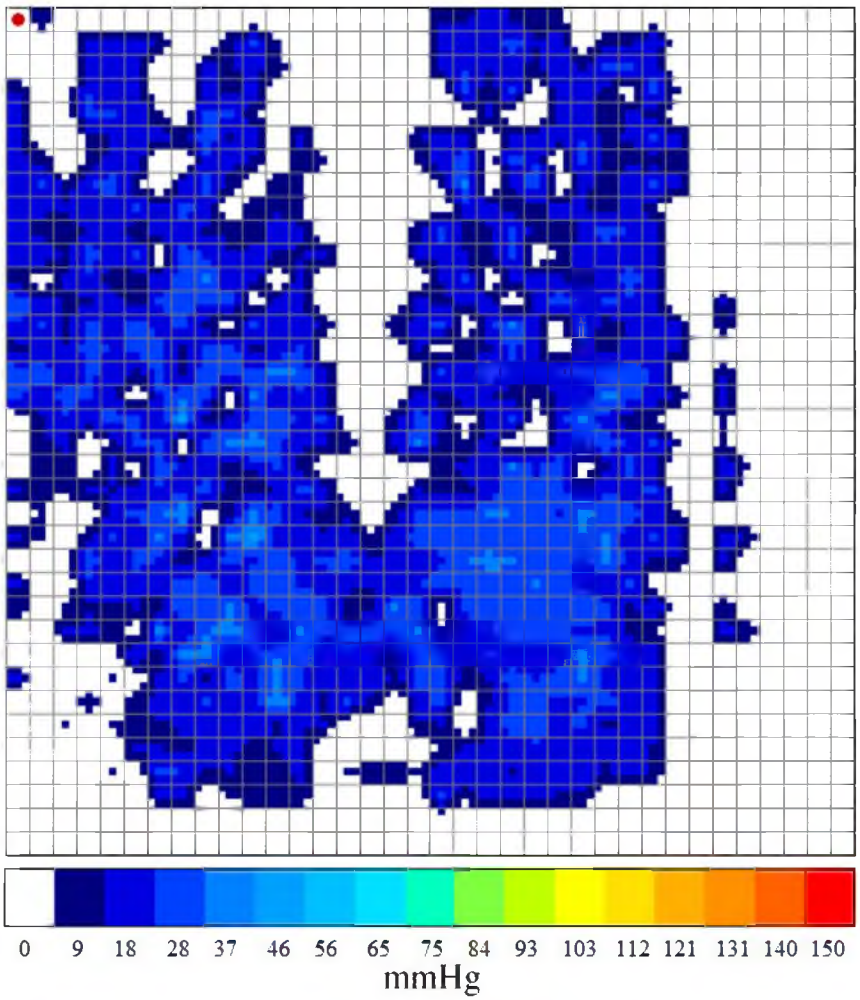

Figure 8 – Air cushion post adjustment. Note the pressure has been distributed away from the ischial tuberosity.

Figure 9 – Subject pressure mapping on the wheel-rim wheelchair.

Figure 10 – Predia shear sensor, manufactured by Molten Corporation.

Figure 11 – 30° inclined sensor validation fixture with sensor cutout.

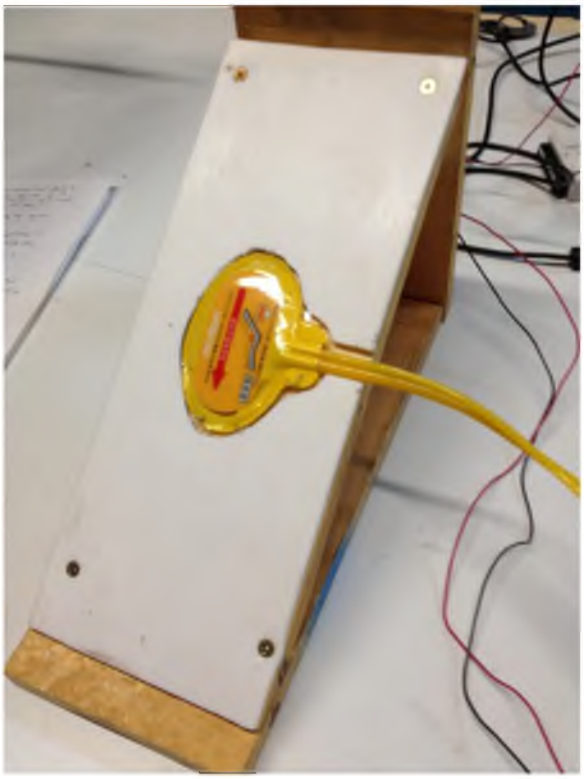

Figure 12 – Predia sensor embedded in validation fixture.

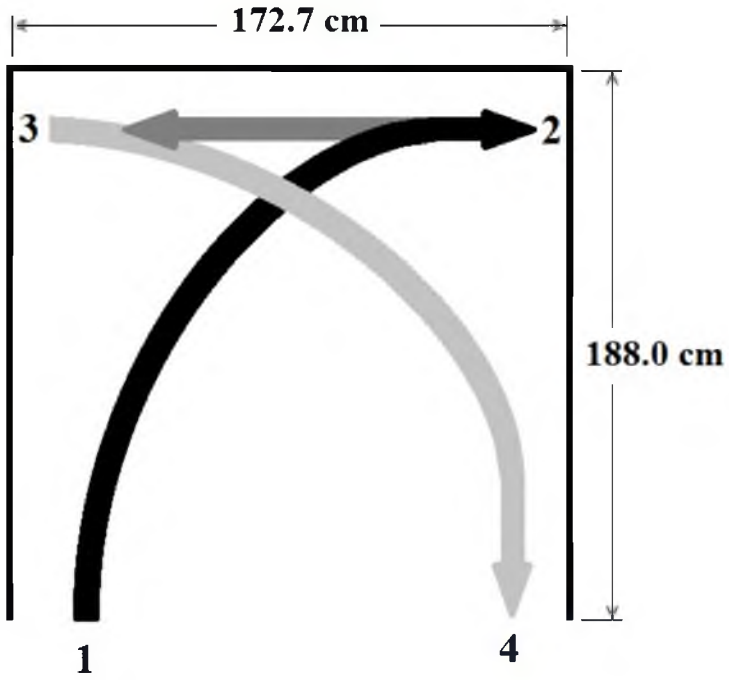

Figure 13 – Right handed turn course. Subject starts, from a complete stop, at number 1 and maneuvers their way through the course to number 4, stopping at each number.

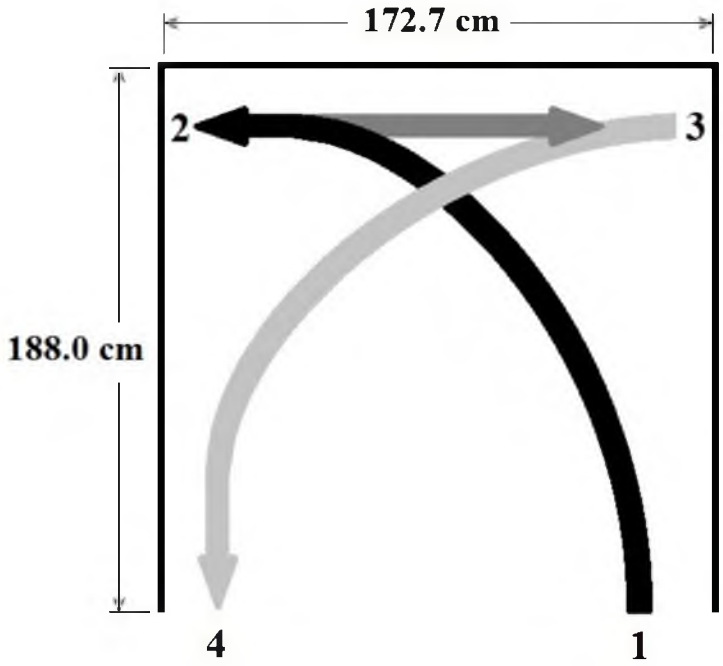

Figure 14 – Left handed turn course. Subject starts, from a complete stop, at number 1 and maneuvers their way through the course to number 4, stopping at each number.

Figure 15 – Participant performing pressure relief lift on wheel-rim wheelchair.

Figure 16 – Test proctor would follow test subject with computer and switch in hand.

Table 2 – Testing matrix for shear testing performed with a right turn and a left turn, three trials each. The testing order for each subject was randomized.

Wheel-rim Chair with Foam Cushion	Lever-arm Chair with Foam Cushion
Wheel-rim Chair with Air Adjusted Cushion	Lever-arm Chair with Air Adjusted Cushion

RESULTS

Pressure Mapping

Pressure mapping data were analyzed based upon the following calculations: average pressure (mmHg), Peak Pressure Index (mmHg), Contact Area (cm^2), and Dispersion Index (%). The average pressure and contact area were calculated from the pressure map data at the end of the 120-second loading period over the surface of the map with a minimum threshold of 5 mmHg. The peak pressure is not a reliable measure as bony prominences, such as the ischial tuberosity, are larger than an individual sensor. The peak pressure index (PPI) takes the average pressure over an area, 9-10 cm^2, which includes the ischial tuberosity ("ISO Working Group Clinical Use Guidelines," 2008). The Dispersion Index is a ratio of the sum of pressure in the ischial tuberosity and sacrum region relative to the sum of the pressure over the entire surface. It is traditionally expressed as a percentage of user loads in the critical areas. Shown in Figure 17 through Figure 20 are the average pressure, PPI, contact area, and dispersion index values for each testing subject, respectively. The significance for the differences between the cushions was calculated for each of the four data points: Average Pressure, PPI, Contact Area, and Dispersion Index; *p*-values are shown in Table 3.

It can be seen from Figure 17 through Figure 20 that the average pressure, peak pressure index, contact area, and dispersion index differ between air and foam cushions for each subject. There were statistically significant differences (p=0.05) for average pressure and PPI between the two cushions for each subject, except subject number nine. There were statistically significant differences (p=0.05) for the dispersion index between cushions for each subject except number seven. There were statistically significant differences (p=0.05) for contact area between the two cushions for all subjects.

As a population, the air cushion measured a significant decrease of average pressure compared to the foam cushion, dropping the average pressure from 29.8 mmHg for the foam cushion to 25.6 mmHg for the air adjustable cushion (p=0.05). The PPI reduced from 50.0 mmHg for the foam cushion to 35.4 mmHg for the air adjustable cushion (p=0.05). The Dispersion Index decreased from 41.6% for the foam cushion to 36.2% for the air adjustable cushion (p=0.05).

A new metric labeled the "Pressure Distribution Index" was created specifically for this study to represent the data. The Pressure Distribution Index is the ratio of Average Pressure to PPI. This value is very similar to the Dispersion Index; however, it is a ratio of a given point relative to the entire surface whereas the Dispersion Index is the ratio of a region relative to the entire surface. The Dispersion Index includes area of potentially low and high pressures, relative to the entire cushion surface. The resolution of this metric does not truly measure the pressure over the boney prominences relative to the surface. The Pressure Distribution Index, however, is a measure of when a surface properly distributes the pressure away from critical points. Ideally, a value closer to 1.0 would indicate the average pressure is equivalent to the PPI, giving an equal pressure

distribution over the surface. The Pressure Distribution Index was calculated for each subject and can be seen in Figure 21. The p-values for the difference between the air and foam cushions are shown in Table 4. For the entire population, the Pressure Distribution Index increased from 0.613 for the foam cushion to 0.739 for the air adjustable cushion (p=0.05).

Shear Measurement

The shear stress measurements at the seating surface were analyzed based upon the static shear (sitting still before the participant started the obstacle course) and the dynamic shear (moving during the obstacle course). The static shear was measured as the shear measured by the Predia sensor. The dynamic shear was analyzed as a range of data, from start to finish of the particular segment of the obstacle course. The decision to analyze dynamic shear as a range allowed the data to be observed as an influence of the chair and cushion over a given movement. The data were also separated from the left turn course to right turn course as differences between the two orientations proved to be significant.

Static Shear Results

Within the static shear data, the data were separated according to the obstacle course segments as defined in Figure 13 and Figure 14 as shown in the METHODS section. The static shear was measured each time was about to begin the next segment. Shown in Figure 22 and Figure 23 is the static shear after the pressure relief lift prior to the movement into the obstacle course for the left and right hand test, respectively. The static shear data prior to the reverse portion of the left and right obstacle courses is shown

in Figure 24 and Figure 25, respectively. Lastly, the static shear data after the reverse to segment three is shown in Figure 26 and Figure 27 for the left and right turn courses, respectively.

Visually, Figure 22 through Figure 27 do not show any trends for a configuration that produced lower shear values. A Least Squares Means analysis was performed on the static shear data. The effects of test subjects, gender, cushion, wheelchair type, turn, gender x cushion, cushion x turn, type of chair x turn, and cushion x chair x turn were evaluated. As a population, the chair type or cushion does not play a significant effect in reducing the shear. However, individual parameters did have a significant effect. For the static shear gathered at zone one, the parameter with the most significant effect at reducing shear was the air cushion over the foam cushion, p=0.0160. The Air cushion combined with right turn produced a significant effect to reduce shear, p=0.0090, and Females crossed the Air cushion produced a significant effect to reduce shear, p=0.0329. For the static shear gathered at zone two, the only significant effects at reducing shear were the air cushion and the air cushion crossed the right turn, p=0.0081 and p=0.0178, respectively. However, for the static shear gathered at zone three, the only significant effect at reducing shear was the use of the air cushion with p=0.0022.

Dynamic Shear Results

The dynamic shear was segmented into the same intervals as defined in Figure 13 and Figure 14. Dynamic shear was measured each time the participant was maneuvering through the obstacle course, separated by sections of the course. Shown in Figure 28 and Figure 29 is the dynamic shear from zone 1-2 for the left and right turns of the obstacle

course, respectively. Section 2-3, the reverse, is shown in Figure 30 and Figure 31 for the left and right obstacle courses, respectfully. Lastly, the dynamic shear zone from 3-4 for the left and right turns of the obstacle course are shown in Figure 32 and Figure 33, respectfully.

As was the case with static shear, the dynamic shear, as shown in Figure 28 through Figure 33, does not produce any configurations that produced lower shear values upon inspection. A Least Squares Means analysis was performed on the dynamic shear data. The effects for the analysis included test subjects, gender, cushion, wheelchair type, turn, gender cross cushion, cushion cross turn, type of chair cross turn, and cushion cross chair cross turn. The dynamic shear did not produce a chair or cushion configuration that produced a significantly lower shear value. Over the population, a few parameters did produce significantly lower shear values. For the dynamic shear from zone one to two, Males, Females crossed with the left turn course, and Females crossed with the Air adjustable cushion produced significance in lowering shear values; $p<0.0001$, $p=0.0005$, and $p=0.0037$, respectfully. For the dynamic shear from zone two to three, no parameters produced significant reductions in shear. Finally, for the dynamic shear zone from three to four, Females crossed with the Air cushion, the Wheel-rim propulsion type, and Males produced significant reductions in shear; $p=0.0009$, $p=0.0112$, and $p=0.0474$, respectfully.

Power calculations based upon given data set indicate that statistical significance between testing configurations might occur with a sample size on the order of 250+, a sample size beyond a reasonable amount for this research project.

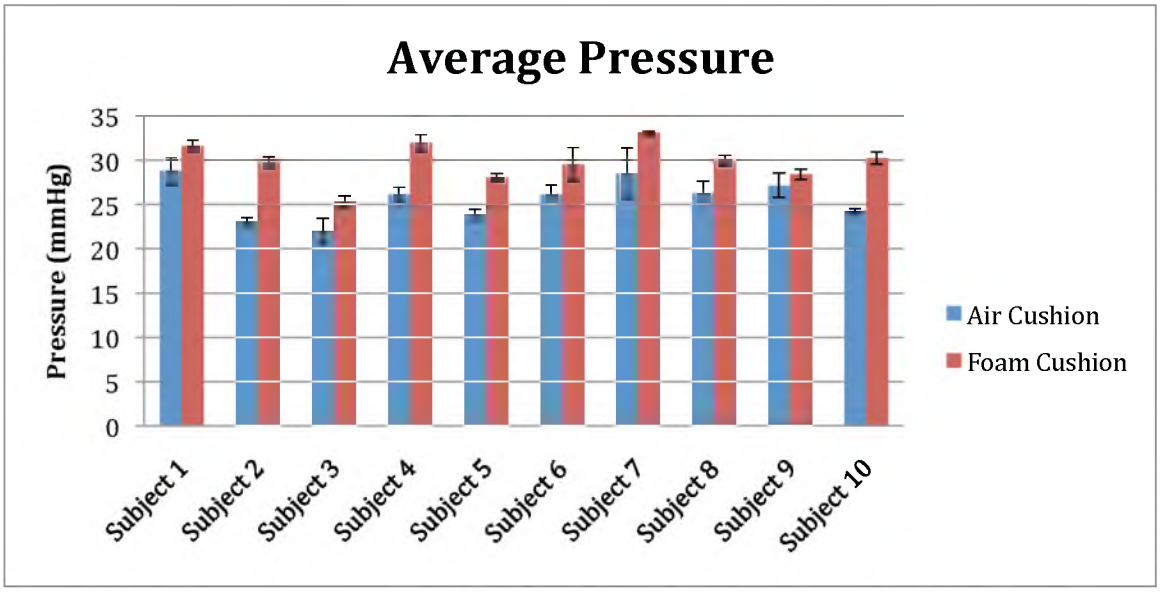

Figure 17 – Average pressure by subject for both air and foam cushions. Error bars indicate confidence intervals to 95%.

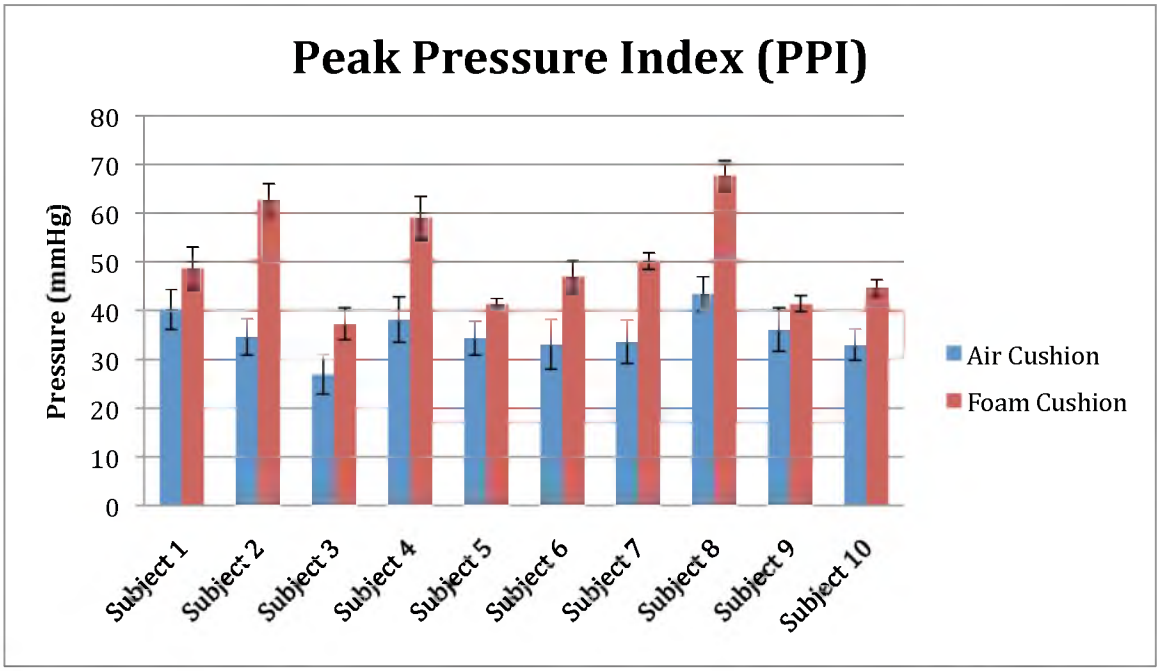

Figure 18 – Peak Pressure Index (PPI) by subject for both air and foam cushions. Error bars indicate confidence intervals to 95%.

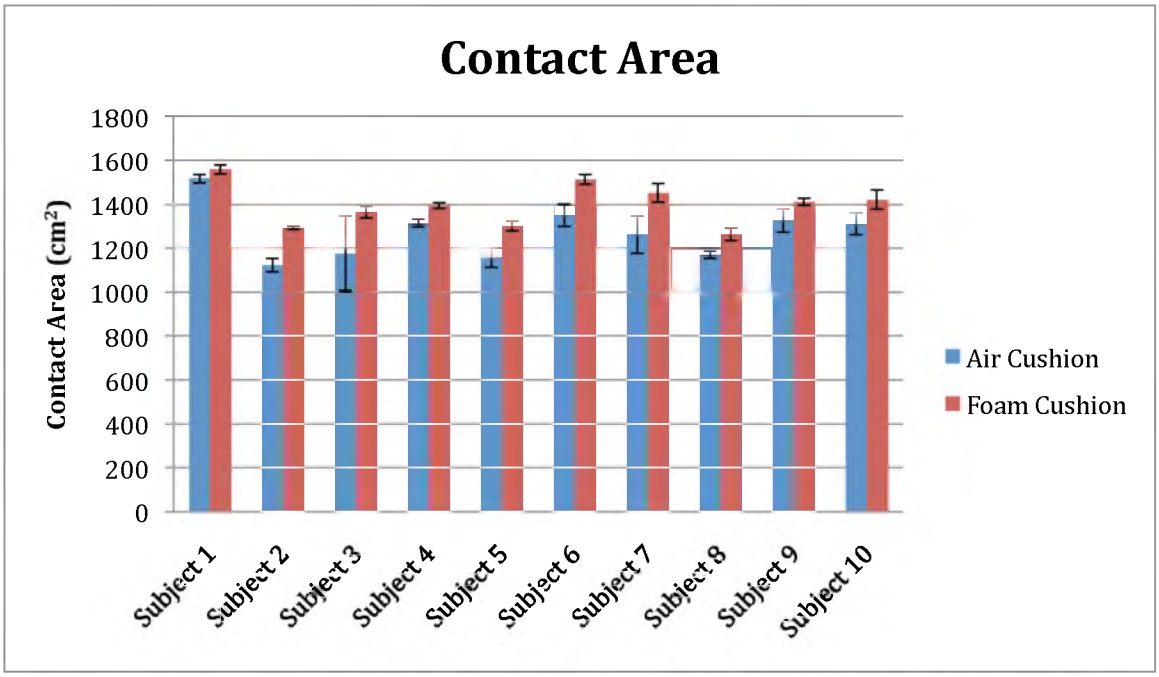

Figure 19 – Contact area by subject for both air and foam cushions. Error bars indicate confidence intervals to 95%.

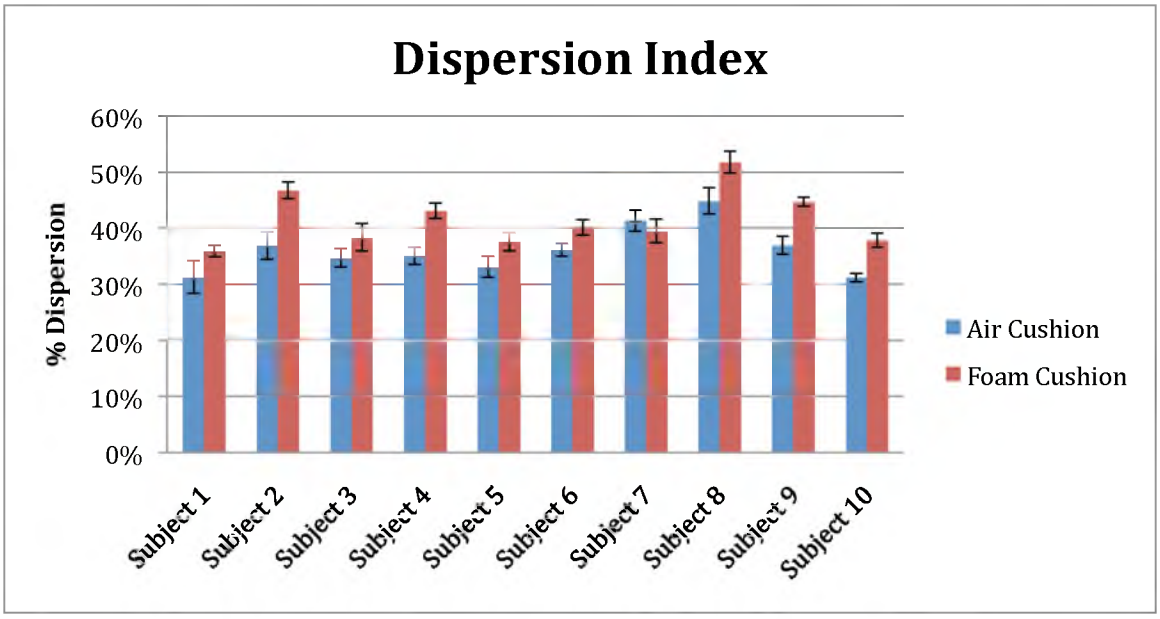

Figure 20 – Dispersion Index by subject for both air and foam cushions. Error bars indicate confidence intervals to 95%.

Table 3 – P-values for the individual subject difference between the air and foam cushions. P-values displayed for Average Pressure, PPI, Contact Area, and Dispersion Index.

	Average Pressure (mmHg)	Peak Pressure Index (mmHg)	Contact Area (cm2)	Dispersion Index (%)
Subject 1	0.0099	0.0248	<0.0001	0.0088
Subject 2	<0.0001	<0.0001	0.0317	<0.0001
Subject 3	0.0027	0.0045	<0.0001	0.0202
Subject 4	<0.0001	0.0002	<0.0001	<0.0001
Subject 5	<0.0001	0.006	0.0002	0.0039
Subject 6	0.0147	0.0022	0.0002	0.0012
Subject 7	0.014	0.0001	0.002	NS*
Subject 8	0.001	<0.0001	0.0003	0.001
Subject 9	NS*	NS*	0.0073	<0.0001
Subject 10	<0.0001	0.0002	0.0055	<0.0001

*NS = Not Significant Difference

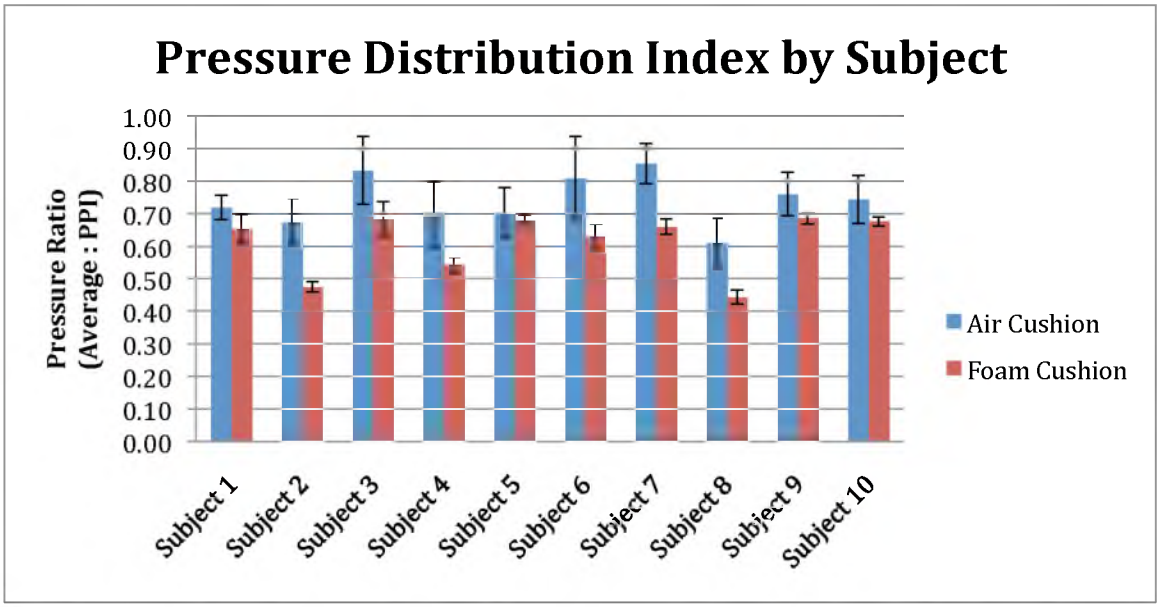

Figure 21 – Pressure Ratio by subject for both air and foam cushions. Pressure Ratio is the ratio of average pressure to PPI. Error bars indicate confidence intervals to 95%.

Table 4 – P-values for the individual subject difference between the air and foam cushions for the Pressure Distribution Index.

	Pressure Distribution Index
Subject 1	0.0276
Subject 2	0.0004
Subject 3	0.0187
Subject 4	0.0096
Subject 5	NS*
Subject 6	0.0149
Subject 7	0.0002
Subject 8	0.0014
Subject 9	0.0353
Subject 10	NS*

*NS = Not Significant Difference

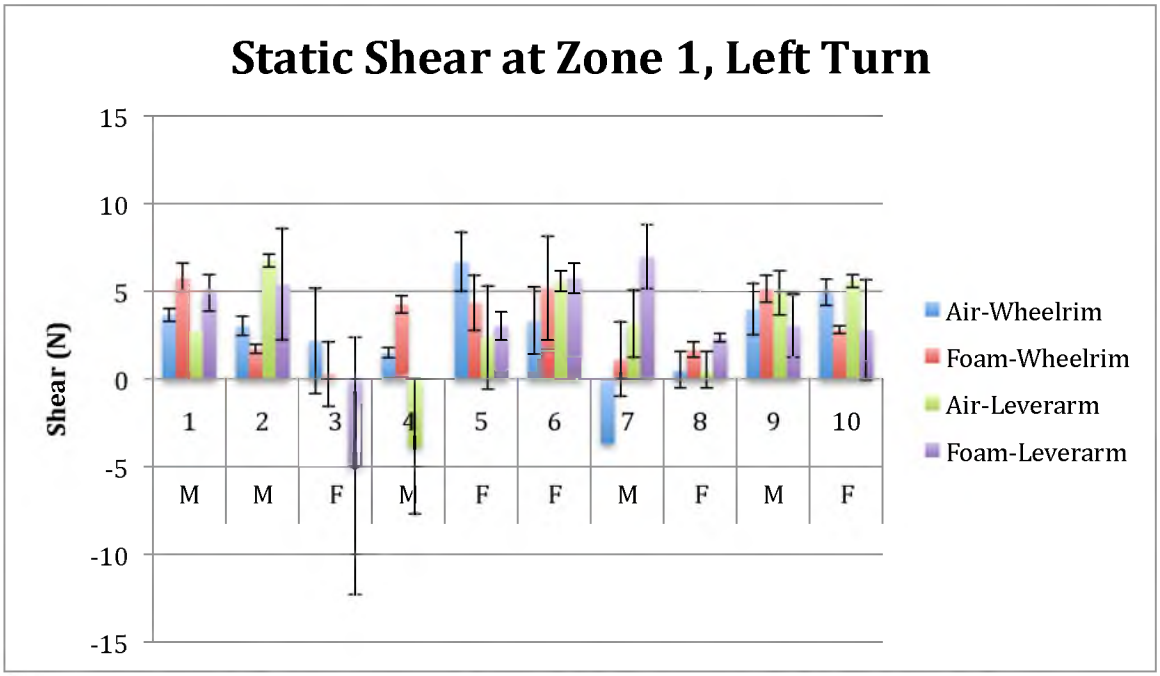

Figure 22 – Static shear at zone 1 of the obstacle course for the left hand turn displaying each testing configuration separated by subject. Error bars indicate confidence interval to 95%.

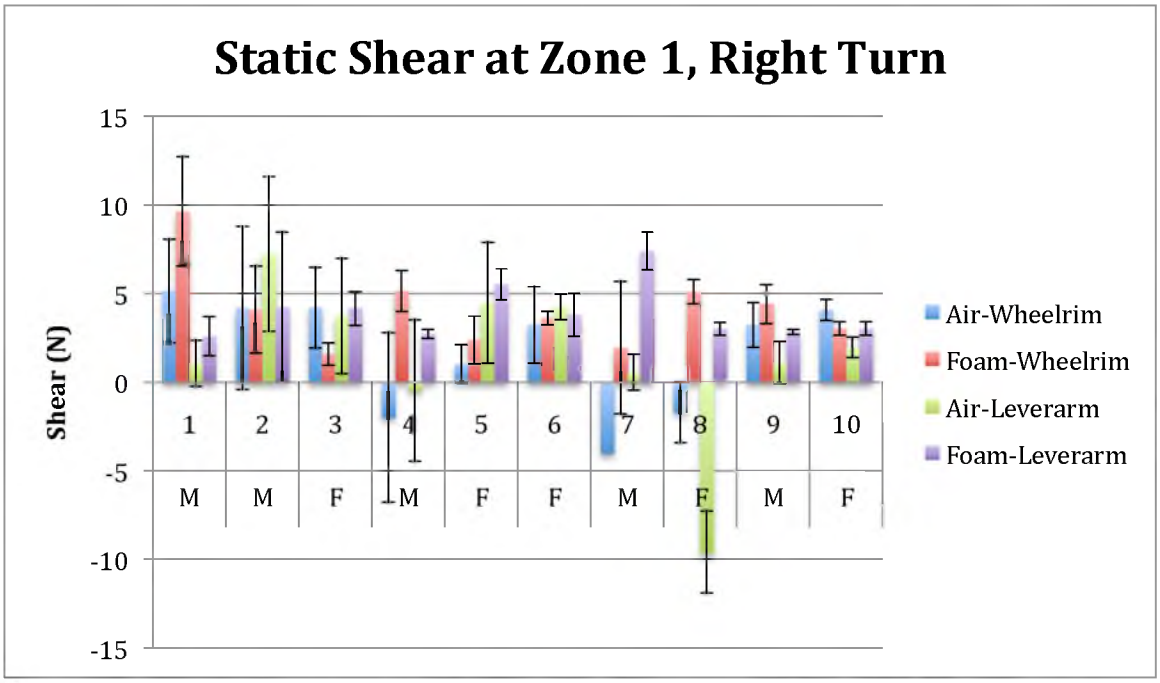

Figure 23 – Static shear at zone 1 of the obstacle course for the right hand turn displaying each testing configuration separated by subject. Error bars indicate confidence interval to 95%.

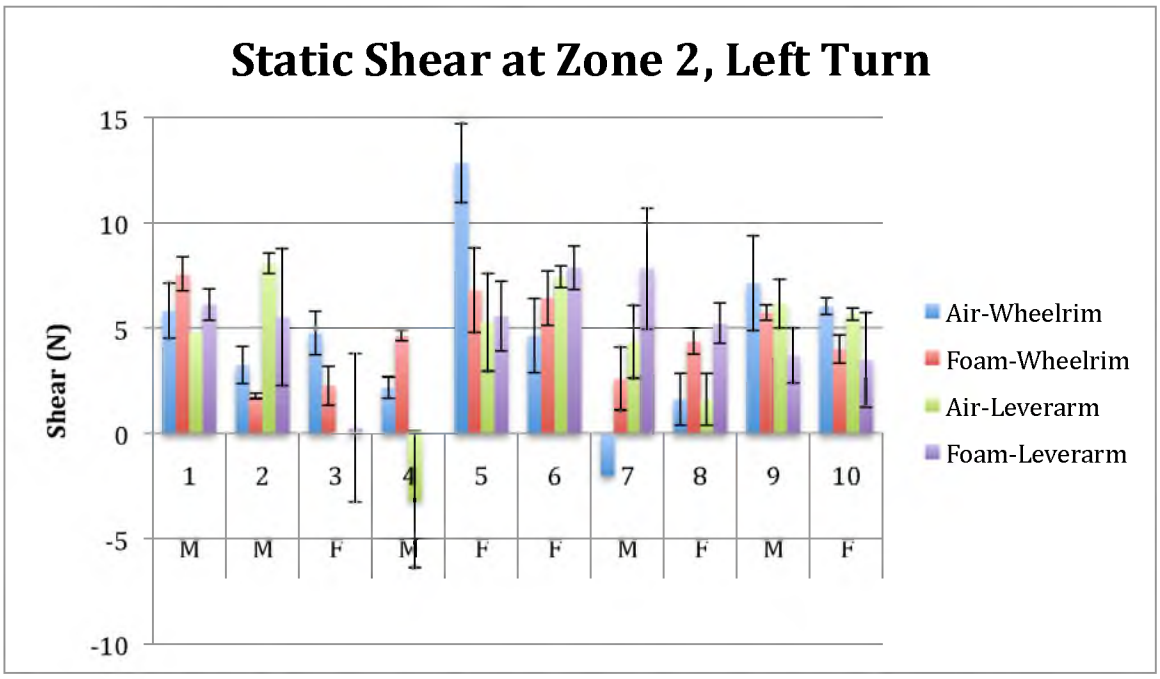

Figure 24 – Static shear at zone 2 of the obstacle course for the left hand turn displaying each testing configuration separated by subject. Error bars indicate confidence interval to 95%.

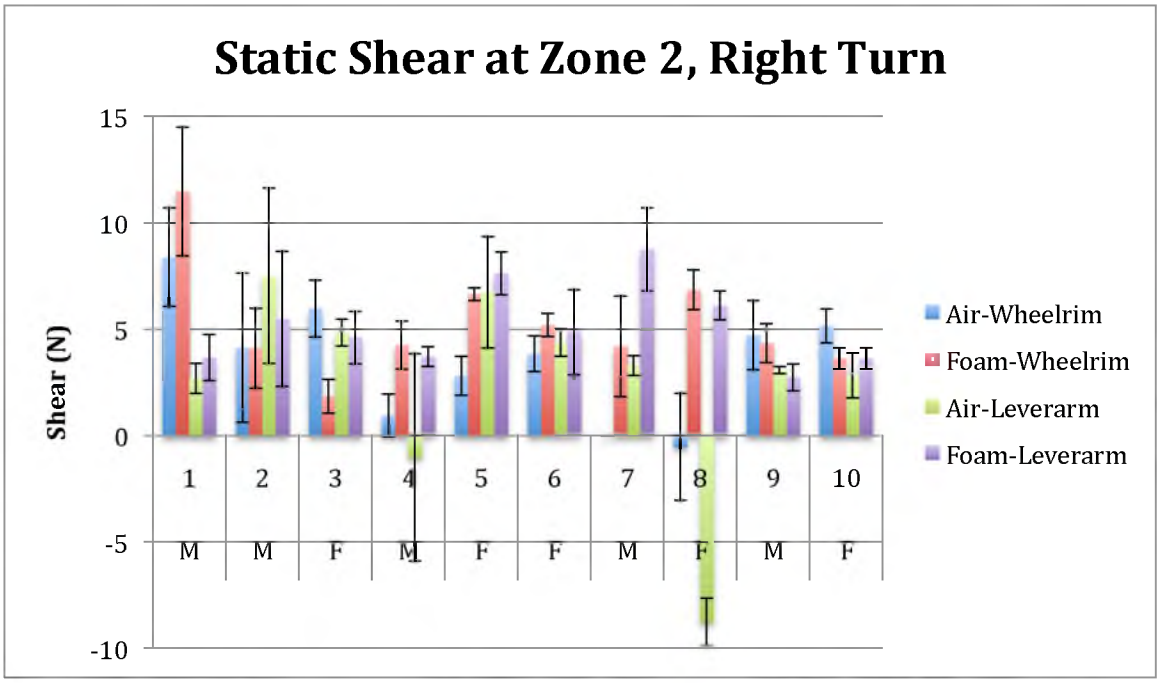

Figure 25 – Static shear at zone 2 of the obstacle course for the right hand turn displaying each testing configuration separated by subject. Error bars indicate confidence interval to 95%.

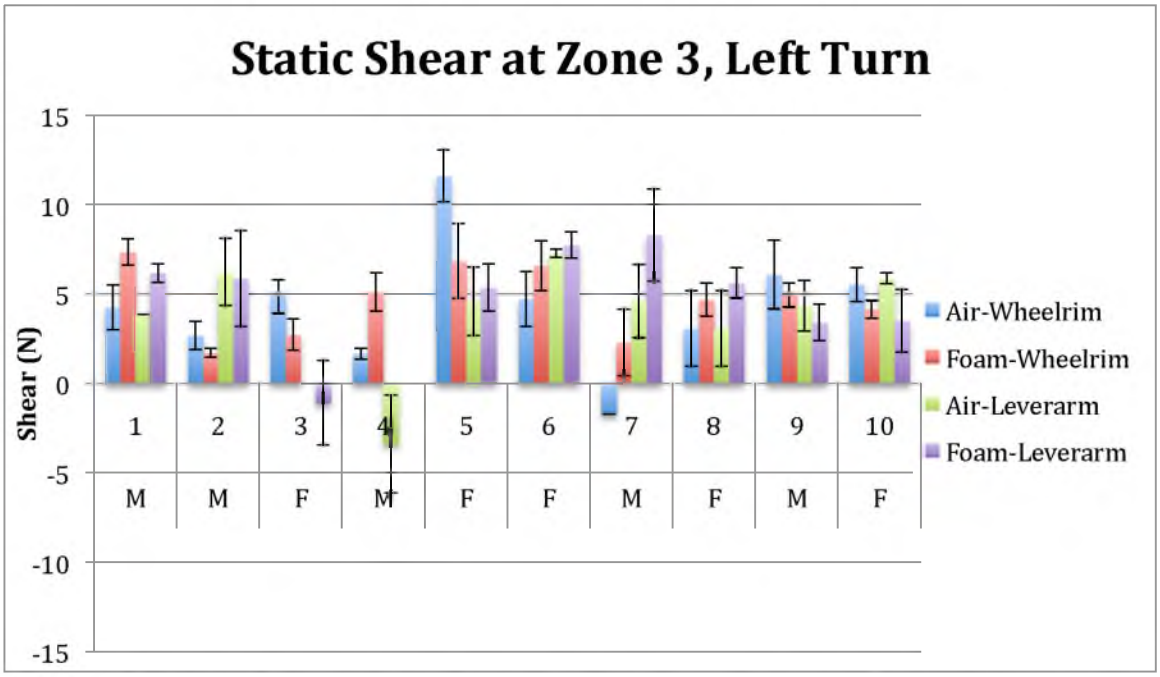

Figure 26 – Static shear at zone 3 of the obstacle course for the left hand turn displaying each testing configuration separated by subject. Error bars indicate confidence interval to 95%.

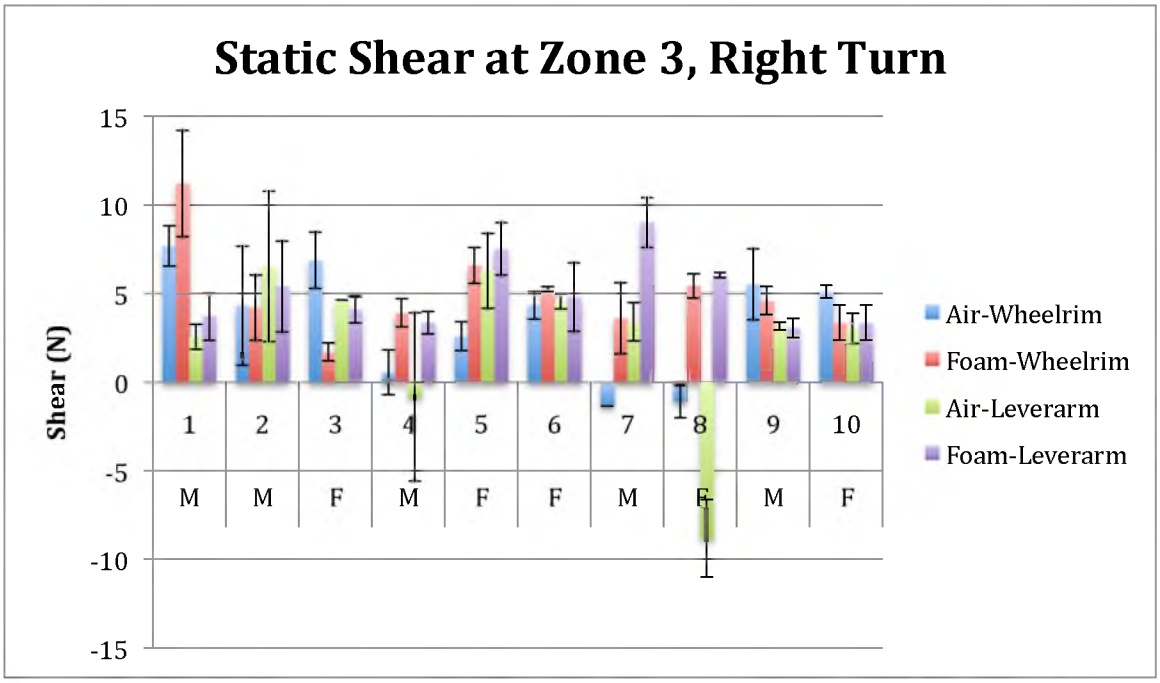

Figure 27 – Static shear at zone 3 of the obstacle course for the right hand turn displaying each testing configuration separated by subject. Error bars indicate confidence interval to 95%.

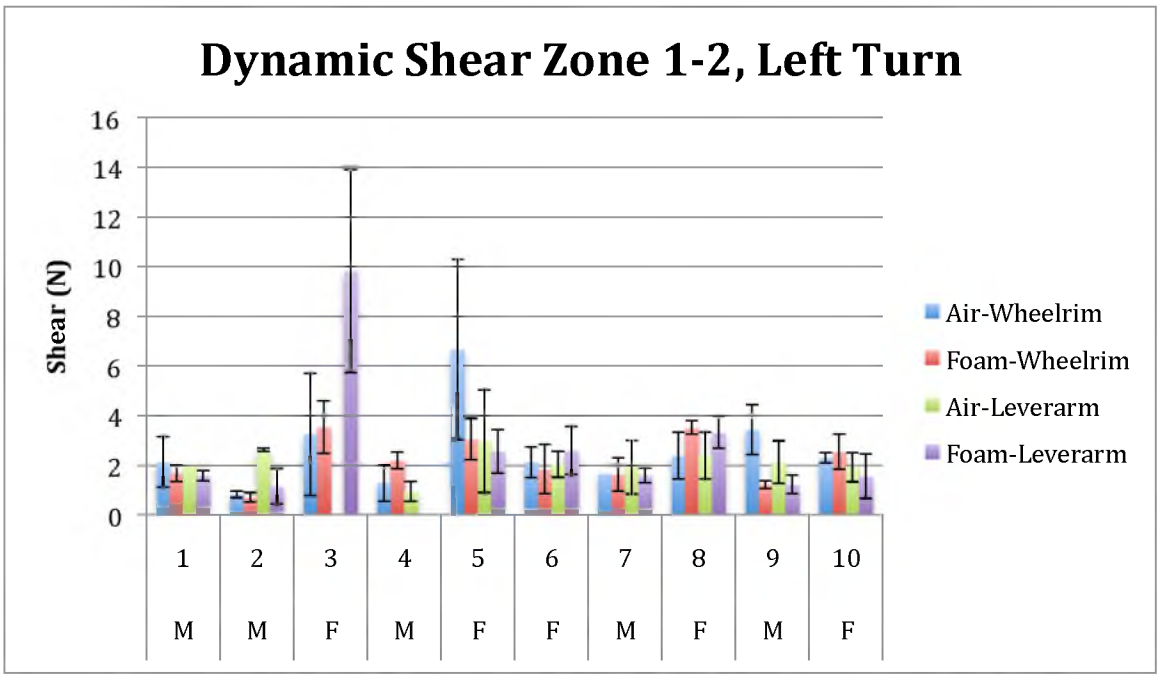

Figure 28 – Dynamic shear during zone 1-2 of the obstacle course for the left hand turn displaying each testing configuration separated by subject. Error bars indicate confidence interval to 95%.

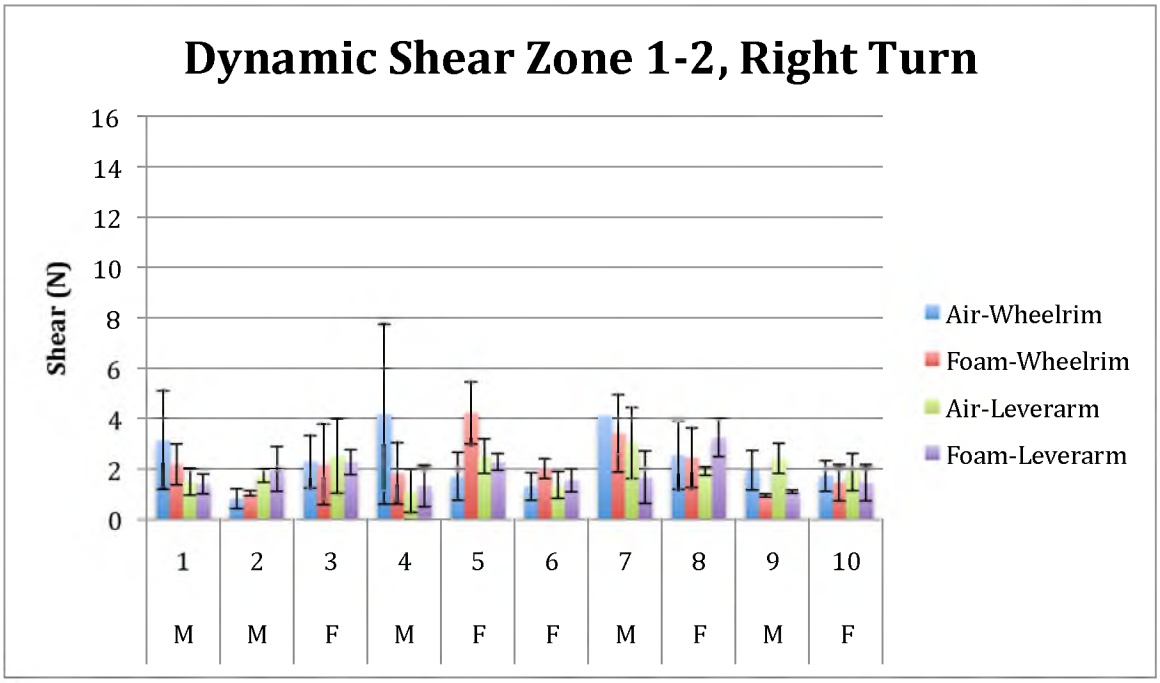

Figure 29 – Dynamic shear during zone 1-2 of the obstacle course for the right hand turn displaying each testing configuration separated by subject. Error bars indicate confidence interval to 95%.

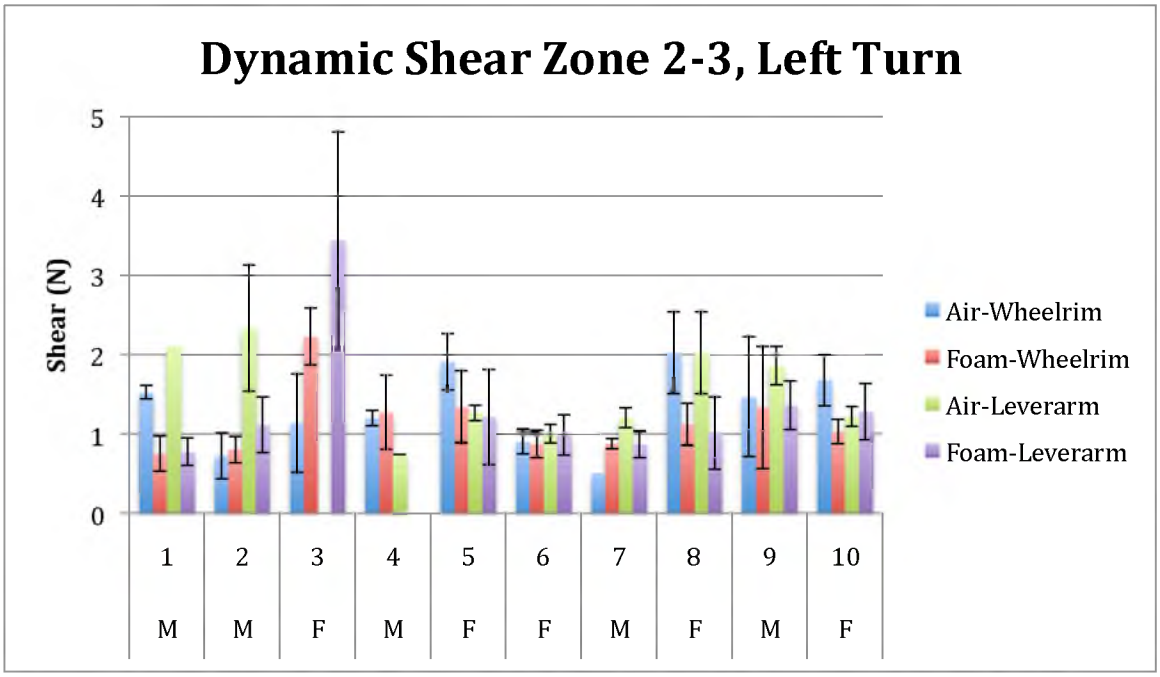

Figure 30 – Dynamic shear during zone 2-3 of the obstacle course for the left hand turn displaying each testing configuration separated by subject. Error bars indicate confidence interval to 95%.

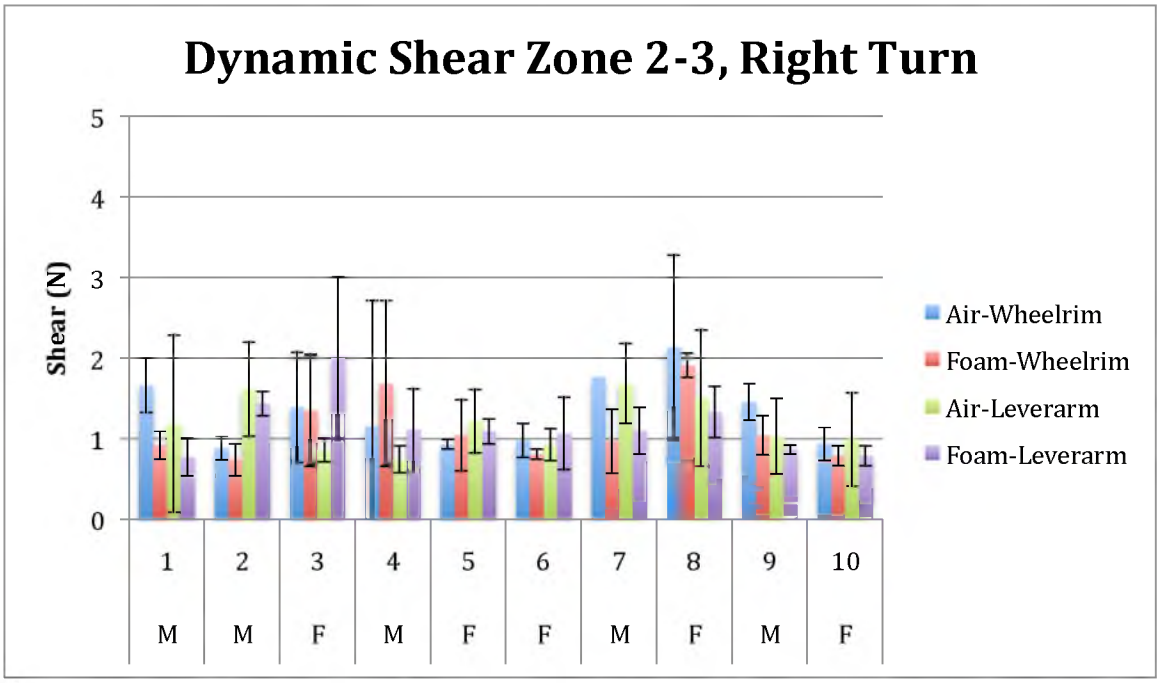

Figure 31 – Dynamic shear during zone 2-3 of the obstacle course for the right hand turn displaying each testing configuration separated by subject. Error bars indicate confidence interval to 95%.

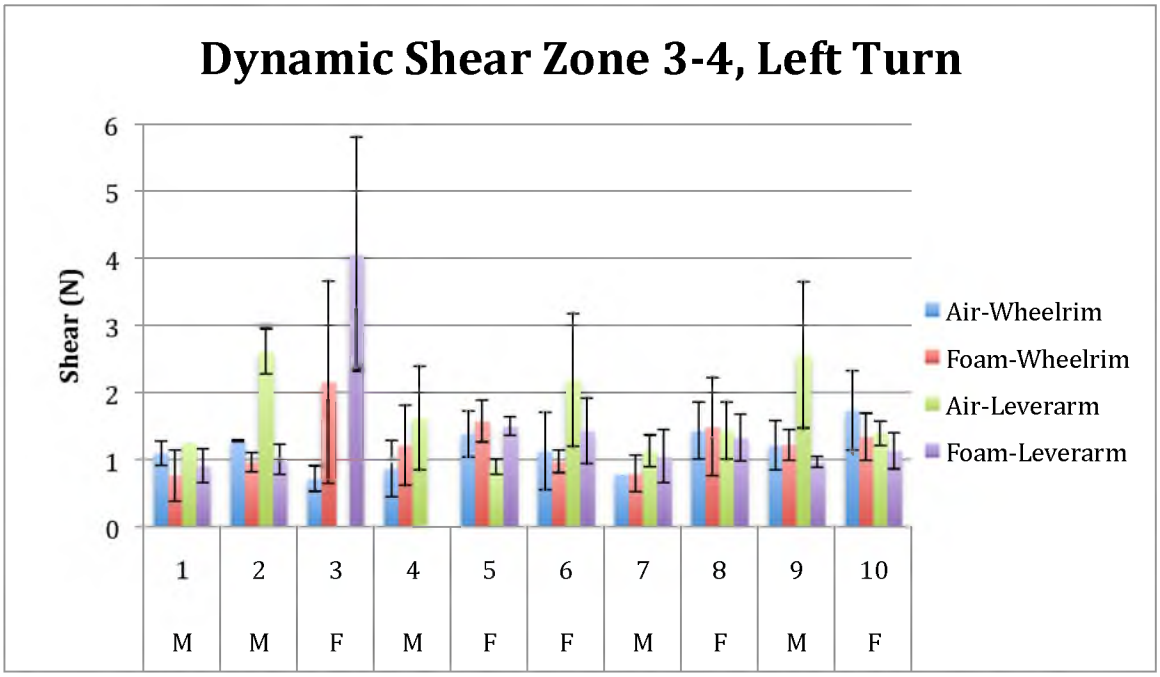

Figure 32 – Dynamic shear during zone 3-4 of the obstacle course for the left hand turn displaying each testing configuration separated by subject. Error bars indicate confidence interval to 95%.

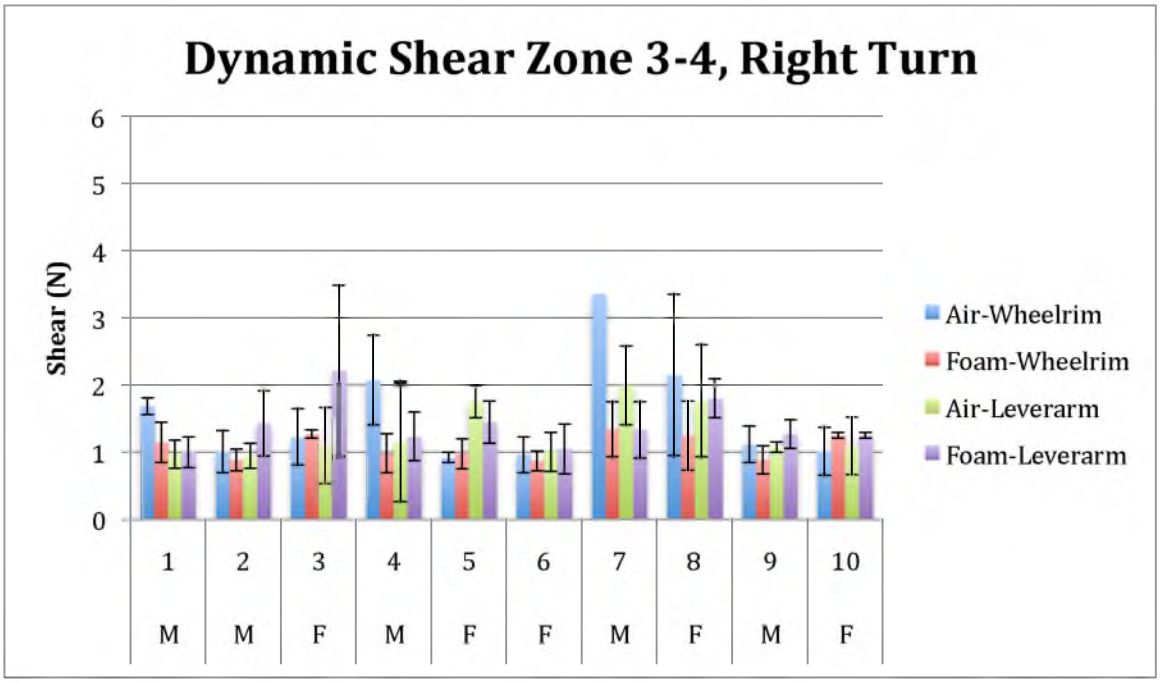

Figure 33 – Dynamic shear during zone 3-4 of the obstacle course for the right hand turn displaying each testing configuration separated by subject. Error bars indicate confidence interval to 95%.

DISCUSSION

Pressure Mapping

Ideally, a good cushion would have a low average pressure, a low PPI, a low dispersion index, and a high contact area (Crawford, Walsh, & Porter-Armstrong, 2006; Ferguson-Pell, Nicholson, Lennon, & Bain, 2001; "ISO Working Group Clinical Use Guidelines," 2008; Nicholson, Ferguson-Pell, Lennon, & Bain, 2001). A low Pressure Distribution Index would indicate the average pressure is much lower than the PPI, suggesting a poor pressure distribution over the surface.

With the exception of subject 9, the air adjustable cushion produced significantly lower average pressures and peak pressure index values for the population. The air cushion did very well at redistributing the peak forces away from critical areas, such as the ischial tuberosities and the sacrum. The foam cushion measured a much larger distinction of pressure accumulation at the ischial tuberosities.

A few gender differences were identified. Females had a much larger percentage of load on the air adjustable cushion compared to males, with 65 ± 9 % of body mass being present on the cushion for females compared to 56 ± 6 % for males. The air adjustable cushion did not produce statistically significant values, but the foam cushion did with a p-value of 0.0145. Females measured 85 ± 8 % of their body mass on the foam cushion, as opposed to 70 ± 7% of the male body mass on the foam cushion. Females also produced a center of pressure more towards the center of the cushion. One

flaw with the body mass calculations is that the resultant force seen by the pressure map is a function of contact area. As seen in Figure 19, the contact area is dramatically lower for the air adjustable cushion. As the cells of the air bladder collapses, gaps can be seen between the cells, causing an area of no contact, thus influencing the resultant load calculations for the air cushion. As well, the functional heights of the foam and air adjustable cushions were quite different, ie the adjusted 13-25mm offset of the air adjustable cushion compared to the compression of the 100mm foam.

A difference in the center of mass from the posterior side of the cushion was identified between genders: females produced a center of pressure 17.9 ± 1.2 cm forward of the posterior side of the cushion, while males produced only 17.4 ± 0.7 cm for the air adjustable cushion. For the foam cushion, females produced a center of pressure 17.9 ± 1.3 cm forward of the posterior side of the cushion while males produced only 16.4 ± 1.0 cm. Though the values are not statistically significant, the trend is that females have a center of pressure closer to the center of the cushion than males. This follows the traditional observed difference that females are more "pair" shaped and carry more of their mass in the pelvic and thigh regions while males are more "apple" shaped and carry more of their mass in the abdomen and upper body (Blaak, 2001; Chaffin et al., 2006).

Pressure mapping was only used in static seating on the cushions. The XSensor X2 pressure map system setup does not easily allow for the map to record data in a mobile test, as cables and the logging computer must be transported with the map. Newer pressure mapping technology allows for wireless logging of data, which would be better suited to measure the dynamic normal loading of the cushion based upon wheelchair propulsion. However, the map should not be used during the course for shear

data collection, as the use of the map at the seating surface will drastically change the shear values because the map is a lower coefficient of friction surface.

The pressure distribution of the two cushions was measured as a function of multiple metrics. The hypothesis, H_1, that the air adjustable cushion would produce greater pressure distribution than the foam cushion can be accepted based upon the metrics: normal pressure, peak pressure index, dispersion index, and pressure distribution index with population data being significant at $p \leq 0.05$. Similar studies follow the trend that an air adjustable cushion produces lower average pressures and peak pressures (Gilsdorf et al., 1991).

Shear Testing

Though not significant in every case, a trend was observed that there was lower shear stress for males than for females. This may likely be a function of normal weight distribution as pressure mapping data measured that the females placed a larger percent of the total body mass on the cushion than the males.

The orientation of the obstacle course proved to play an influence, though it was not significant over all testing configurations. The Predia sensor was adhered on the left side of the subject, and the trend concluded that shear was largest on the left turn where the sensor would be at a smaller turning radius.

A few remarks made by some of the testing subjects indicated that they never consistently felt a large amount of shear or sliding at the cushion surface. The subjects felt that if the obstacle course were longer and allowed for greater speeds to be achieved that perhaps more shear could be measured. Another problem occurred where a few of the data points gathered by the Predia had to be discarded when the data was a flat line,

measuring no shear at all. A more robust sensor and connection to LabView may produce better results for future research.

No wheelchair propulsion type, cushion type, or wheelchair propulsion method and cushion configuration could be identified that resulted in a consistent reduction of shear stresses at the seating surface. A trend was noticed that in a few situations, the air adjustable cushion measured lower shear than the foam cushion, but this was not consistent or significant for the population. Hypotheses H_2, H_3, and H_4 could not be accepted with this data set for either static or dynamic shear.

CONCLUSIONS

Excess pressure over time can lead to detrimental and even dangerous skin or deep tissue break down resulting a pressure ulcer. The addition of shear stress can further reduce the pressure at which tissue breakdown can occur. This study was undertaken to measure the normal pressure and shear stress involved with various forms of wheelchair propulsion and cushion configurations to help identify a wheelchair designs that might reduce shear and normal pressure. Two cushions were used during this study, high resiliency polyurethane foam and an air adjustable cushion readily available in the wheelchair cushion market. Two wheelchair propulsions methods were used in conjunction with the two cushions to measure a difference in the seating stresses.

The following hypotheses were tested:

H_1: The air adjustable cushion will result in greater pressure distribution than the foam cushion.

H_2: The air adjustable cushion will result in less shear stress than the foam cushion.

H_3: The lever-arm wheelchair propulsion method will result in less shear stress than the wheel-rim propulsion method.

H_4: The combination of lever-arm wheelchair propulsion and air adjustable cushion will produce less shear stress than the combination of wheel-rim wheelchair propulsion and the form cushion.

The hypothesis, H_1, that the air adjustable cushion better distributes normal pressure over the surface of the cushion can be accepted based upon the sample size tested. The average pressure, peak pressure index, dispersion index, and pressure distribution index all produced significant differences between the two cushions, indicating the air adjustable cushion produced better pressure distribution than the foam cushion.

The hypothesis, H_2, that the air adjustable cushion produces less shear stress than the foam cushion cannot be accepted based upon the sample size tested. A trend was noticed that the air cushion produced less shear, but it was not a significant difference for the population.

Hypotheses H_3 and H_4, that the lever-arm wheelchair propulsion method would produce less shear than the traditional wheel-rim propulsion method and the combination of air cushion paired with the lever-arm wheelchair propulsion method would produce less shear than the foam cushion and wheel-rim propulsion method, could not be accepted with the sample size tested, respectively. No trend was identified that one chair or one cushion and propulsion type configuration produced less shear than any of the others.

APPENDIX A

PRESSURE MAPPING DATA

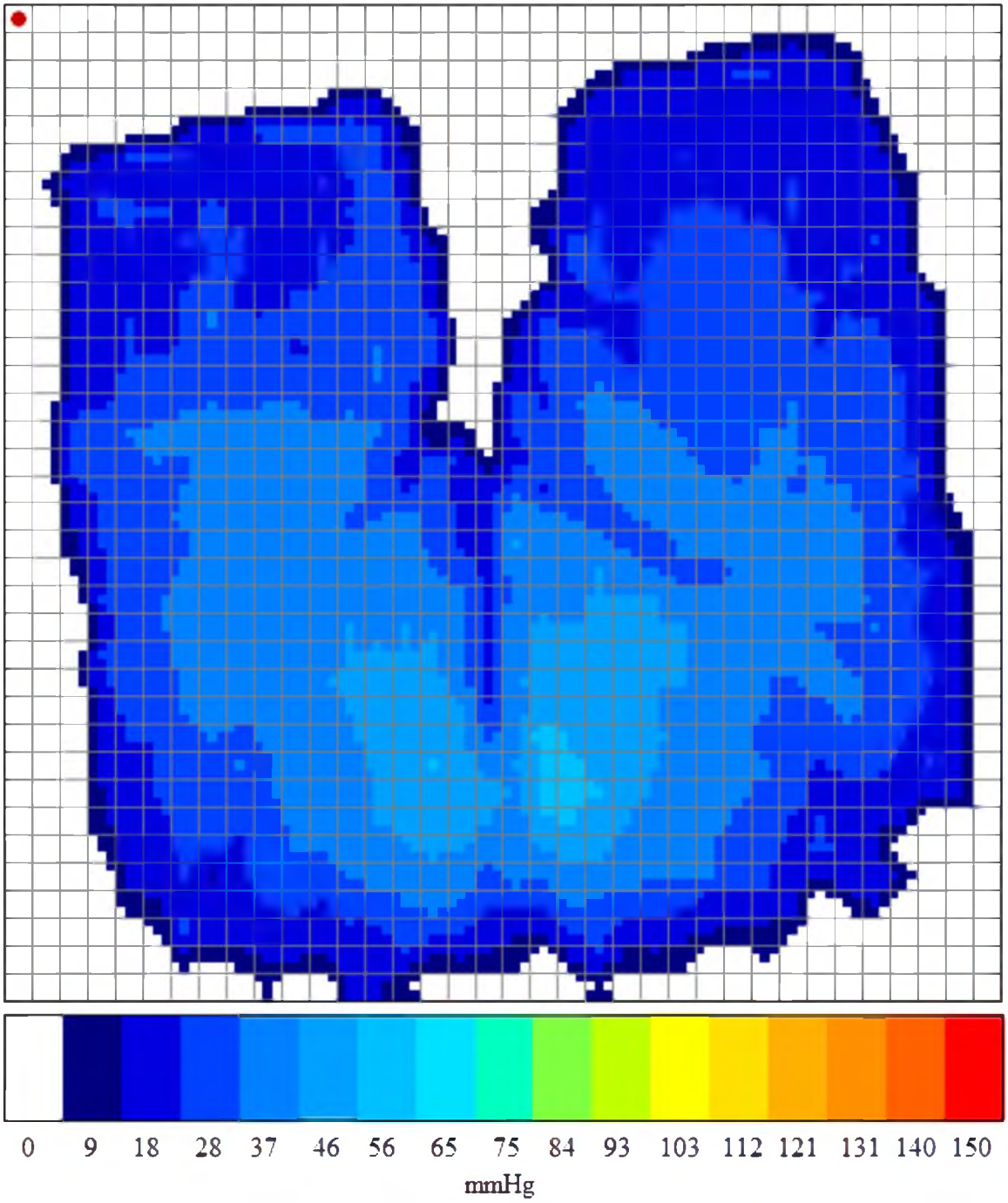

Figure 34 – Test subject #1 on foam cushion after 120 second loading.

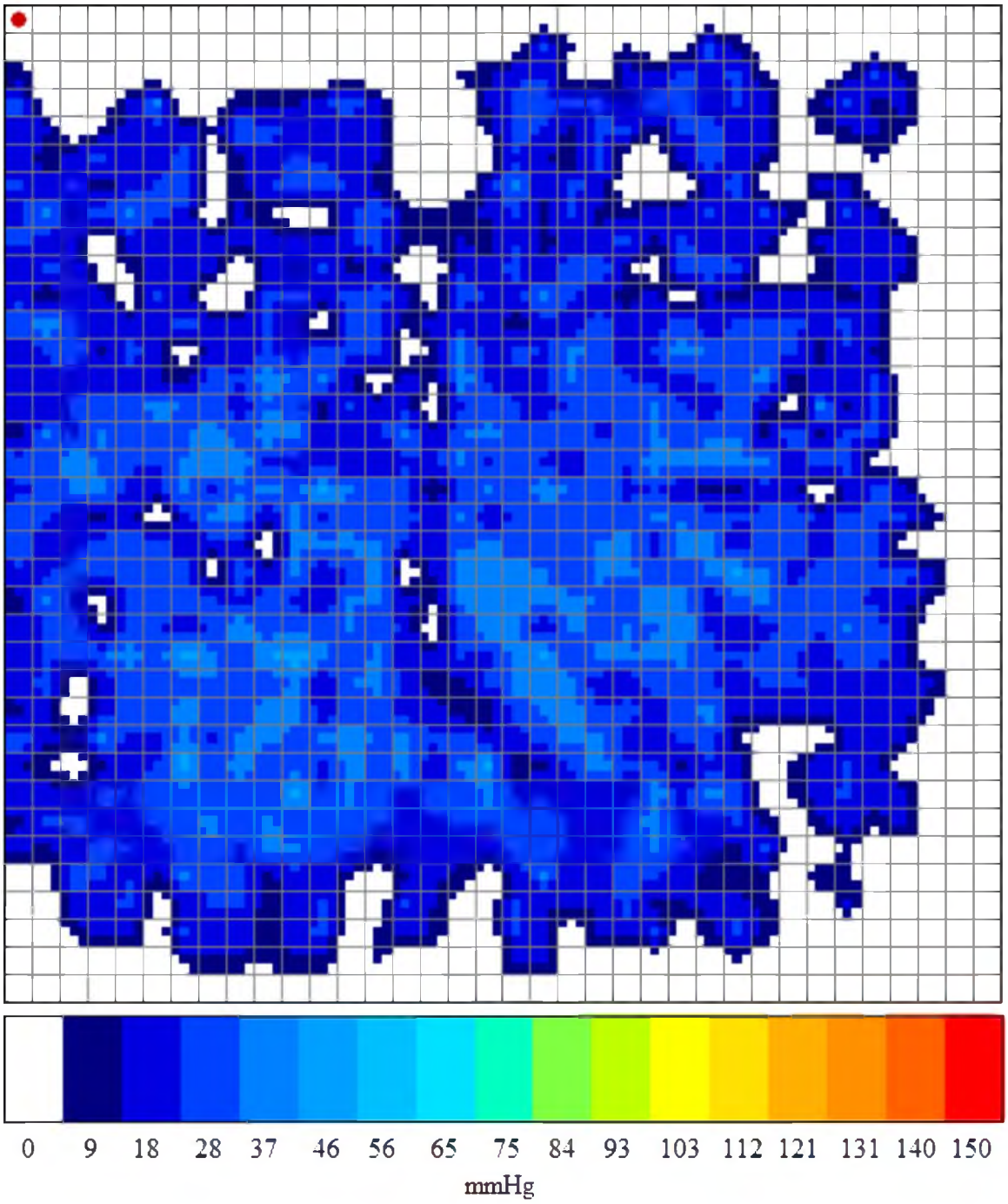

Figure 35 – Test subject #1 on adjusted air cushion after 120 second loading.

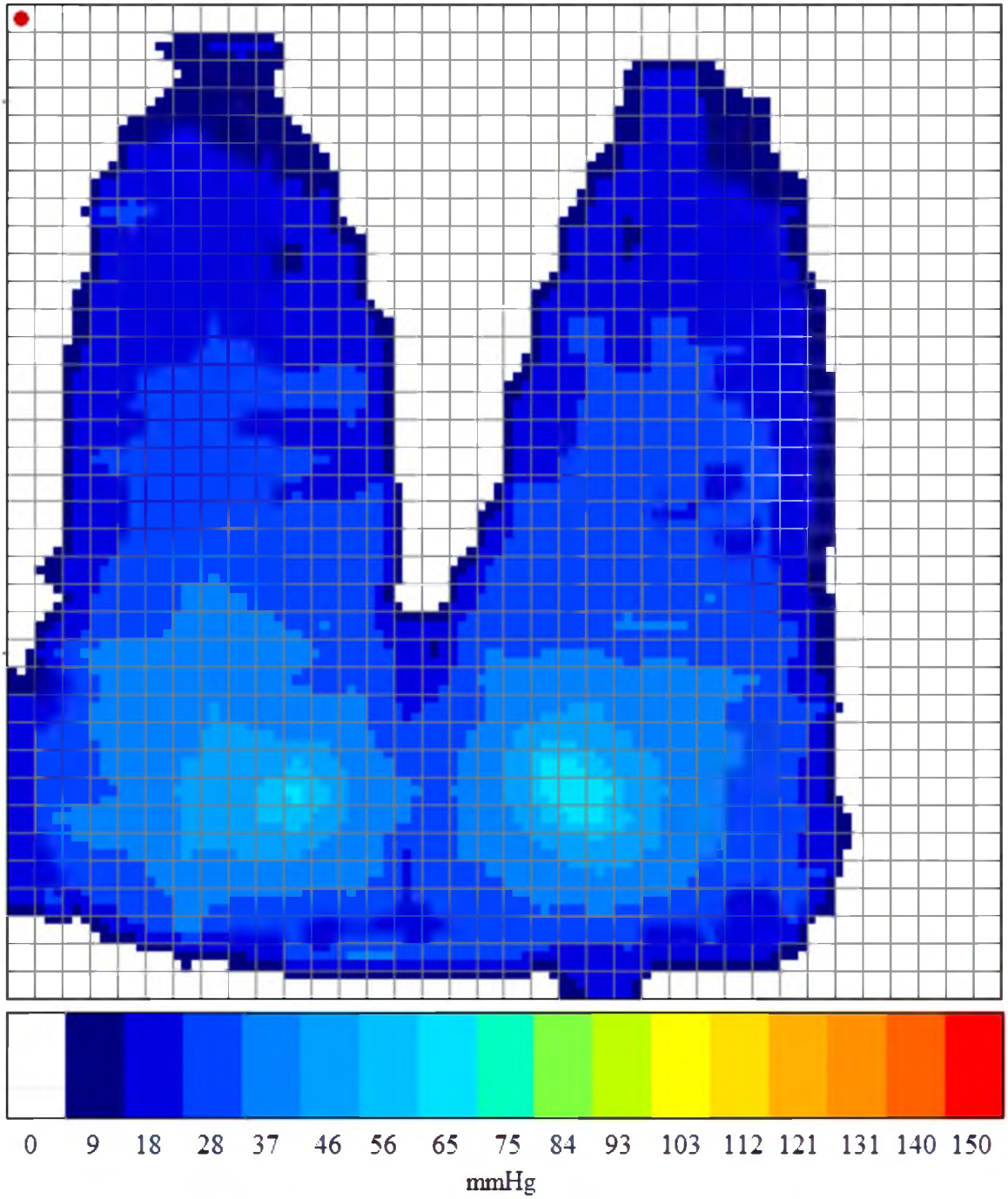

Figure 36 – Test subject #2 on foam cushion after 120 second loading.

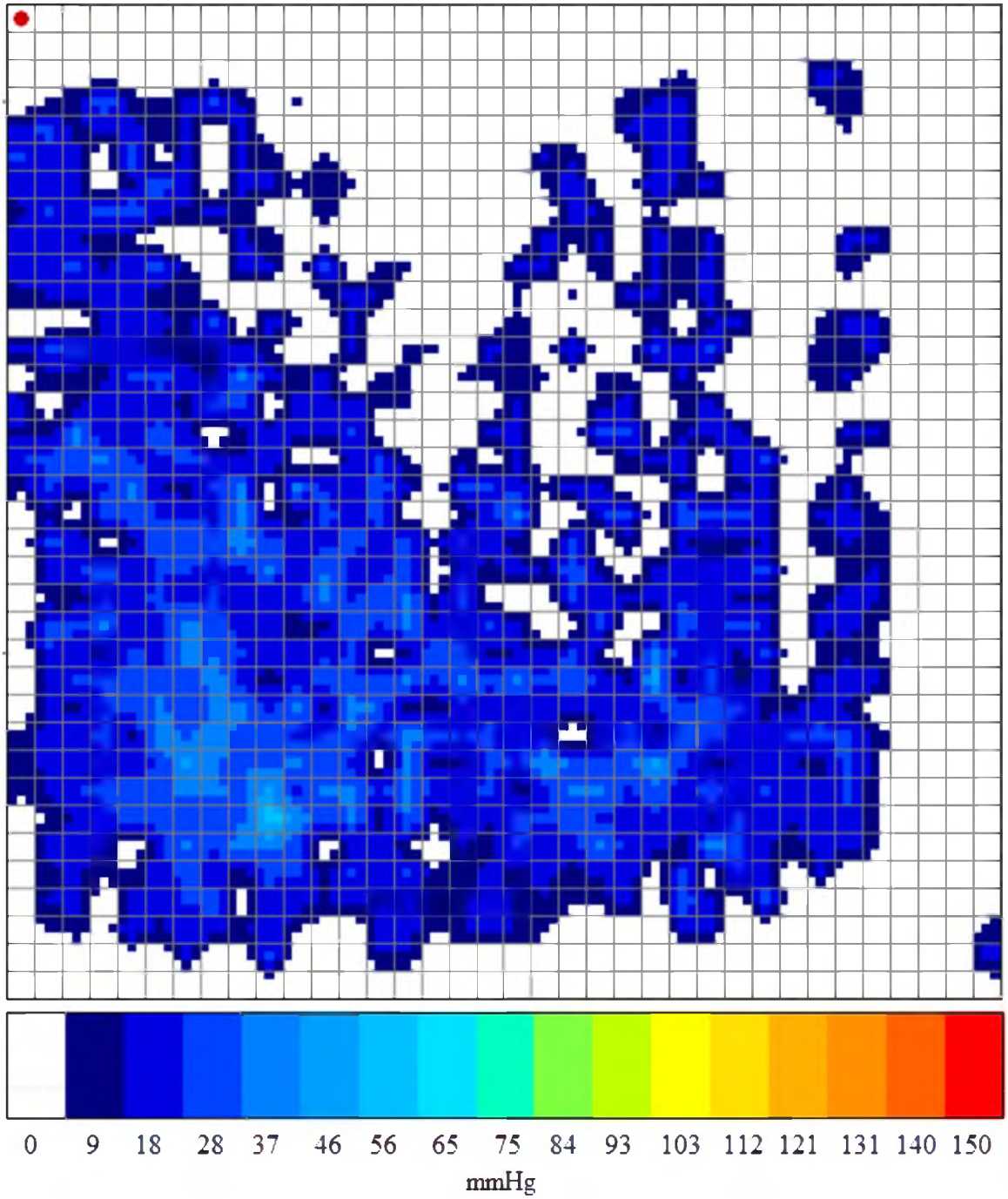

Figure 37 – Test subject #2 on adjusted air cushion after 120 second loading.

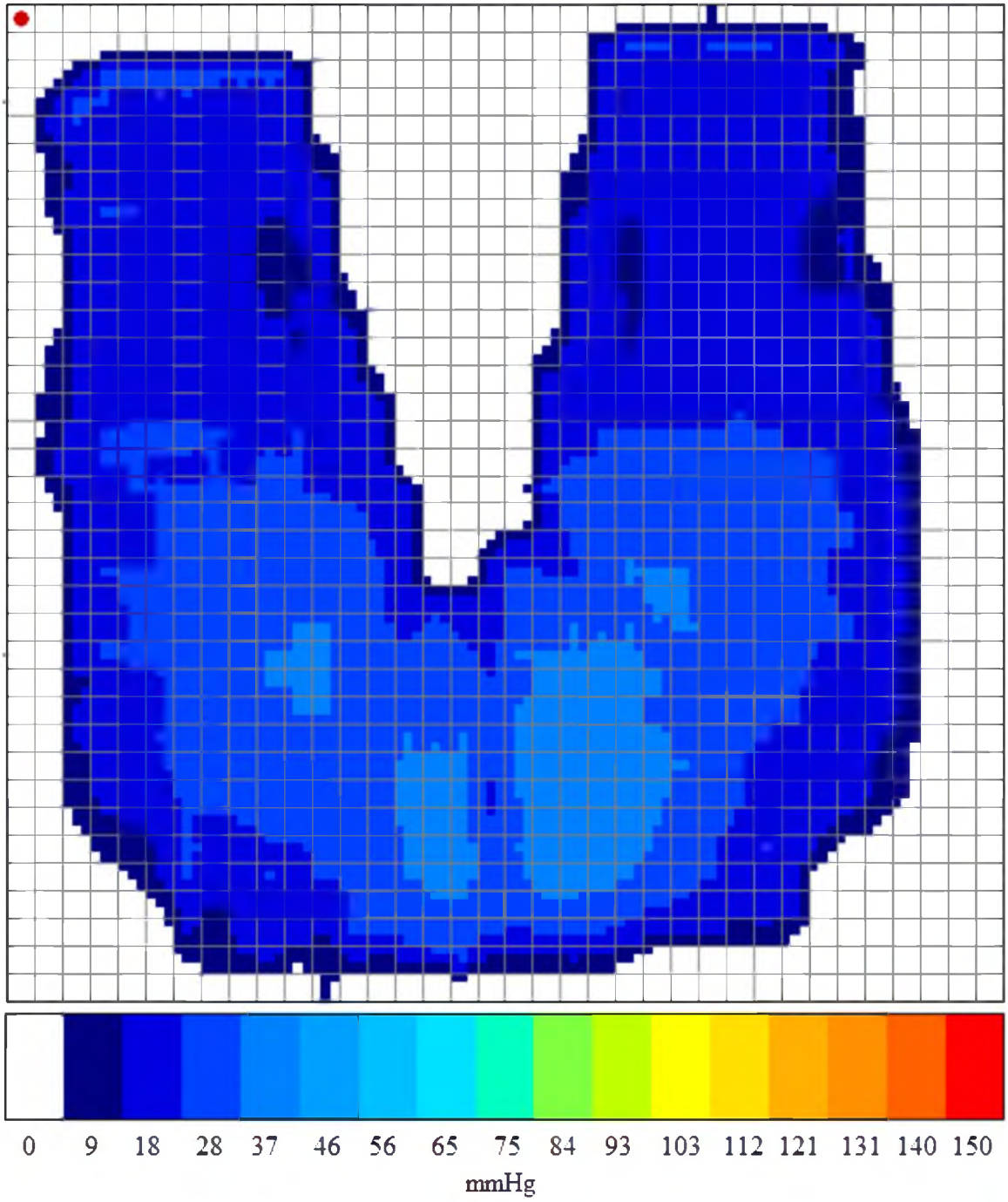

Figure 38 – Test subject #3 on foam cushion after 120 second loading.

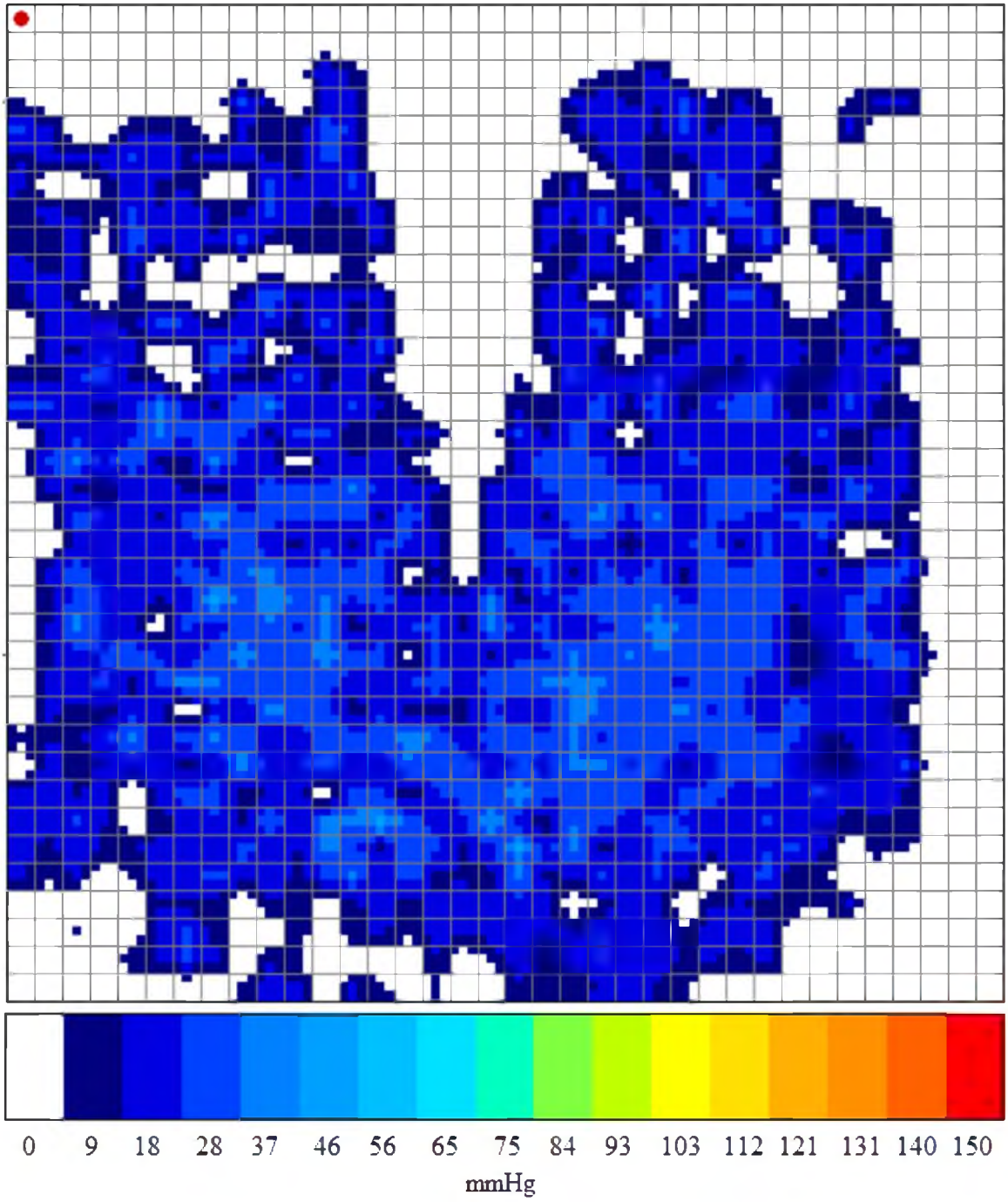

Figure 39 – Test subject #3 on adjusted air cushion after 120 second loading.

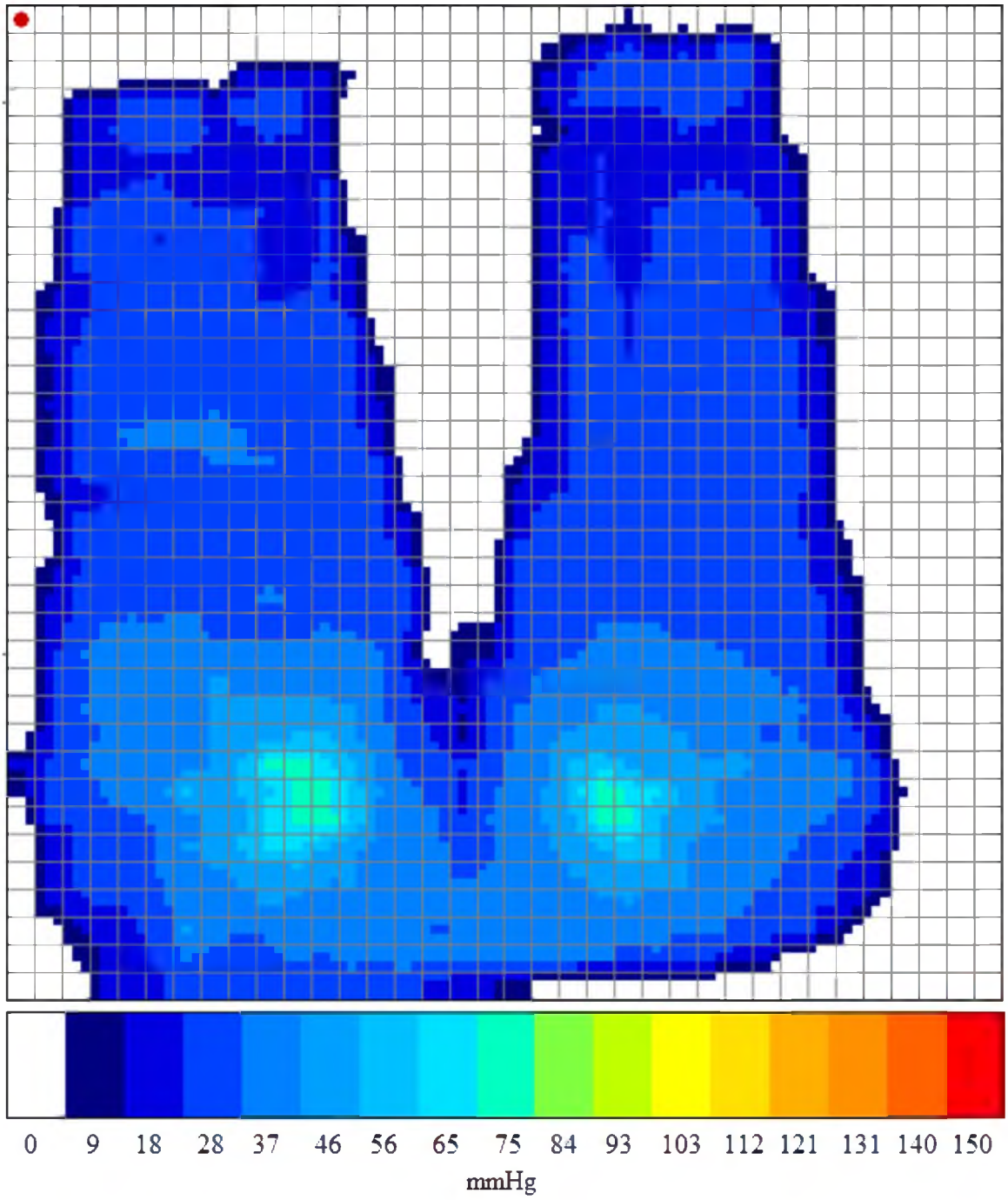

Figure 40 – Test subject #4 on foam cushion after 120 second loading.

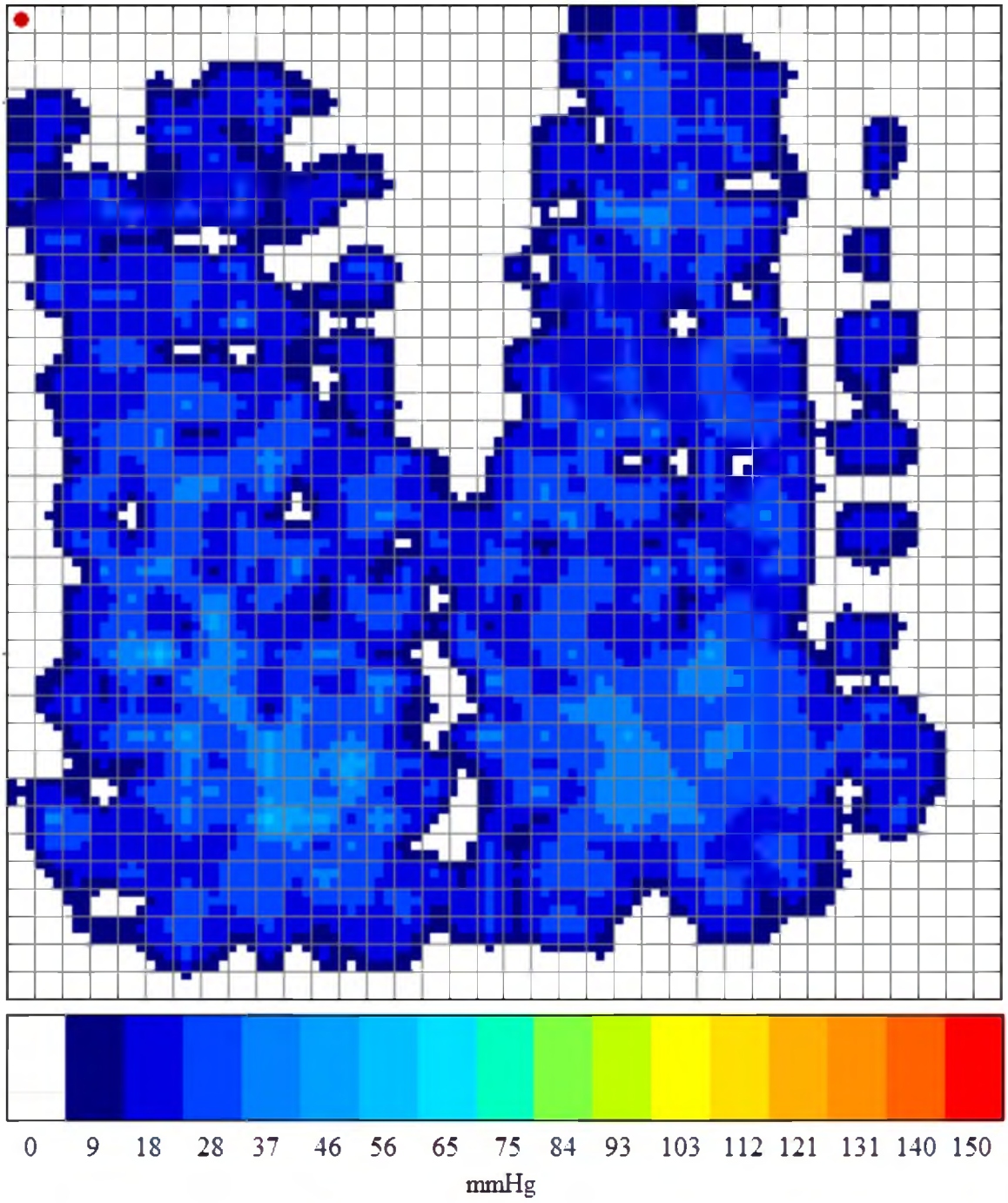

Figure 41 – Test subject #4 on adjusted air cushion after 120 second loading.

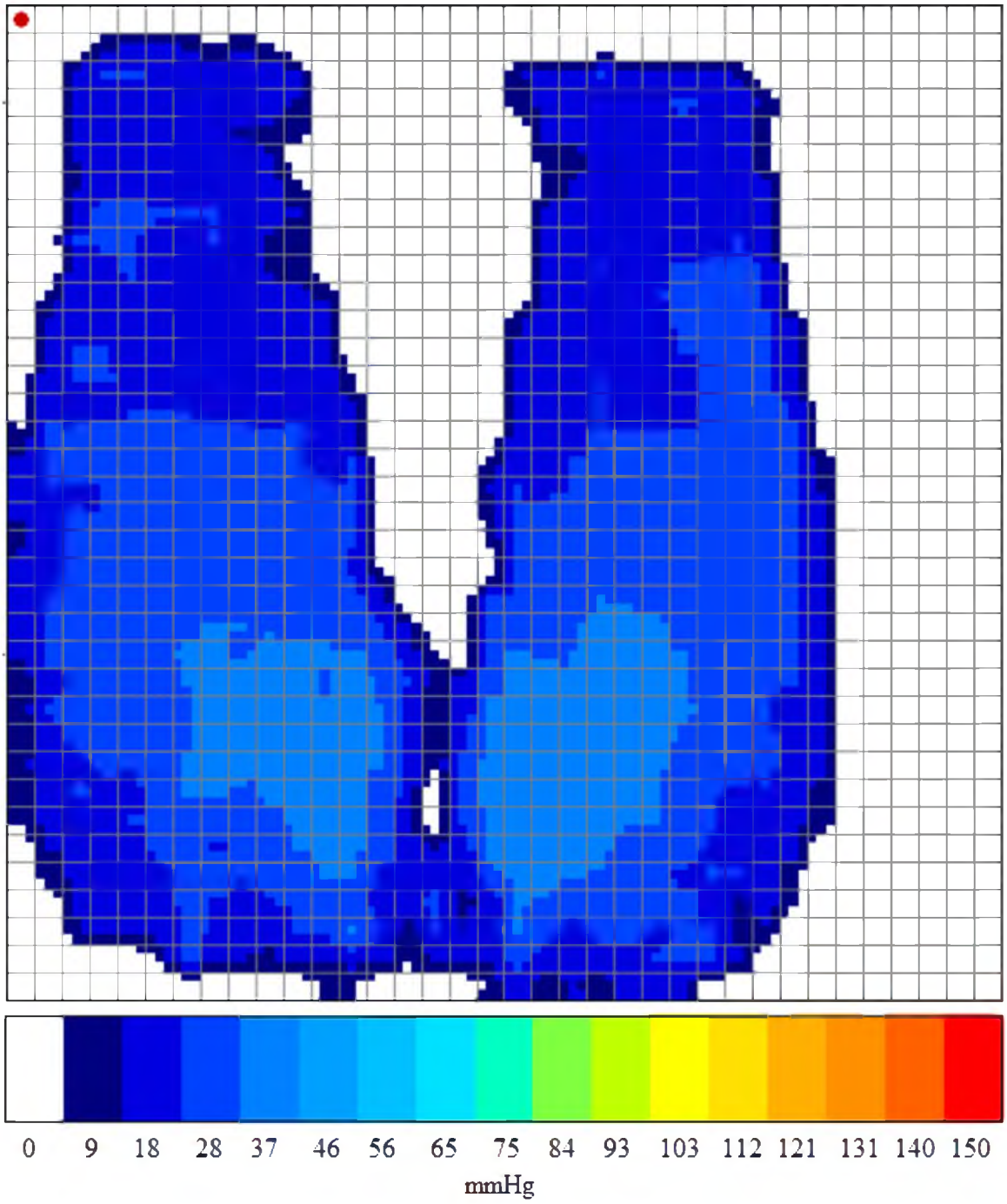

Figure 42 – Test subject #5 on foam cushion after 120 second loading.

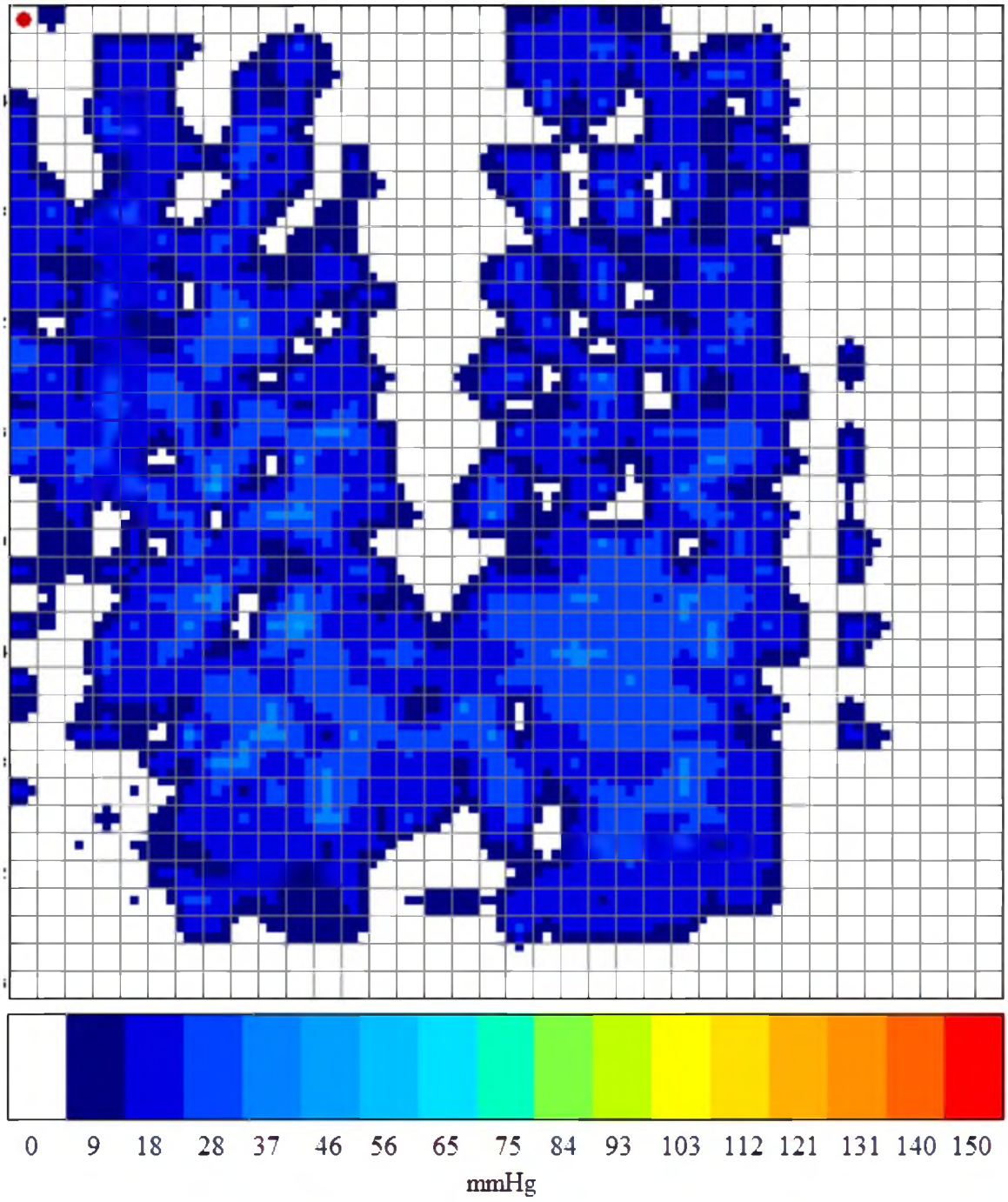

Figure 43 – Test subject #5 on adjusted air cushion after 120 second loading.

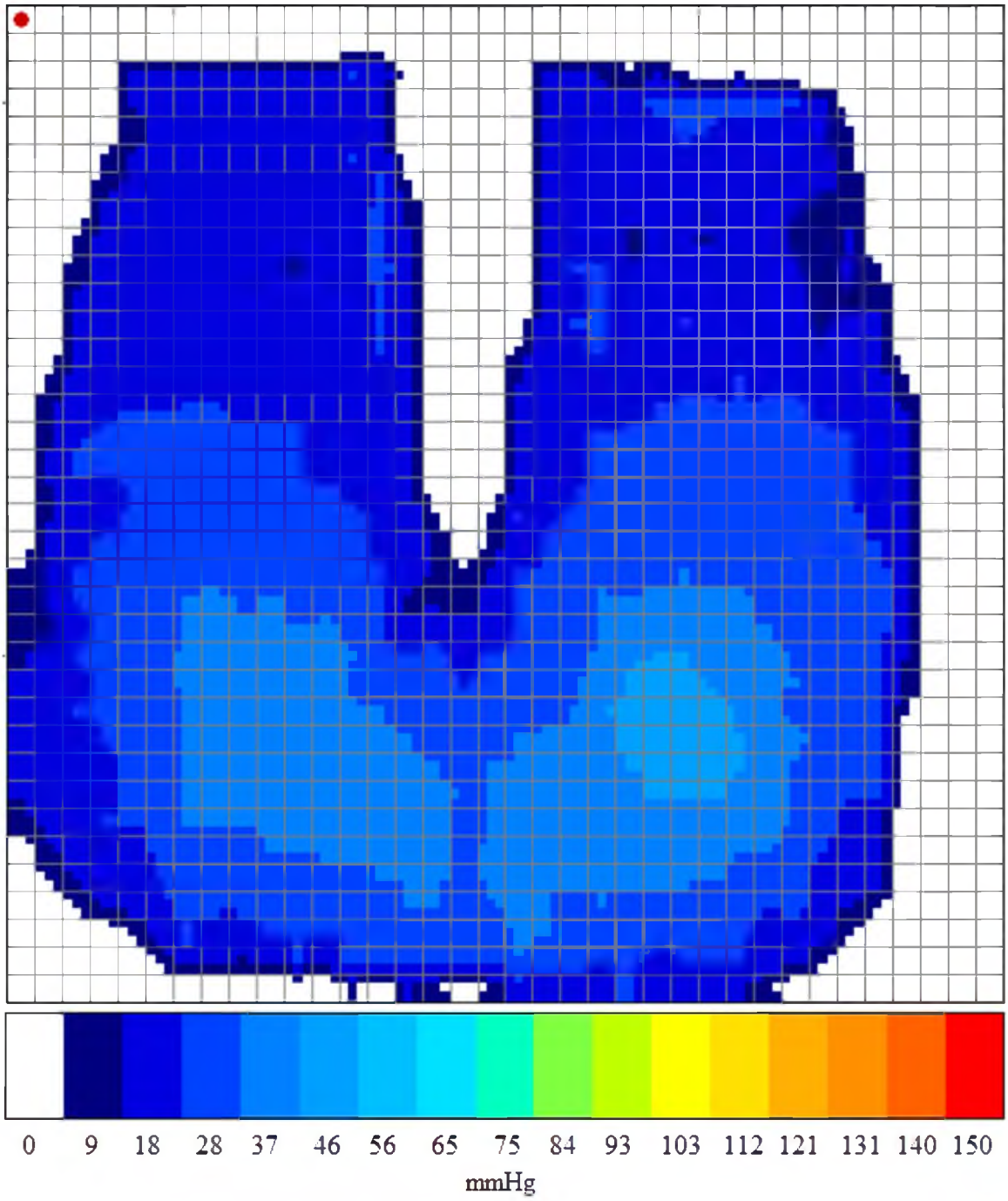

Figure 44 – Test subject #6 on foam cushion after 120 second loading.

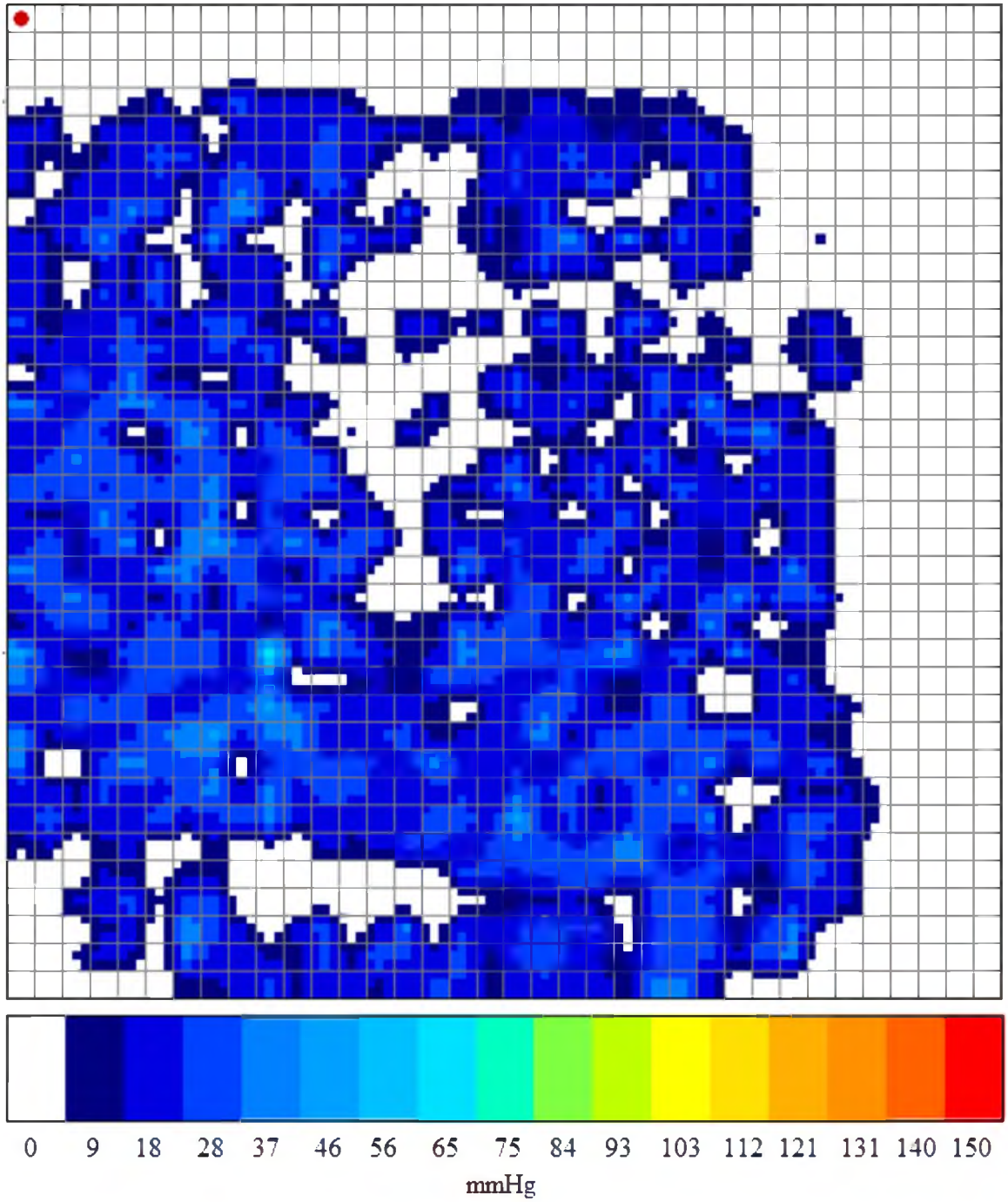

Figure 45 – Test subject #6 on adjusted air cushion after 120 second loading.

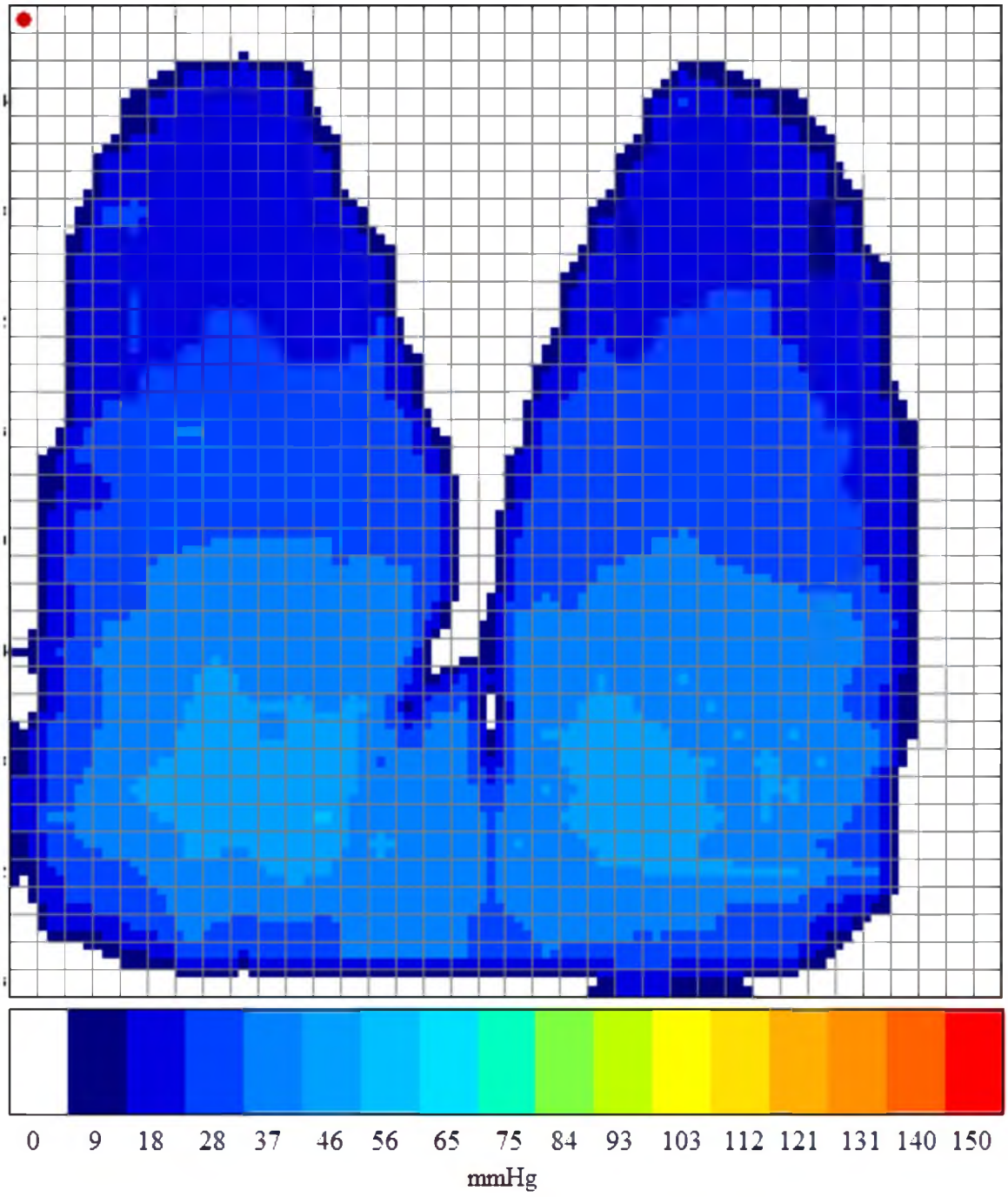

Figure 46 – Test subject #7 on foam cushion after 120 second loading.

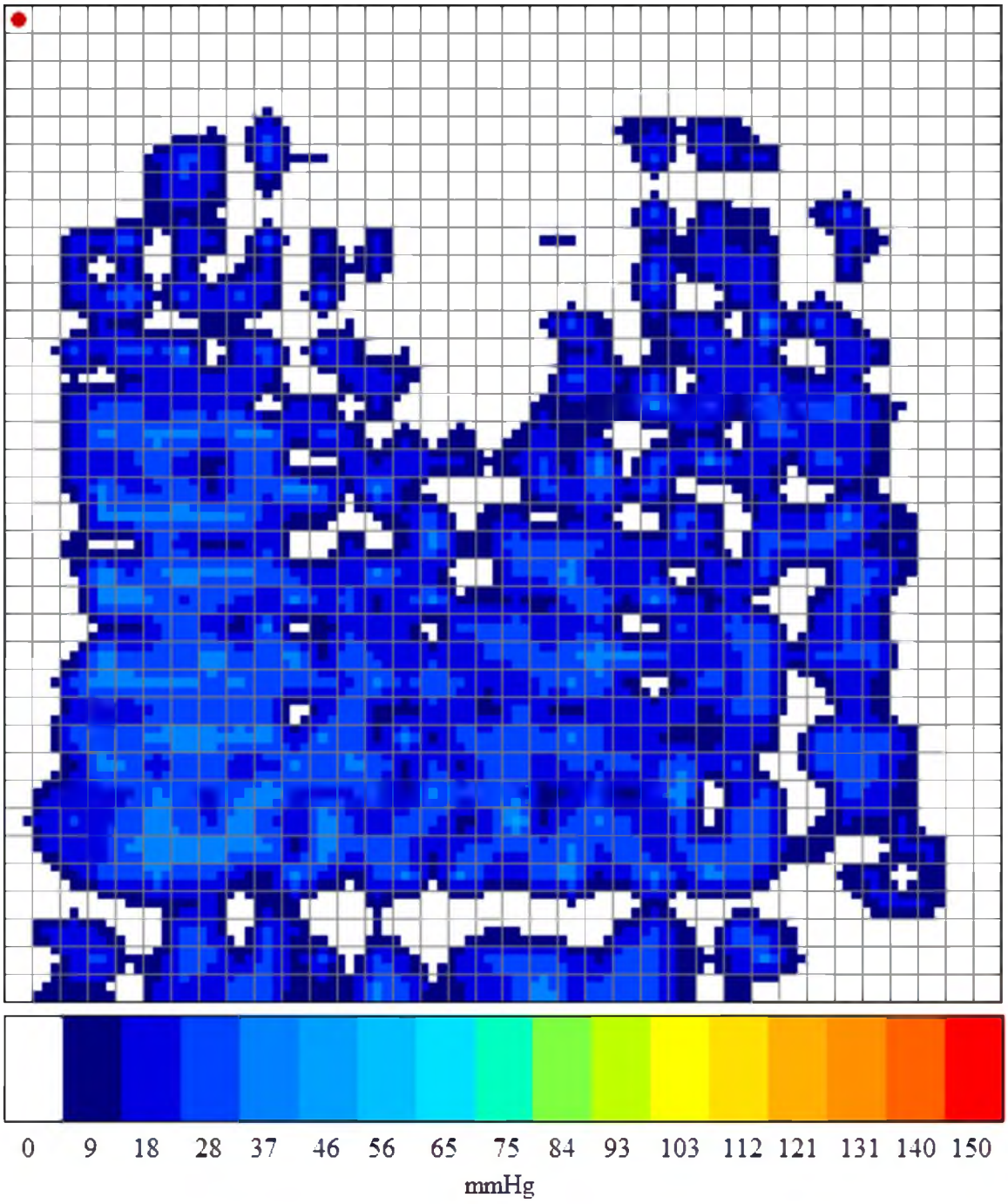

Figure 47 – Test subject #7 on adjusted air cushion after 120 second loading.

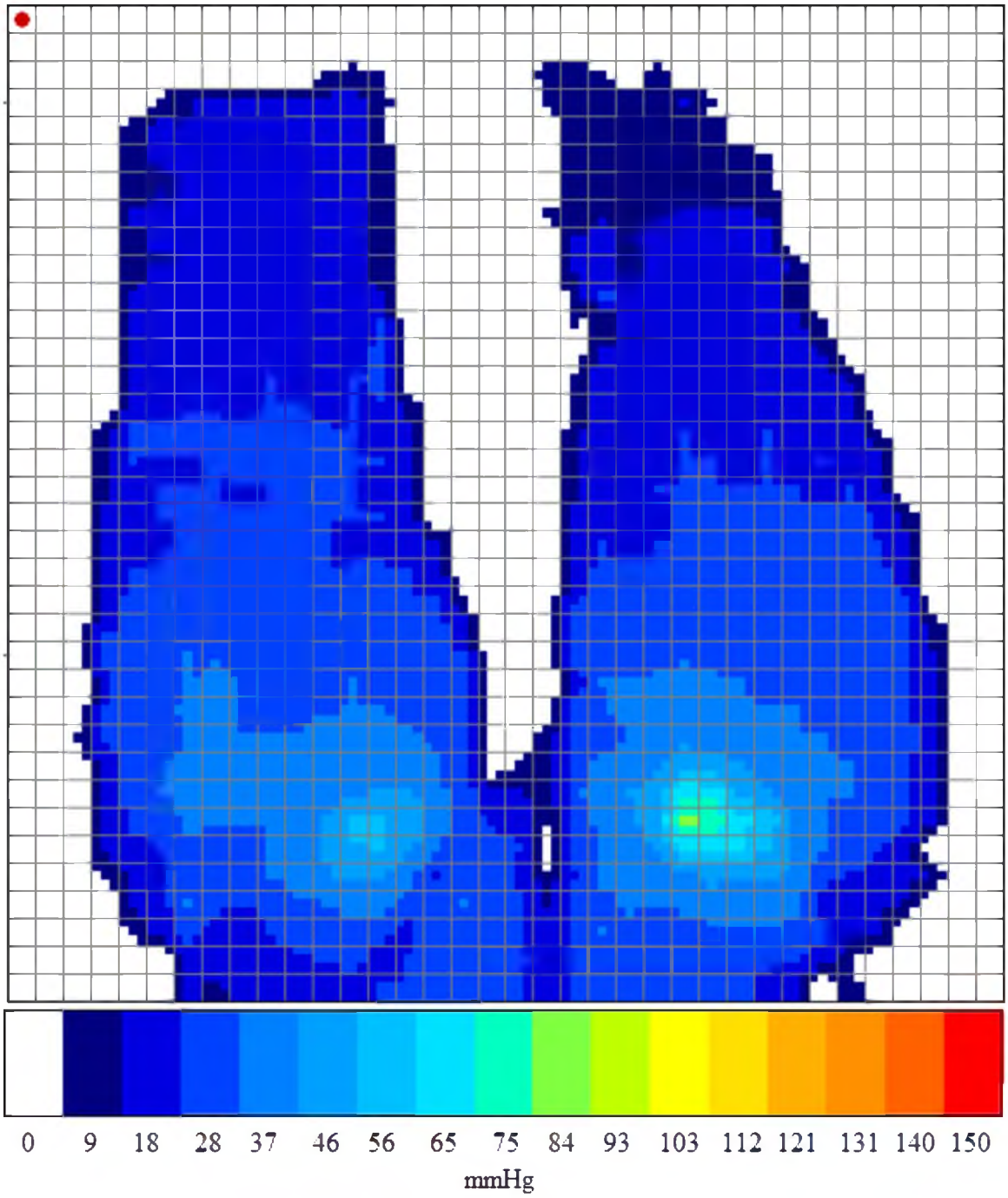

Figure 48 – Test subject #8 on foam cushion after 120 second loading.

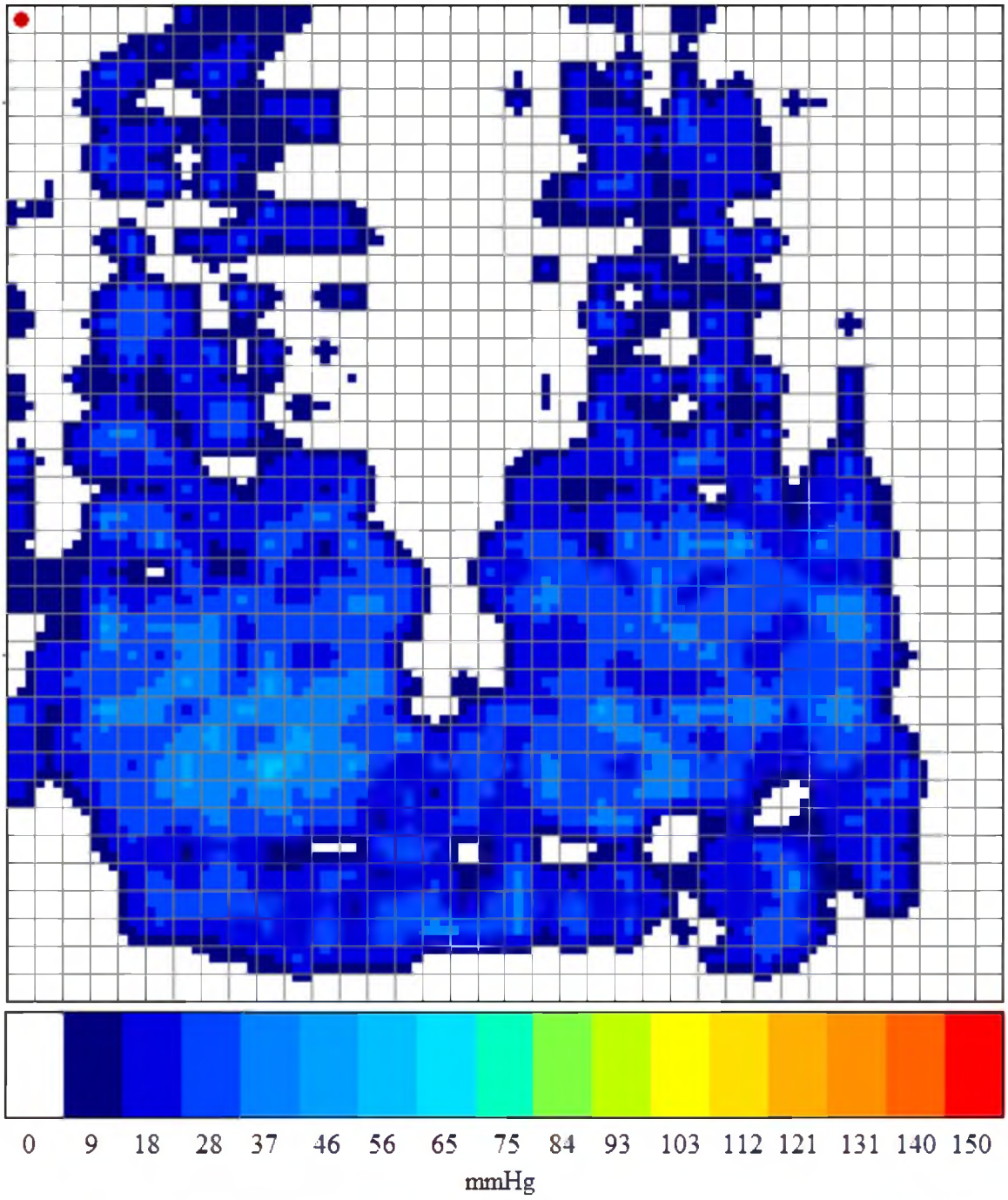

Figure 49 – Test subject #8 on adjusted air cushion after 120 second loading.

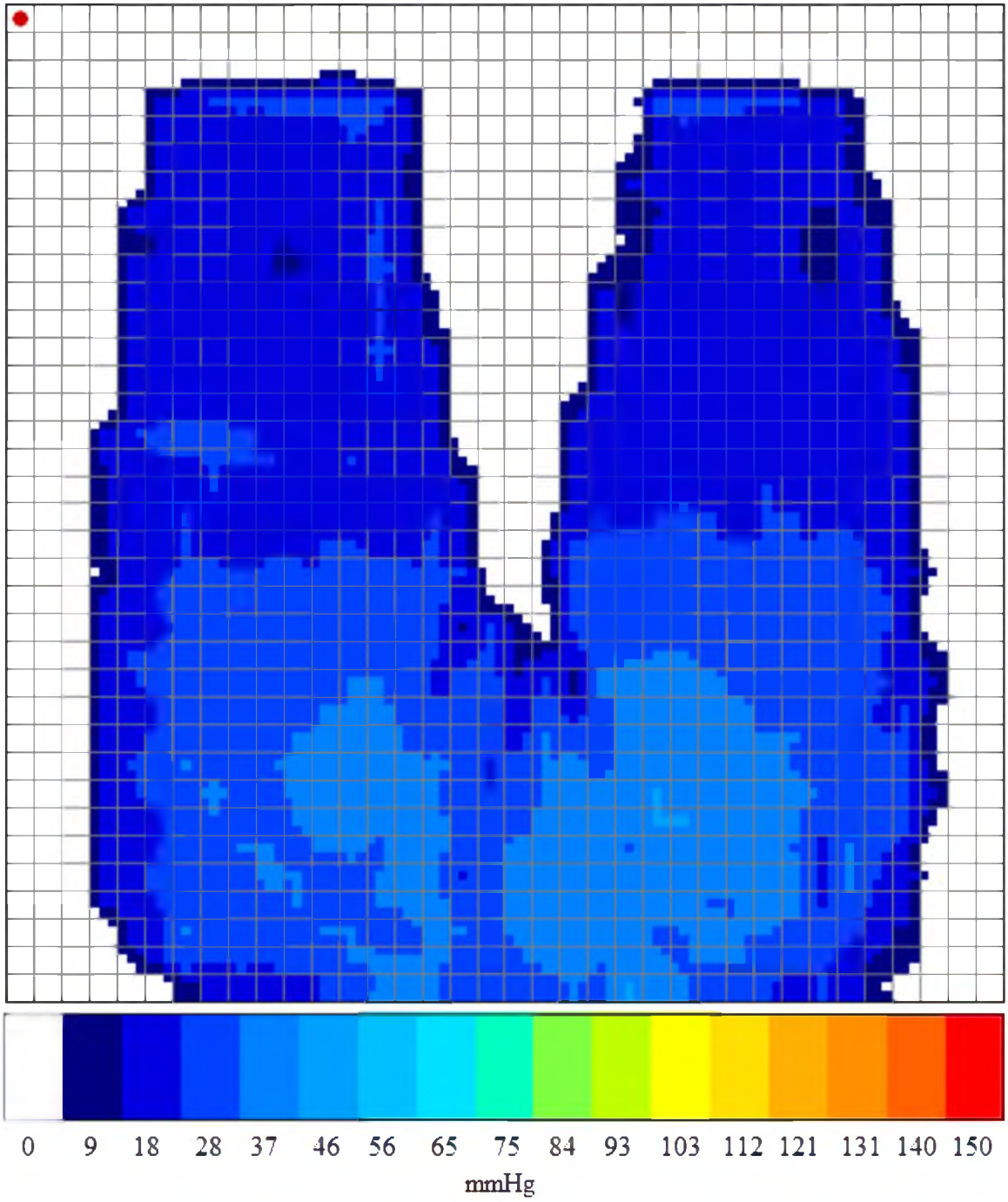

Figure 50 – Test subject #9 on foam cushion after 120 second loading.

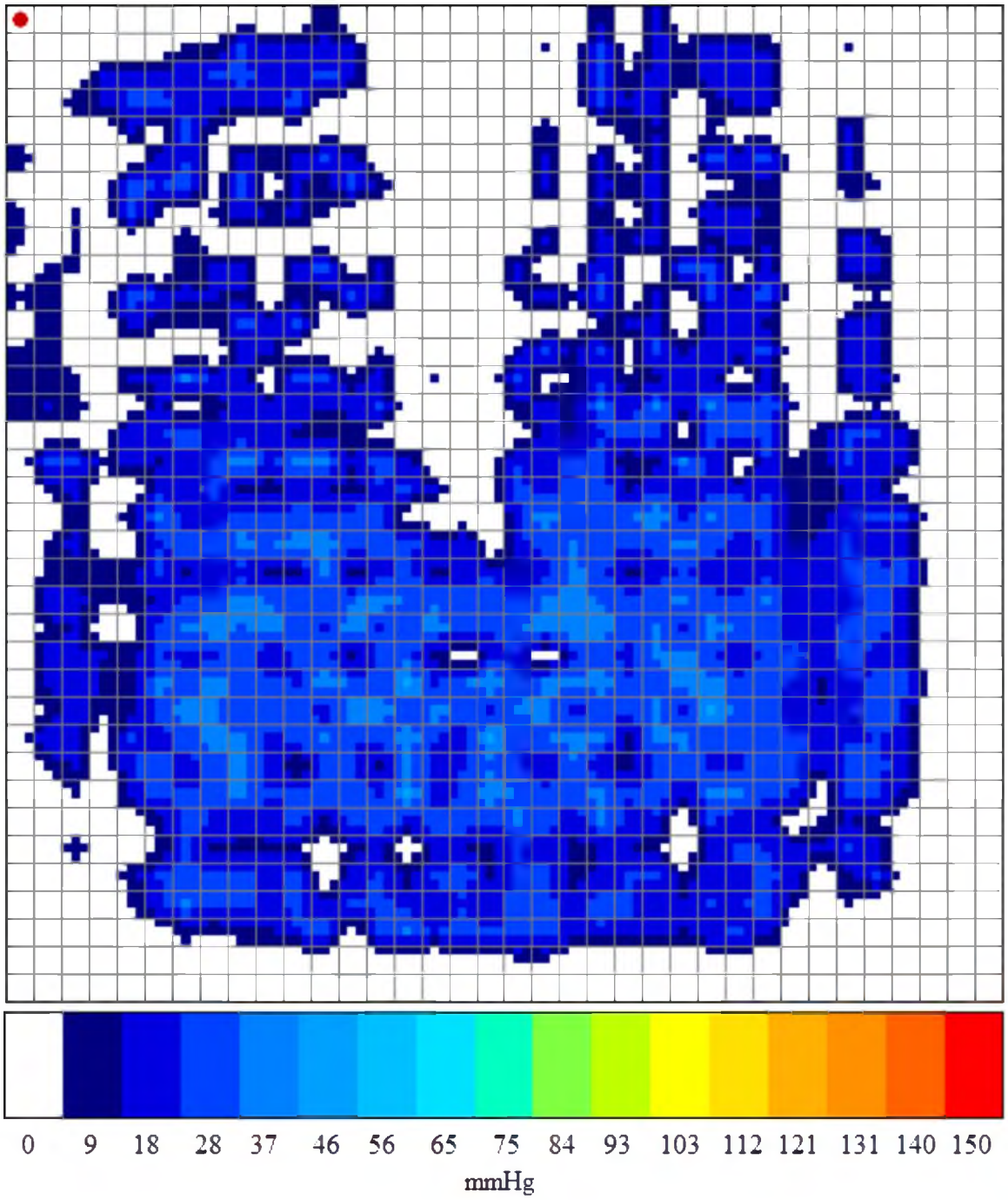

Figure 51 – Test subject #9 on adjusted air cushion after 120 second loading.

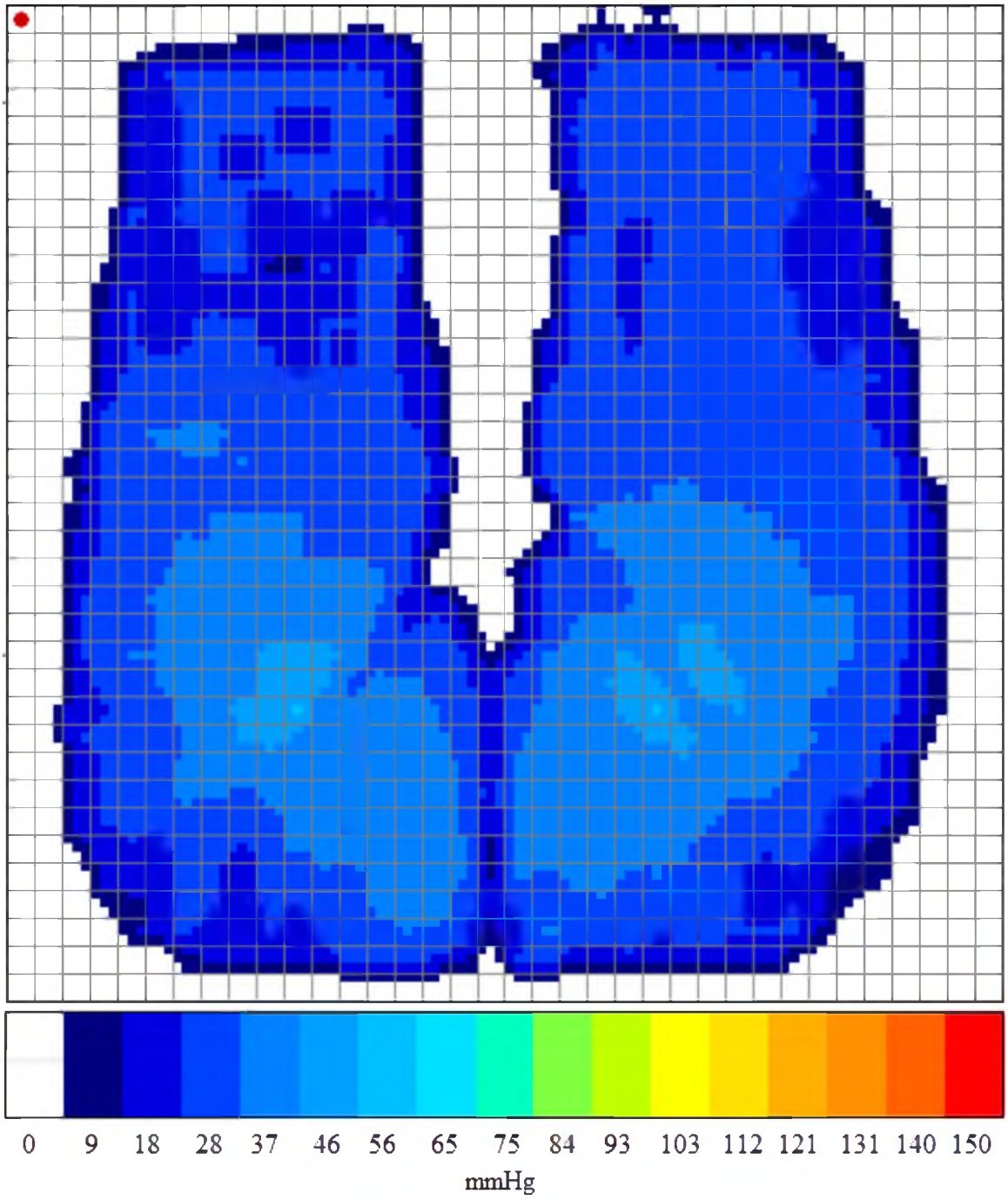

Figure 52 – Test subject #10 on foam cushion after 120 second loading.

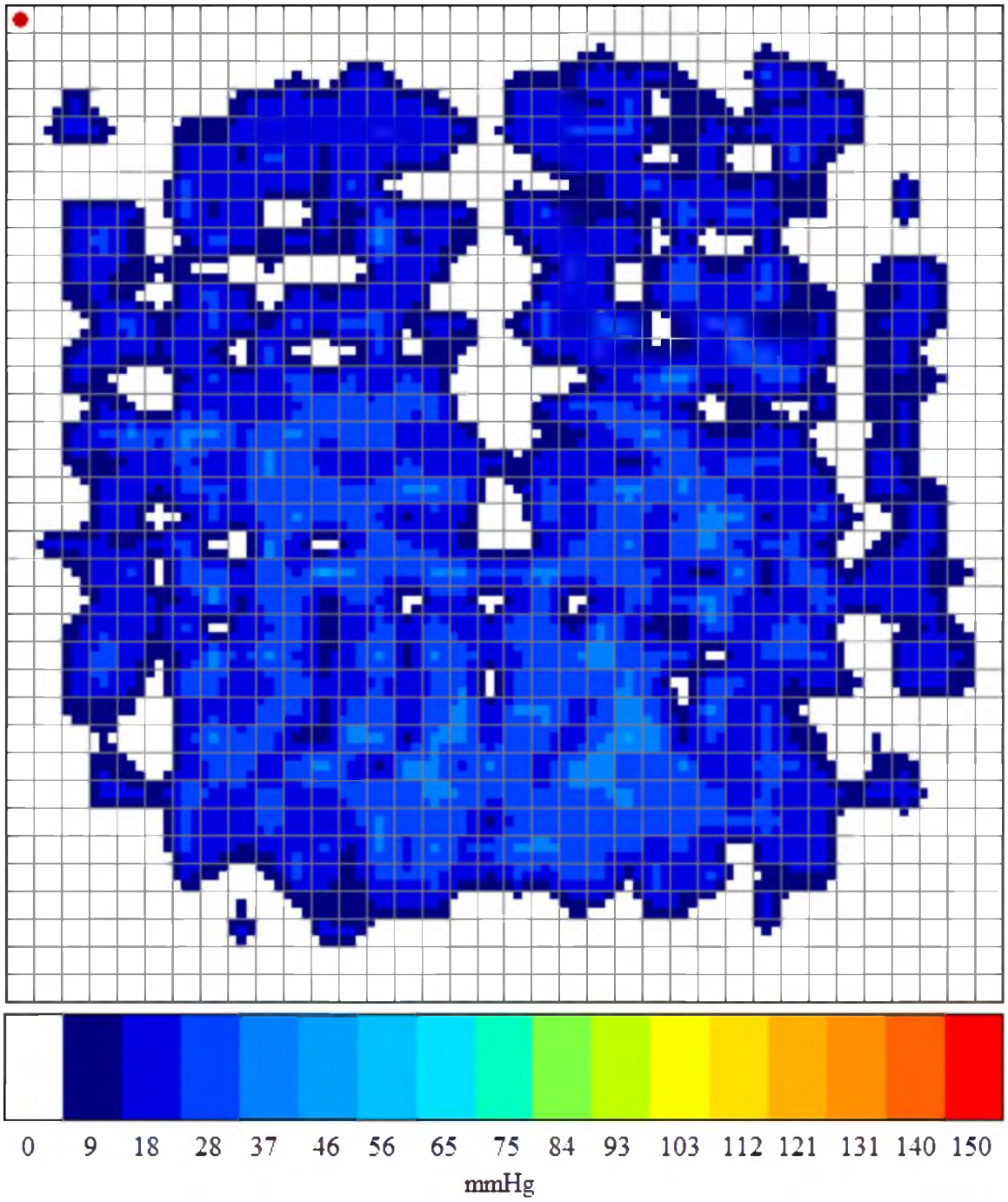

Figure 53 – Test subject #10 on adjusted air cushion after 120 second loading.

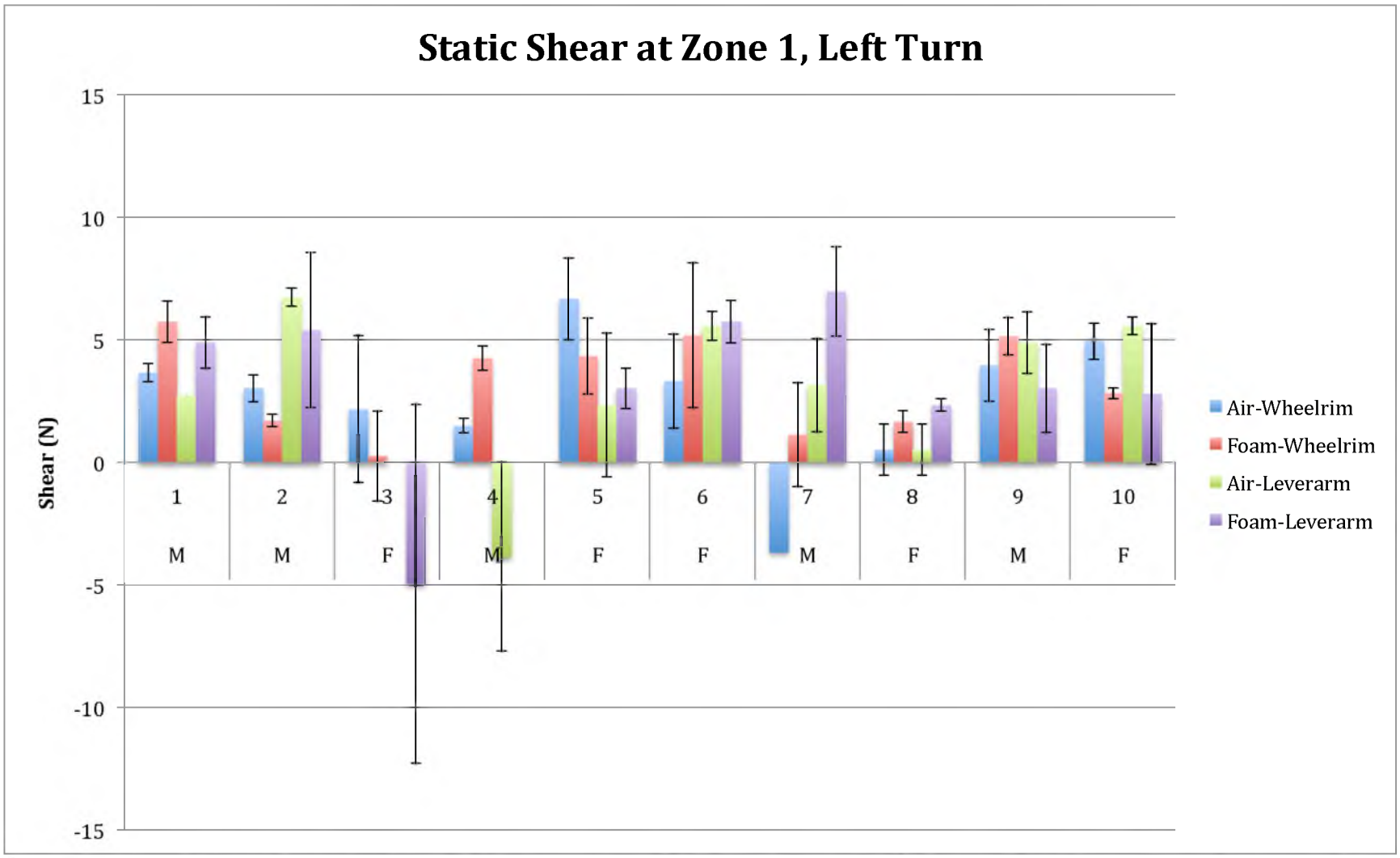

Figure 54 – Static shear at zone 1 of the obstacle course for the left hand turn displaying each testing configuration separated by subject. Error bars indicate confidence interval to 95%.

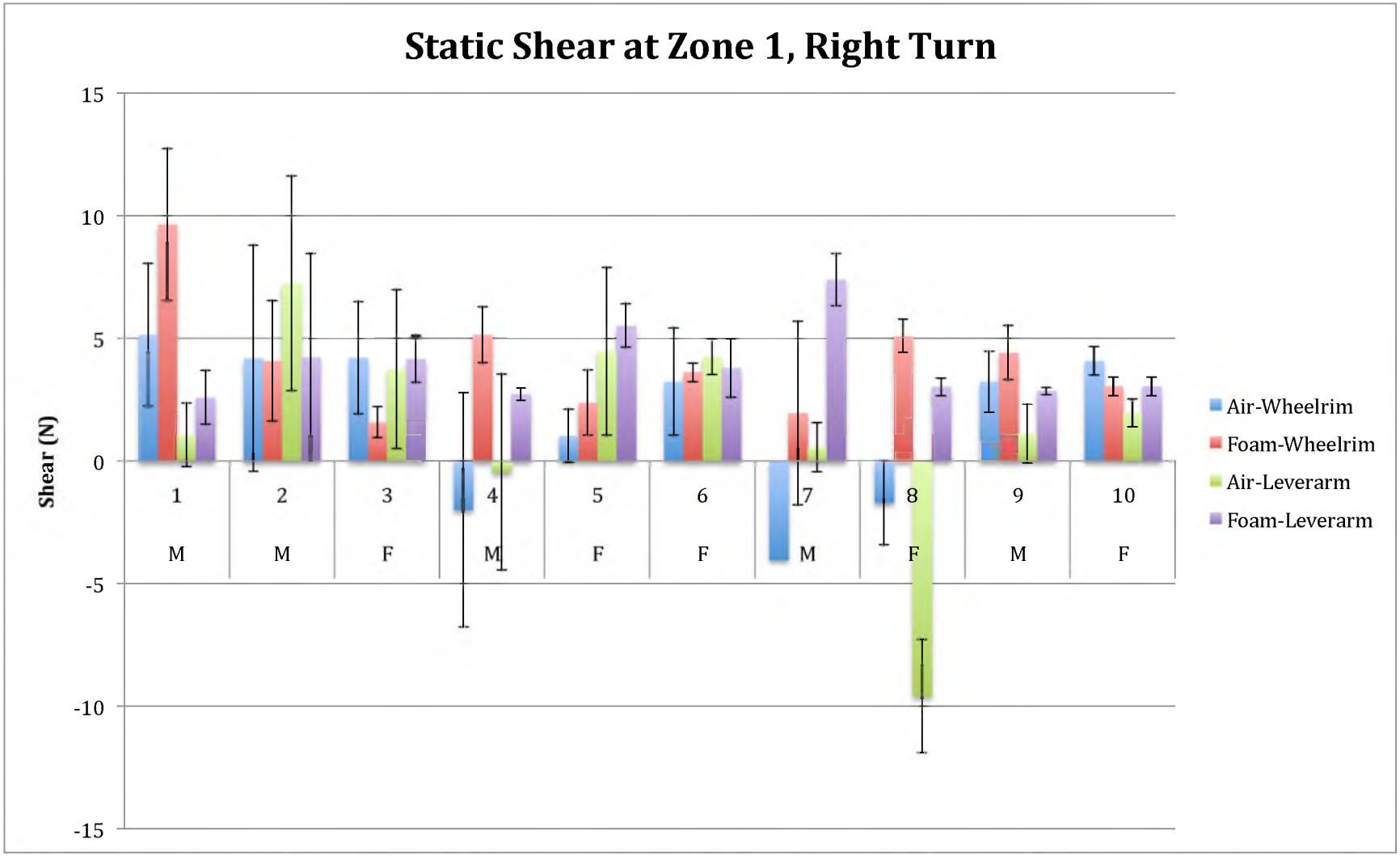

Figure 55 – Static shear at zone 1 of the obstacle course for the right hand turn displaying each testing configuration separated by subject. Error bars indicate confidence interval to 95%.

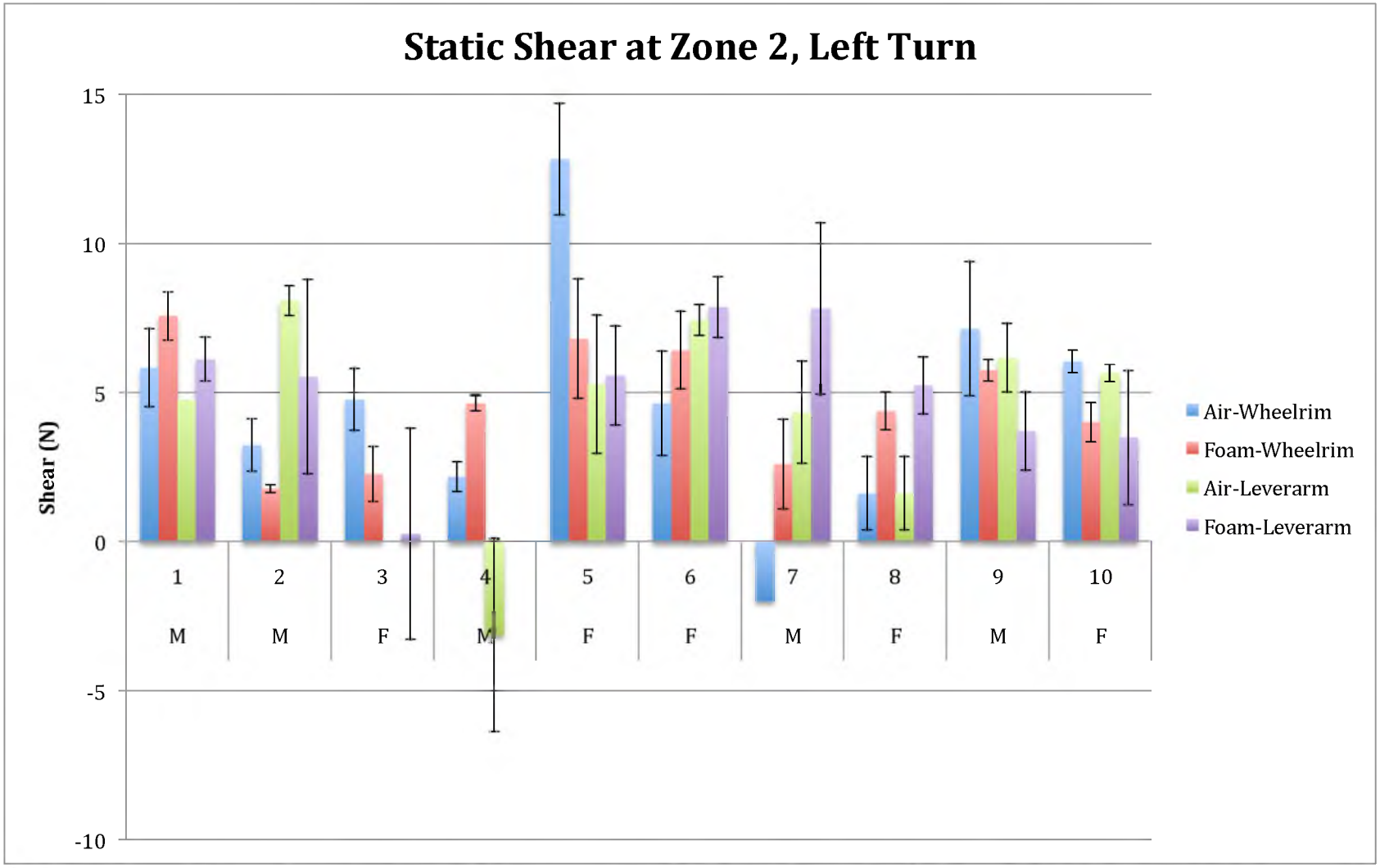

Figure 56 – Static shear at zone 2 of the obstacle course for the left hand turn displaying each testing configuration separated by subject. Error bars indicate confidence interval to 95%.

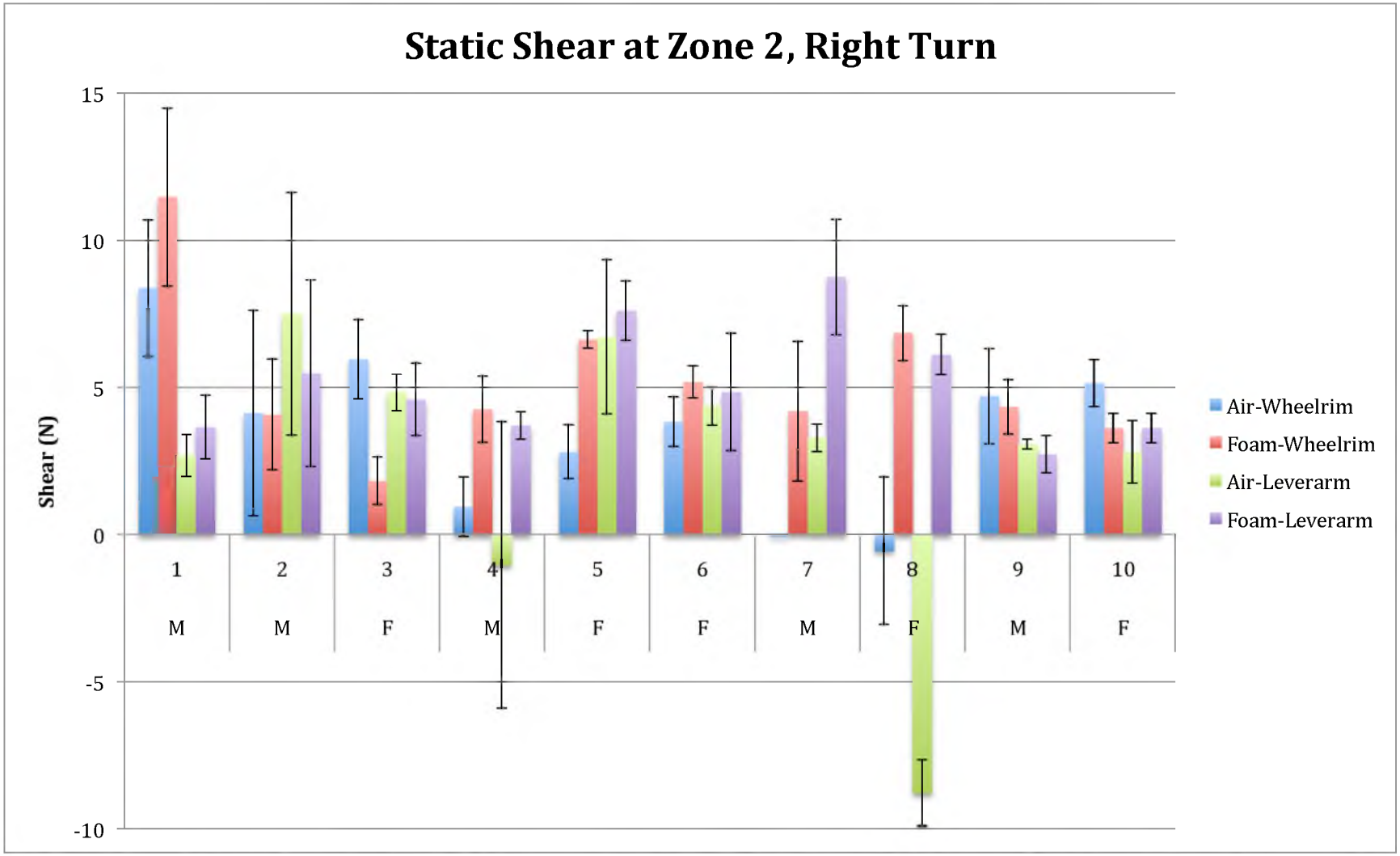

Figure 57 – Static shear at zone 2 of the obstacle course for the right hand turn displaying each testing configuration separated by subject. Error bars indicate confidence interval to 95%.

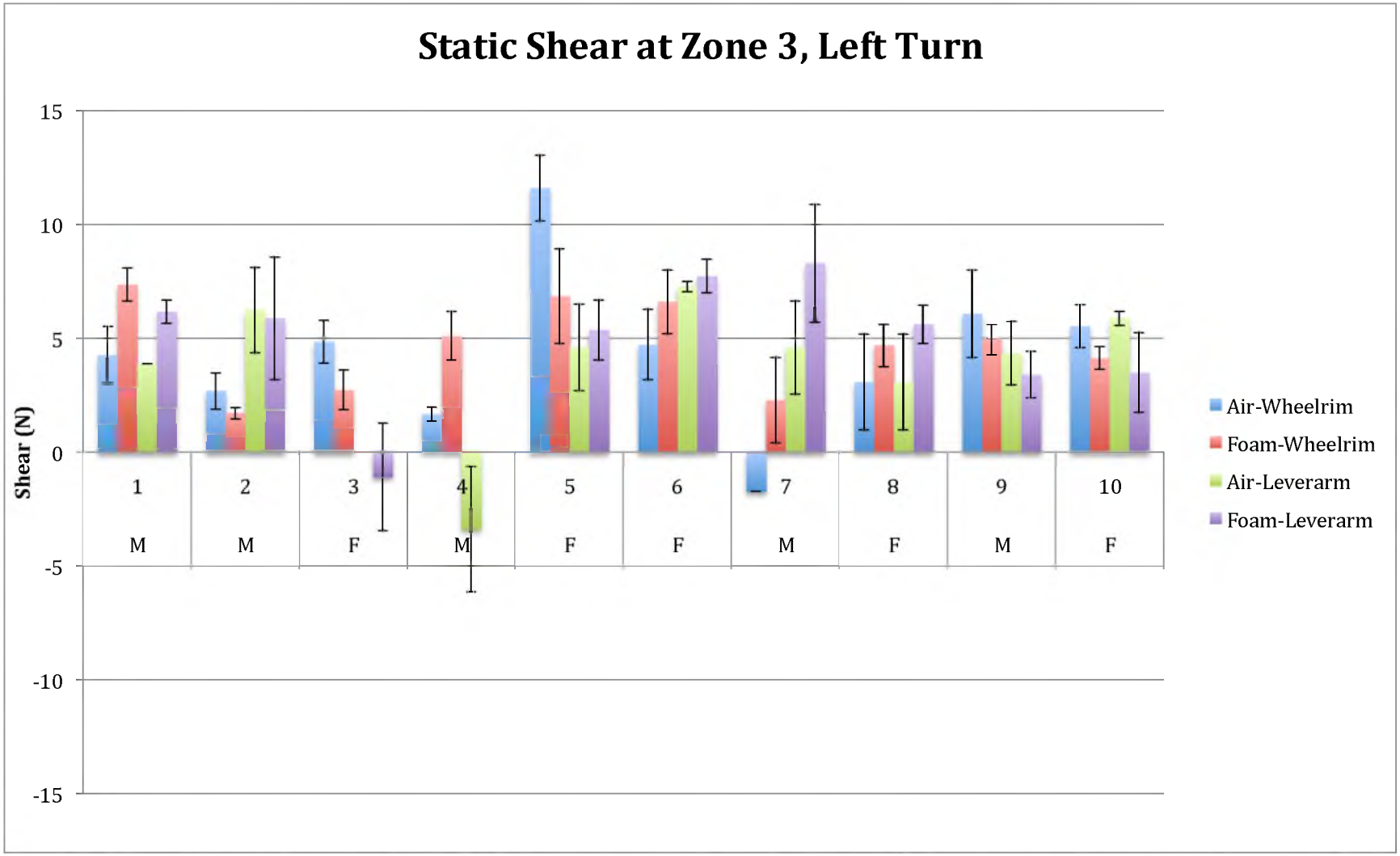

Figure 58 – Static shear at zone 3 of the obstacle course for the left hand turn displaying each testing configuration separated by subject. Error bars indicate confidence interval to 95%.

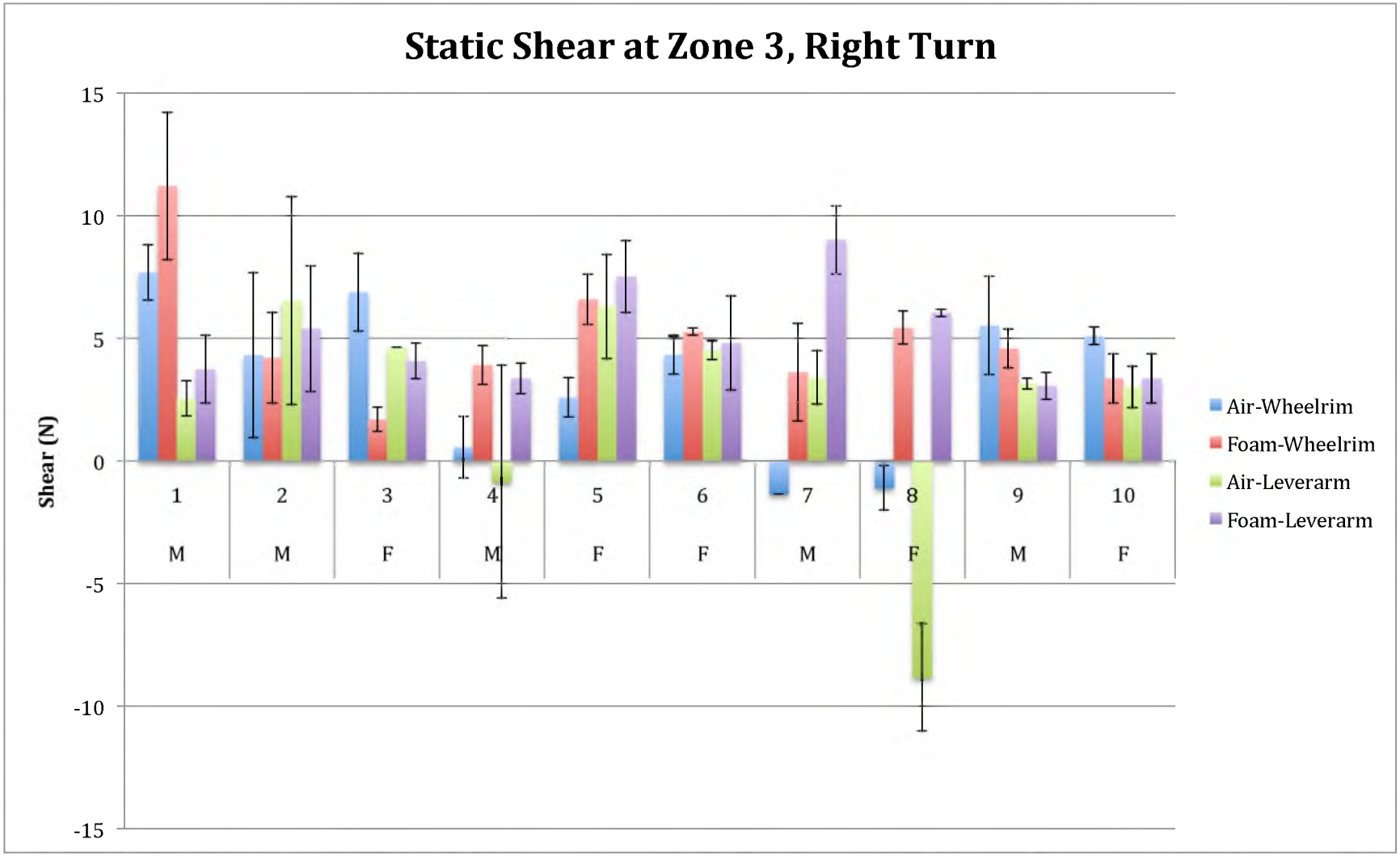

Figure 59 – Static shear at zone 3 of the obstacle course for the right hand turn displaying each testing configuration separated by subject. Error bars indicate confidence interval to 95%.

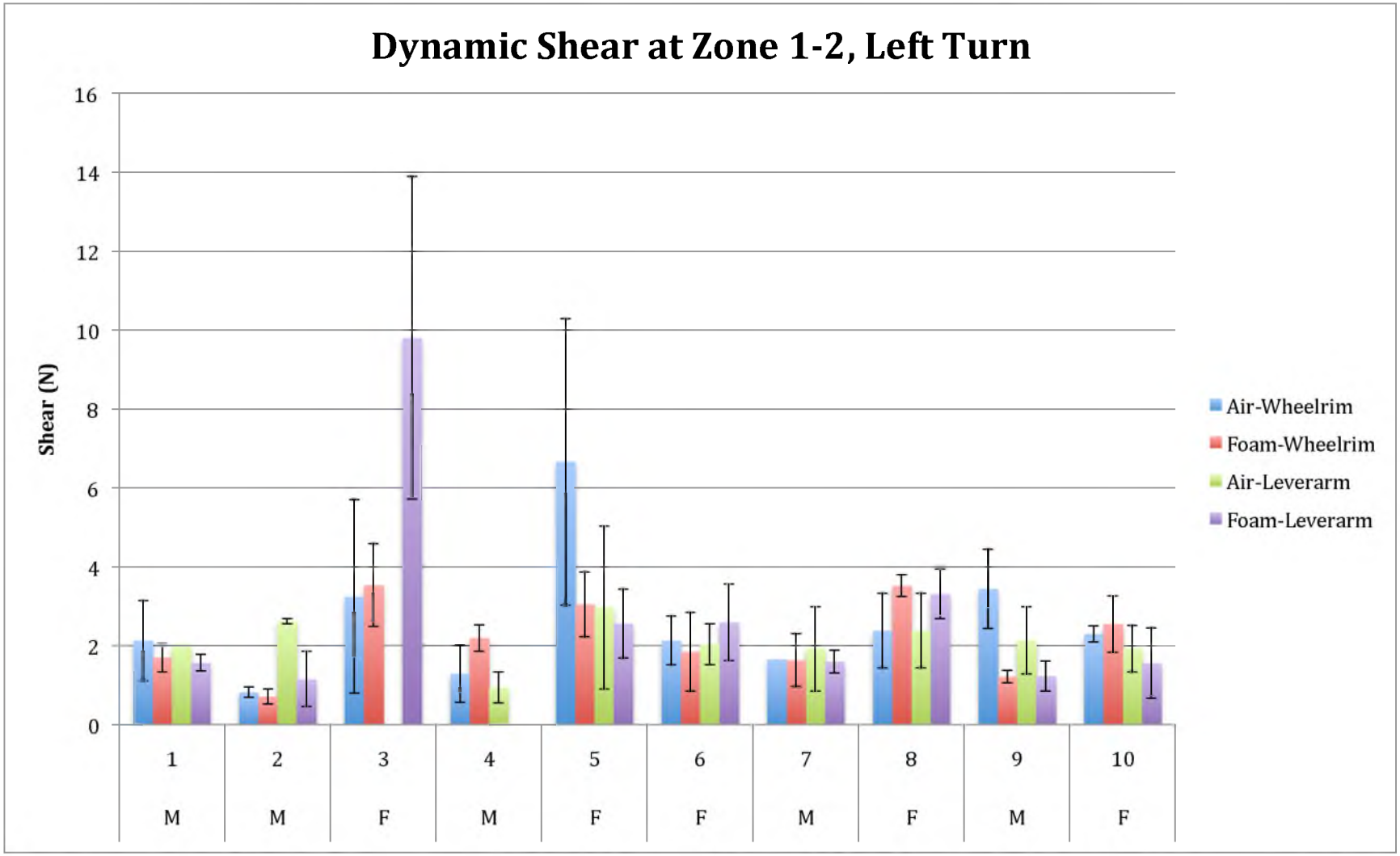

Figure 60 – Dynamic shear during zone 1-2 of the obstacle course for the left hand turn displaying each testing configuration separated by subject. Error bars indicate confidence interval to 95%.

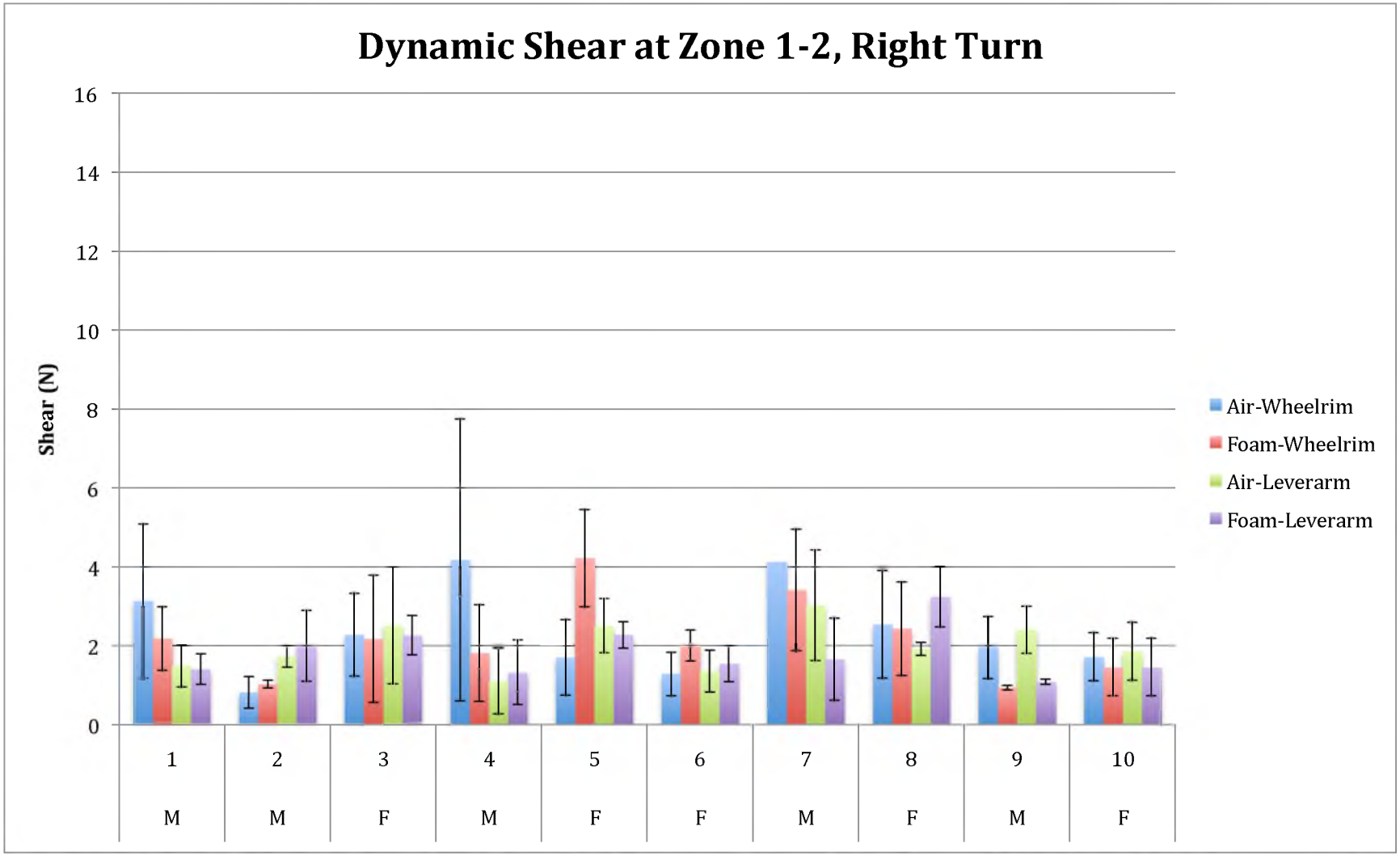

Figure 61 – Dynamic shear during zone 1-2 of the obstacle course for the right hand turn displaying each testing configuration separated by subject. Error bars indicate confidence interval to 95%.

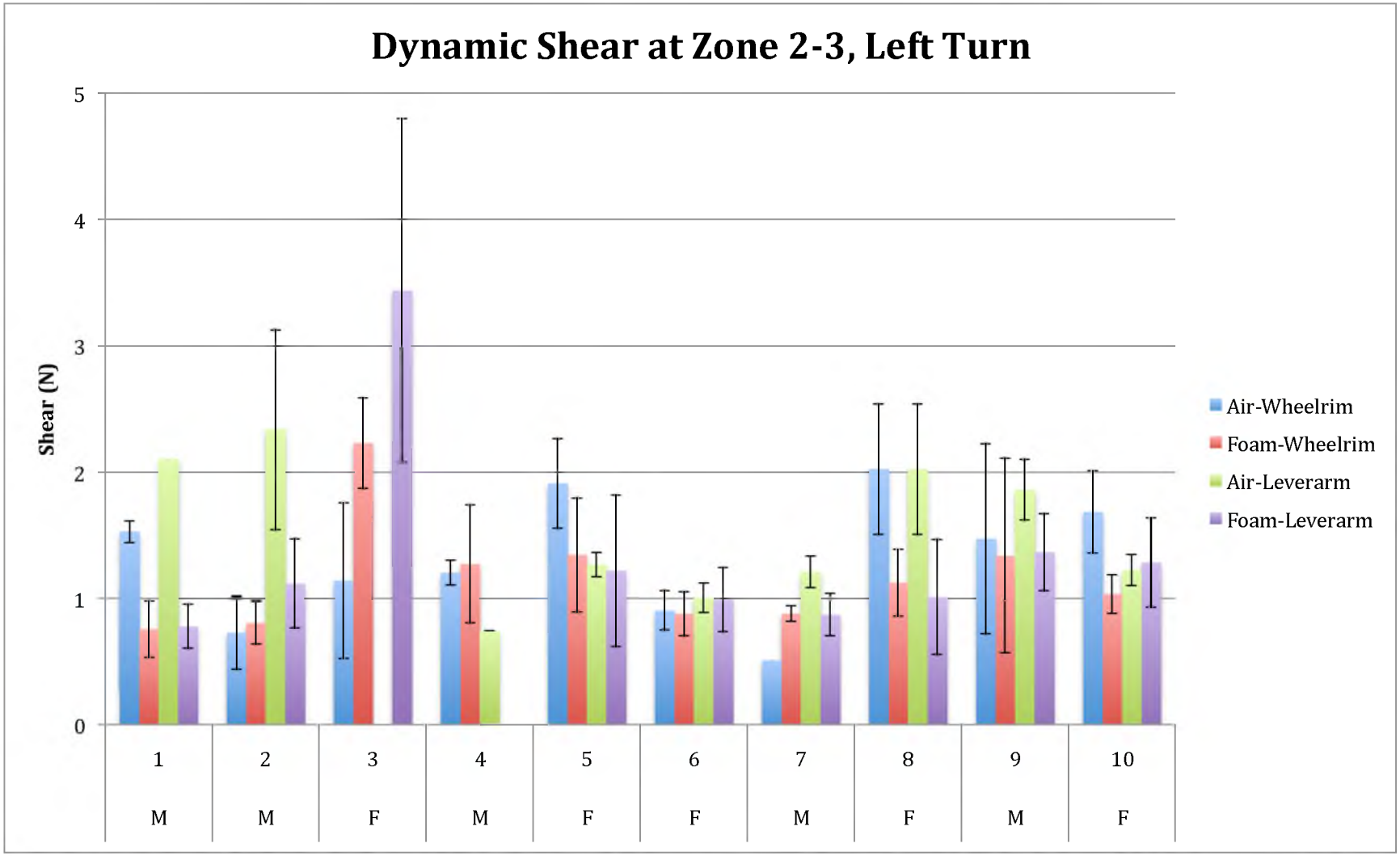

Figure 62 – Dynamic shear during zone 2-3 of the obstacle course for the left hand turn displaying each testing configuration separated by subject. Error bars indicate confidence interval to 95%.

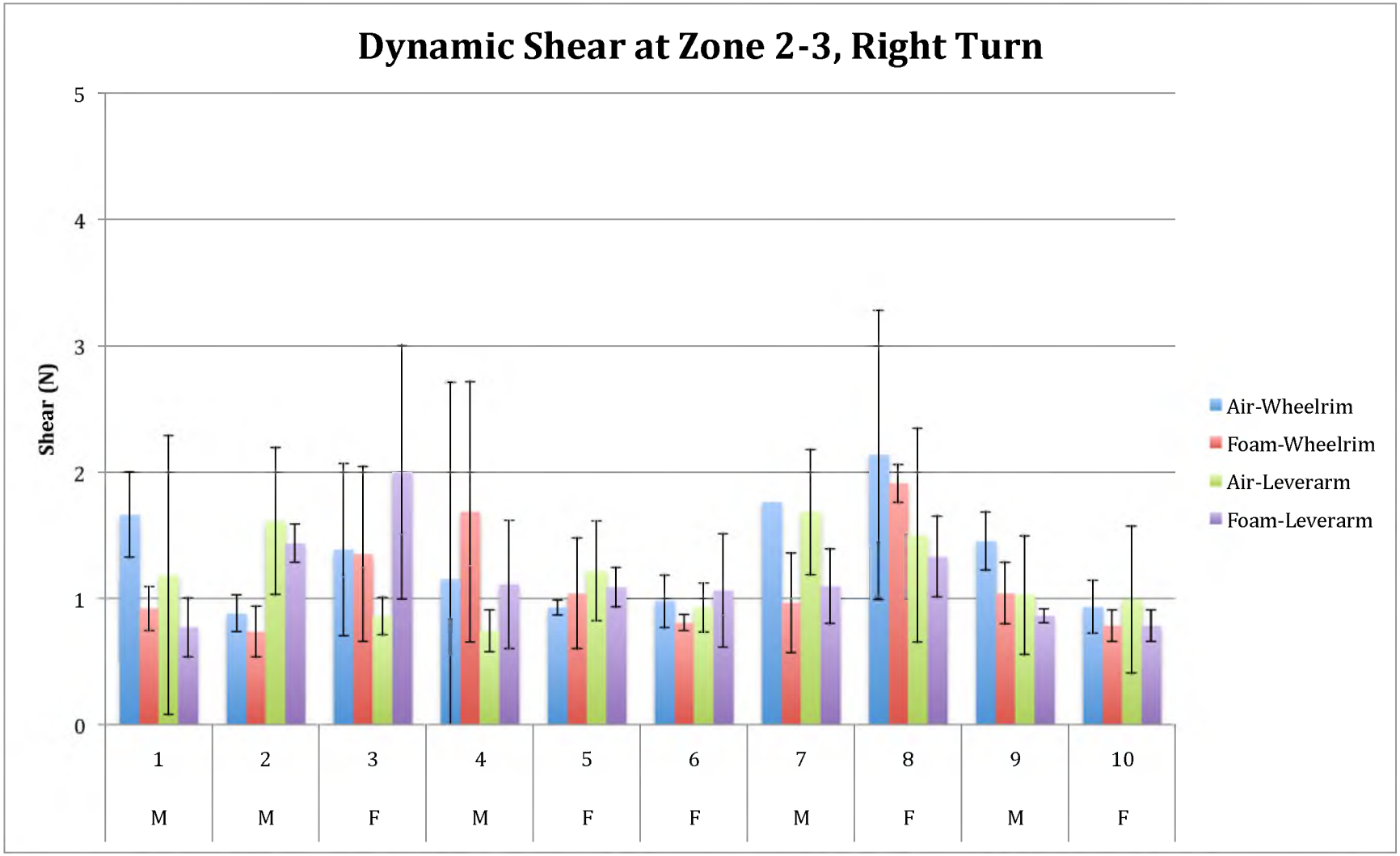

Figure 63 – Dynamic shear during zone 2-3 of the obstacle course for the right hand turn displaying each testing configuration separated by subject. Error bars indicate confidence interval to 95%.

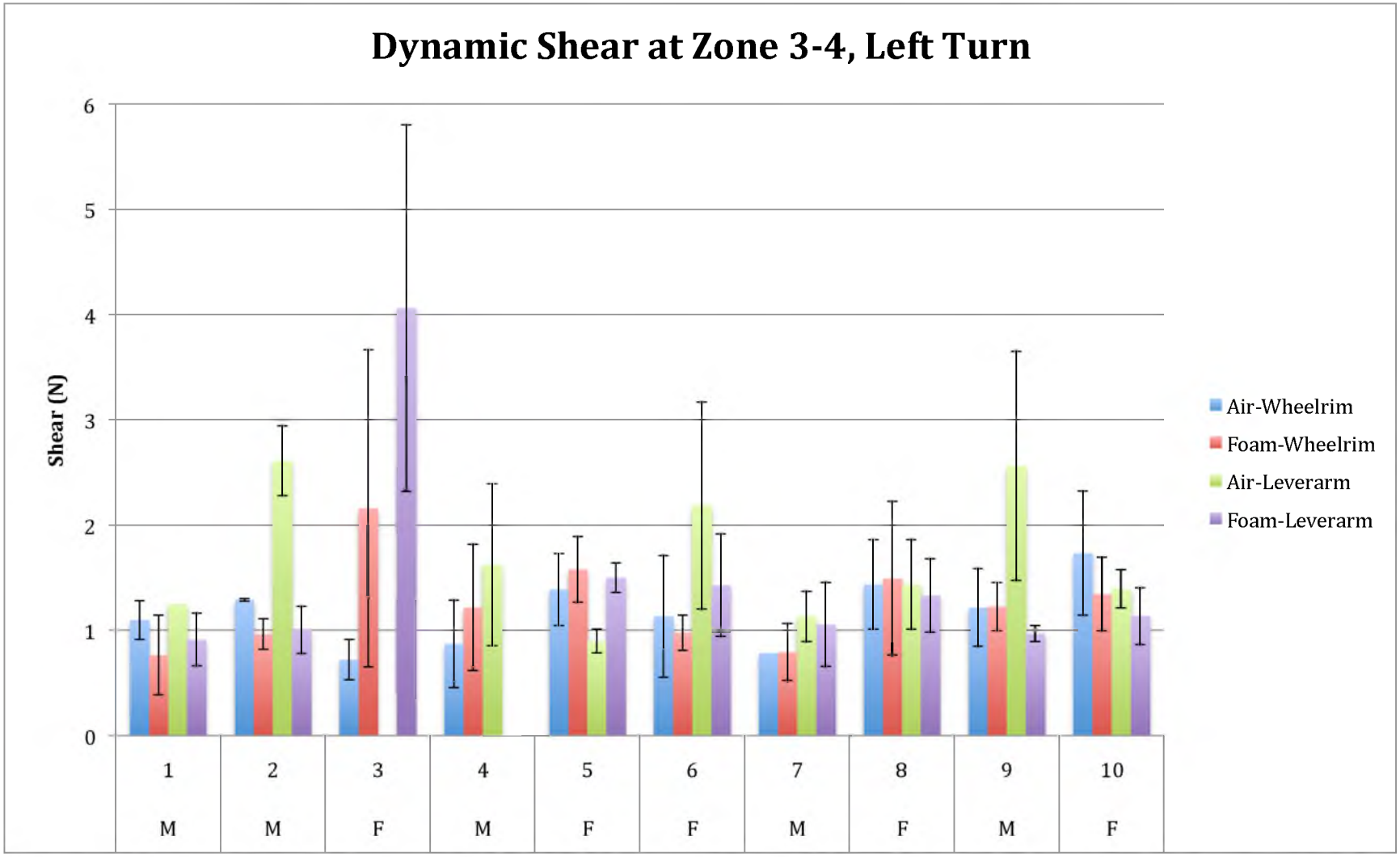

Figure 64 – Dynamic shear during zone 3-4 of the obstacle course for the left hand turn displaying each testing configuration separated by subject. Error bars indicate confidence interval to 95%.

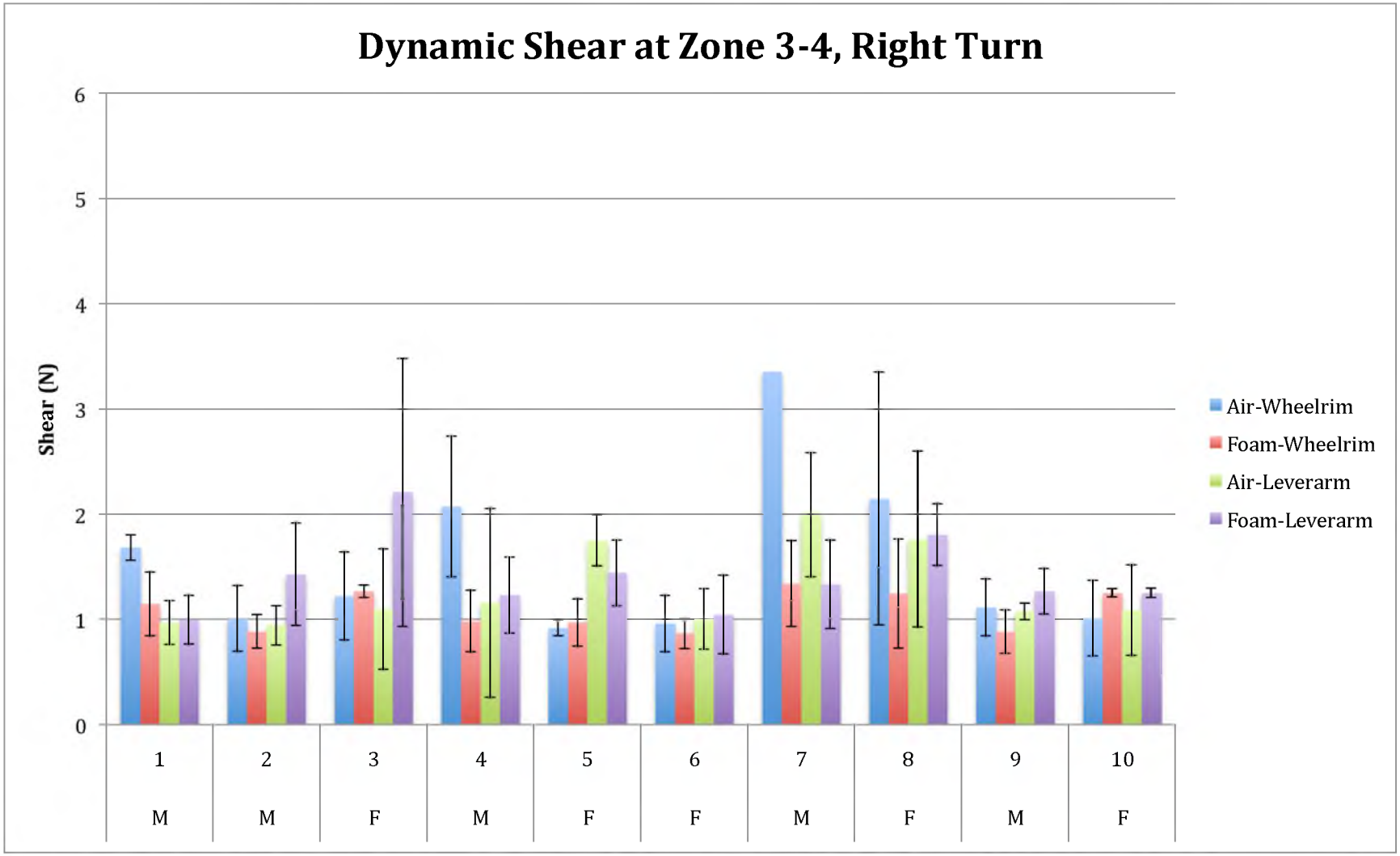

Figure 65 – Dynamic shear during zone 3-4 of the obstacle course for the right hand turn displaying each testing configuration separated by subject. Error bars indicate confidence interval to 95%.

Table 5 – Average static shear data for left turn obstacle course. Error bars indicate confidence interval to 95%.

	Average Static Shear 1 (N)			
	Air-Wheelrim	Foam-Wheelrim	Air-Leverarm	Foam-Leverarm
1	3.66 ±0.36	5.75 ±0.84	2.73	4.90 ±1.04
2	3.03 ±0.55	1.71 ±0.25	6.74 ±0.37	5.41 ±3.17
3	2.18 ±3.00	0.27 ±1.84	--	-4.96 ±7.33
4	1.50 ±0.30	4.26 ±0.50	-3.83 ±3.87	--
5	6.68 ±1.66	4.34 ±1.55	2.35 ±2.93	3.03 ±0.82
6	3.32 ±1.92	5.19 ±2.96	5.58 ±0.58	5.75 ±0.87
7	-3.64	1.14 ±2.12	3.15 ±1.90	6.98 ±1.83
8	0.52 ±1.04	1.67 ±0.44	0.52 ±1.04	2.35 ±0.25
9	3.96 ±1.46	5.15 ±0.76	4.90 ±1.26	3.03 ±1.79
10	4.94 ±0.74	2.81 ±0.22	5.58 ±0.36	2.79 ±2.87
	Average Static Shear 2 (N)			
	Air-Wheelrim	Foam-Wheelrim	Air-Leverarm	Foam-Leverarm
1	5.83 ±1.31	7.57 ±0.80	4.77	6.13 ±0.74
2	3.24 ±0.88	1.77 ±0.12	8.08 ±0.50	5.53 ±3.26
3	4.77 ±1.04	2.26 ±0.93	--	0.27 ±3.54
4	2.18 ±0.51	4.64 ±0.25	-3.13 ±3.25	--
5	12.84 ±1.88	6.81 ±2.00	5.28 ±2.32	5.58 ±1.66
6	4.64 ±1.75	6.42 ±1.30	7.44 ±0.52	7.87 ±1.02
7	-1.98	2.60 ±1.50	4.34 ±1.72	7.83 ±2.88
8	1.63 ±1.23	4.39 ±0.63	1.63 ±1.23	5.24 ±0.96
9	7.15 ±2.25	5.75 ±0.36	6.17 ±1.15	3.71 ±1.31
10	6.04 ±0.38	4.00 ±0.66	5.66 ±0.29	3.49 ±2.25
	Average Static Shear 3 (N)			
	Air-Wheelrim	Foam-Wheelrim	Air-Leverarm	Foam-Leverarm
1	4.26 ±1.26	7.36 ±0.73	3.88	6.17 ±0.52
2	2.69 ±0.79	1.71 ±0.25	6.23 ±1.87	5.87 ±2.68
3	4.85 ±0.94	2.73 ±0.88	--	-1.09 ±2.36
4	1.67 ±0.30	5.11 ±1.06	-3.39 ±2.75	--
5	11.61 ±1.44	6.85 ±2.09	4.60 ±1.90	5.36 ±1.31
6	4.73 ±1.54	6.59 ±1.40	7.27 ±0.22	7.74 ±0.74
7	-1.73	2.28 ±1.87	4.60 ±2.05	8.29 ±2.58
8	3.07 ±2.10	4.68 ±0.93	3.07 ±2.10	5.62 ±0.84
9	6.09 ±1.92	4.94 ±0.67	4.34 ±1.40	3.41 ±1.01
10	5.53 ±0.95	4.13 ±0.50	5.87 ±0.30	3.49 ±1.75

Table 6 – Static shear data for right turn obstacle course. Error bars indicate confidence interval to 95%.

	Average Static Shear 1 (N)			
	Air-Wheelrim	Foam-Wheelrim	Air-Leverarm	Foam-Leverarm
1	5.15 ±2.92	9.65 ±3.10	1.07 ±1.30	2.60 ±1.09
2	4.20 ±4.62	4.09 ±2.46	7.25 ±4.37	4.24 ±4.23
3	4.22 ±2.28	1.58 ±0.63	3.75 ±3.25	4.17 ±0.96
4	-1.98 ±4.78	5.15 ±1.14	-0.46 ±4.00	2.73 ±0.25
5	1.03 ±1.08	2.39 ±1.34	4.47 ±3.42	5.53 ±0.88
6	3.24 ±2.18	3.62 ±0.38	4.26 ±0.72	3.79 ±1.20
7	-4.02	1.97 ±3.75	0.56 ±1.01	7.40 ±1.06
8	-1.69 ±1.72	5.11 ±0.68	-9.59 ±2.31	3.03 ±0.36
9	3.24 ±1.25	4.43 ±1.10	1.12 ±1.20	2.86 ±0.14
10	4.09 ±0.58	3.05 ±0.37	1.97 ±0.58	3.05 ±0.37
	Average Static Shear 2 (N)			
	Air-Wheelrim	Foam-Wheelrim	Air-Leverarm	Foam-Leverarm
1	8.38 ±2.32	11.48 ±3.03	2.69 ±0.71	3.66 ±1.08
2	4.13 ±3.50	4.09 ±1.88	7.51 ±4.12	5.49 ±3.17
3	5.96 ±1.34	1.84 ±0.80	4.83 ±0.62	4.60 ±1.23
4	0.95 ±1.01	4.26 ±1.13	-1.03 ±4.87	3.71 ±0.46
5	2.81 ±0.92	6.64 ±0.30	6.72 ±2.62	7.61 ±1.01
6	3.83 ±0.84	5.19 ±0.55	4.39 ±0.66	4.85 ±1.99
7	-0.07	4.20 ±2.37	3.28 ±0.46	8.76 ±1.96
8	-0.54 ±2.51	6.85 ±0.93	-8.78 ±1.12	6.13 ±0.68
9	4.70 ±1.62	4.34 ±0.93	3.07 ±0.17	2.73 ±0.63
10	5.15 ±0.80	3.62 ±0.50	2.81 ±1.06	3.62 ±0.50
	Average Static Shear 3 (N)			
	Air-Wheelrim	Foam-Wheelrim	Air-Leverarm	Foam-Leverarm
1	7.70 ±1.13	11.22 ±3.00	2.56 ±0.71	3.75 ±1.38
2	4.32 ±3.37	4.22 ±1.84	6.55 ±4.25	5.41 ±2.56
3	6.89 ±1.58	1.71 ±0.50	4.64	4.09 ±0.73
4	0.56 ±1.25	3.92 ±0.79	-0.84 ±4.74	3.37 ±0.63
5	2.60 ±0.80	6.59 ±1.02	6.30 ±2.12	7.53 ±1.47
6	4.34 ±0.79	5.28 ±0.14	4.51 ±0.38	4.81 ±1.92
7	-1.35	3.62 ±2.00	3.41 ±1.09	9.02 ±1.40
8	-1.09 ±0.90	5.45 ±0.68	-8.82 ±2.19	6.04 ±0.14
9	5.53 ±2.00	4.60 ±0.79	3.15 ±0.22	3.07 ±0.55
10	5.11 ±0.36	3.37 ±1.00	3.03 ±0.84	3.37 ±1.00

Table 7 – Dynamic shear data for left turn obstacle course. Error bars indicate confidence interval to 95%.

	Average Dynamic Shear 1 (N)			
	Air-Wheelrim	Foam-Wheelrim	Air-Leverarm	Foam-Leverarm
1	2.13 ±1.01	1.70 ±0.36	1.97	1.57 ±0.21
2	0.83 ±0.13	0.71 ±0.19	2.62 ±0.06	1.15 ±0.70
3	3.25 ±2.46	3.54 ±1.05	--	9.80 ±4.09
4	1.29 ±0.73	2.19 ±0.33	0.94 ±0.40	--
5	6.66 ±3.63	3.04 ±0.82	2.97 ±2.07	2.56 ±0.88
6	2.13 ±0.62	1.85 ±0.99	2.04 ±0.52	2.59 ±0.97
7	1.66	1.64 ±0.67	1.92 ±1.07	1.59 ±0.29
8	2.39 ±0.94	3.52 ±0.27	2.39 ±0.94	3.31 ±0.63
9	3.44 ±1.00	1.22 ±0.16	2.13 ±0.85	1.23 ±0.38
10	2.30 ±0.20	2.55 ±0.71	1.93 ±0.59	1.56 ±0.89
	Average Dynamic Shear 2 (N)			
	Air-Wheelrim	Foam-Wheelrim	Air-Leverarm	Foam-Leverarm
1	1.53 ±0.09	0.76 ±0.22	2.10	0.78 ±0.17
2	0.73 ±0.29	0.81 ±0.17	2.34 ±0.79	1.12 ±0.35
3	1.14 ±0.62	2.23 ±0.36	--	3.44 ±1.36
4	1.20 ±0.10	1.27 ±0.47	0.74	--
5	1.91 ±0.35	1.34 ±0.45	1.27 ±0.10	1.22 ±0.60
6	0.91 ±0.16	0.88 ±0.17	1.01 ±0.12	0.99 ±0.25
7	0.51	0.88 ±0.06	1.21 ±0.12	0.87 ±0.17
8	2.02 ±0.52	1.13 ±0.26	2.02 ±0.52	1.01 ±0.45
9	1.47 ±0.75	1.34 ±0.77	1.86 ±0.24	1.37 ±0.31
10	1.68 ±0.33	1.03 ±0.15	1.22 ±0.12	1.28 ±0.35
	Average Dynamic Shear 3 (N)			
	Air-Wheelrim	Foam-Wheelrim	Air-Leverarm	Foam-Leverarm
1	1.10 ±0.18	0.76 ±0.38	1.25	0.91 ±0.25
2	1.29 ±0.01	0.97 ±0.15	2.61 ±0.33	1.01 ±0.22
3	0.72 ±0.19	2.16 ±1.50	--	4.06 ±1.74
4	0.87 ±0.42	1.22 ±0.60	1.62 ±0.77	--
5	1.39 ±0.34	1.58 ±0.31	0.90 ±0.11	1.50 ±0.14
6	1.13 ±0.58	0.98 ±0.17	2.19 ±0.98	1.43 ±0.49
7	0.79	0.80 ±0.27	1.13 ±0.24	1.05 ±0.40
8	1.44 ±0.42	1.49 ±0.73	1.44 ±0.42	1.33 ±0.35
9	1.22 ±0.37	1.22 ±0.23	2.56 ±1.09	0.97 ±0.08
10	1.73 ±0.59	1.34 ±0.35	1.39 ±0.18	1.14 ±0.27

Table 8 – Dynamic shear data for right turn obstacle course. Error bars indicate confidence interval to 95%.

	Average Dynamic Shear 1 (N)			
	Air-Wheelrim	Foam-Wheelrim	Air-Leverarm	Foam-Leverarm
1	3.14 ±1.95	2.18 ±0.81	1.49 ±0.54	1.41 ±0.39
2	0.82 ±0.40	1.03 ±0.10	1.73 ±0.27	1.99 ±0.90
3	2.28 ±1.05	2.17 ±1.61	2.52 ±1.48	2.26 ±0.50
4	4.18 ±3.57	1.81 ±1.22	1.10 ±0.83	1.32 ±0.82
5	1.71 ±0.95	4.22 ±1.24	2.51 ±0.69	2.27 ±0.33
6	1.29 ±0.55	2.00 ±0.39	1.36 ±0.53	1.54 ±0.45
7	4.12	3.42 ±1.54	3.03 ±1.40	1.66 ±1.04
8	2.54 ±1.37	2.43 ±1.19	1.92 ±0.16	3.24 ±0.77
9	1.95 ±0.79	0.93 ±0.06	2.41 ±0.60	1.08 ±0.06
10	1.72 ±0.61	1.45 ±0.73	1.86 ±0.73	1.45 ±0.73
	Average Dynamic Shear 2 (N)			
	Air-Wheelrim	Foam-Wheelrim	Air-Leverarm	Foam-Leverarm
1	1.66 ±0.34	0.92 ±0.17	1.18 ±1.10	0.77 ±0.23
2	0.88 ±0.15	0.74 ±0.20	1.61 ±0.58	1.44 ±0.15
3	1.39 ±0.68	1.35 ±0.69	0.86 ±0.15	2.00 ±1.01
4	1.15 ±1.56	1.68 ±1.03	0.74 ±0.17	1.11 ±0.51
5	0.93 ±0.06	1.04 ±0.44	1.22 ±0.40	1.09 ±0.16
6	0.98 ±0.21	0.81 ±0.06	0.93 ±0.20	1.06 ±0.45
7	1.76	0.97 ±0.40	1.68 ±0.50	1.10 ±0.29
8	2.14 ±1.14	1.91 ±0.15	1.50 ±0.85	1.33 ±0.32
9	1.45 ±0.23	1.04 ±0.24	1.03 ±0.47	0.86 ±0.06
10	0.93 ±0.21	0.79 ±0.12	0.99 ±0.58	0.79 ±0.12
	Average Dynamic Shear 3 (N)			
	Air-Wheelrim	Foam-Wheelrim	Air-Leverarm	Foam-Leverarm
1	1.68 ±0.12	1.15 ±0.30	0.97 ±0.21	1.00 ±0.23
2	1.01 ±0.31	0.88 ±0.16	0.94 ±0.19	1.43 ±0.49
3	1.22 ±0.42	1.27 ±0.06	1.10 ±0.57	2.21 ±1.27
4	2.07 ±0.67	0.98 ±0.29	1.16 ±0.90	1.23 ±0.36
5	0.92 ±0.07	0.97 ±0.22	1.75 ±0.24	1.44 ±0.31
6	0.96 ±0.27	0.87 ±0.15	1.01 ±0.29	1.05 ±0.37
7	3.36	1.34 ±0.41	1.99 ±0.59	1.33 ±0.42
8	2.15 ±1.20	1.25 ±0.52	1.76 ±0.84	1.80 ±0.29
9	1.11 ±0.27	0.88 ±0.21	1.08 ±0.08	1.27 ±0.22
10	1.01 ±0.36	1.25 ±0.04	1.09 ±0.43	1.25 ±0.04

APPENDIX B

SHEAR MEASUREMENT DATA

REFERENCES

[1] Aissaoui, R., Arabi, H., Lacoste, M., Zalzal, V., & Dansereay, J. (2002). Biomechanics of manual wheelchair propulsion in elderly: System tilt and tack recline angles. *American Journal of Physical Medicine & Rehabilitation, 81*(2), 94-100.

[2] Akins, J. S., Karg, P. E., & Brienza, D. M. (2011). Interface shear and pressure characteristics of wheelchair seat cushions. [Research Support, Non-U.S. Gov't Research Support, U.S. Gov't, Non-P.H.S.]. *J Rehabil Res Dev, 48*(3), 225-234. doi: 10.1682

[3] Armstrong, T. J. (1985). Mechanical considerations of skin in work. *American Journal of Industrial Medicine, 8*, 463-472.

[4] Bader, D., Bouten, C., Colin, D., & Oomens, C. (2005). *Pressure Ulcer Research*. NY: Springer.

[5] Blaak, E. (2001). Gender differences in fat metabolism. [Review]. *Curr Opin Clin Nutr Metab Care, 4*(6), 499-502.

[6] Bloswick, D. S., Erickson, J., Browns, D. R., Howell, G., & Mecham, W. (2003). Maneuverability and usability analysis of three knee-extension propelled wheelchairs. *Disability and Rehabilitation, 25*, 197-206.

[7] Boninger, M. L., Baldwin, M., Cooper, R. A., Koontz, A., & Chan, L. (2000). Manual wheelchair pushrim biomechanics and axle position. [Research Support, Non-U.S. Gov't Research Support, U.S. Gov't, Non-P.H.S. Research Support, U.S. Gov't, P.H.S.]. *Arch Phys Med Rehabil, 81*(5), 608-613.

[8] Brienza, D. M., Geyer, M. J., Karg, P., & Jan, Y.-K. (2001). *Tissue integrity management: State of the science white paper on tissue integrity management.* Paper presented at the A State of the Science Conference on Seating Issues for Persons with Disabilities, Orlando, FL.

[9] Brienza, D. M., & Karg, P. E. (1998). A method for contoured cushion design using pressure measurements. *RESNA '98*, 125-127.

[10] Brienza, D. M., Karg, P. E., Geyer, M. J., Kelsey, S., & Trefler, E. (2001). The Relationship between pressure ulcer invidence and buttock-seat cushion

interface pressure in at-risk elderly wheelchair users. *Arch Phys Med Rehabil, 82*(April 2001), 529-533.

[11] Chaffin, D. B., Andersson, G. B. J., & Martin, B. J. (2006). *Occupational biomechanics* (4th ed.). Hoboken, NJ: John Wiley & Sons, Inc.

[12] Crawford, S. A., Walsh, D. M., & Porter-Armstrong, A. P. (2006). Hammocking: the effect of cushion covers on interface pressure measurements. [Research Support, Non-U.S. Gov't]. *Disabil Rehabil Assist Technol, 1*(1-2), 141-144.

[13] Doughty, D., Ramundo, J., Bonham, P., Beitz, J., Erwin-Toth, P., Anderson, R., & Rolstad, B. S. (2006). Issues and challenges in staging of pressure ulcers. [Consensus Development Conference]. *J Wound Ostomy Continence Nurs, 33*(2), 125-130; quiz 131-122.

[14] Edwards, C., & Marks, R. (1995). Evaluation of biomechanical properties of human skin. [Review]. *Clin Dermatol, 13*(4), 375-380.

[15] Ferguson-Pell, M., Nicholson, G., Lennon, P., & Bain, D. (2001). *Comparative evaluation of pressure mapping systems (2): Cushion testing.* Paper presented at the Proceedings of the RESNA 2001 Annual Conference: The AT Odyssey Continues, Reno, NV.

[16] Ferrarin, M., Andreoni, G., & Pedotti, A. (2000). Comparative biomechanical evaluation of different wheelchair seat cushions. [Clinical TrialComparative Study Research Support, Non-U.S. Gov't]. *J Rehabil Res Dev, 37*(3), 315-324.

[17] Gilsdorf, P., Patterson, R., & Fisher, S. (1991). Thirty-minute continuous sitting force measurements with different support surfaces in the spinal cord injured and able-bodied. [Research Support, Non-U.S. Gov't]. *J Rehabil Res Dev, 28*(4), 33-38. doi: 10.1682/JRRD.1991.10.0033

[18] Gilsdorf, P., Patterson, R., Fisher, S., & Appel, N. (1990). Sitting forces and wheelchair mechanics. [Research Support, Non-U.S. Gov't]. *J Rehabil Res Dev, 27*(3), 239-246.

[19] Hanson, D., Langemo, D. K., Anderson, J., Thompson, P., & Hunter, S. (2010). Friction and shear considerations in pressure ulcer development. [Review]. *Adv Skin Wound Care, 23*(1), 21-24. doi: 10.1097/01.ASW.0000363489.38996.13

[20] Hendrik, R., & Goossens, M. (1994). *Biomechanics of body support: A study of load distribution, shear, decubitus risk and form of the spine.* Erasmus University Rotterdam, Joop Noppen, Rotterdam.

[21] ISO Working Group Clinical Use Guidelines. (2008, 05-April-2008). *Pressure Mapping* Retrieved August 2012, from http://www.pressuremappingwiki.com/index.php?title=ISO_Working_Group_Clinical_Use_Guidelines#Pressure_Mapping_Systems_Clinical_Useage_Checklist_and_Guidelines

[22] Manorama, A. A., Baek, S., Vorro, J., Sikorskii, A., & Bush, T. R. (2010). Blood perfusion and transcutaneous oxygen level characterizations in human skin with changes in normal and shear loads--implications for pressure ulcer formation. *Clin Biomech (Bristol, Avon), 25*(8), 823-828. doi: 10.1016/j.clinbiomech.2010.06.003

[23] Minkel, J. L. (2000). Seating and mobility considerations for people with spinal cord injury. *Physical Therapy, 80*(7), 701-709.

[24] Nicholson, G., Ferguson-Pell, M., Lennon, P., & Bain, D. (2001). *Comparative evaluation of pressure mapping systems (1): Bench testing results*. Paper presented at the Proceedings of the RESNA 2001 Annual Conference: The AT Odyssey Continues, Reno, NV.

[25] Ohura, T., Takahashi, M., & Ohura, N. (2008). Influence of external forces (pressure and shear force) on superficial layer and subcutis of percine skin and effects of dressing materials: Are dressing materials beneficial for reducing pressure and shear force in tissues? *Wound Repair Regeneration, 16*, 102-107.

[26] Raphael, M., Merryweather, A., Butler, L., & Bloswick, D. (2011). *Testing and comparison of four manual wheelchair designs.* University of Utah, Salt Lake City, UT.

[27] Reichel, S. M. (1958). Shearing force as a factor in decubitus ulcers in paraplegics. *JAMA, 166*(7), 762-763.

[28] Reuler, J. B., & Cooney, T. G. (1981). The pressure sore: pathophysiology and principles of management. [Research Support, U.S. Gov't, Non-P.H.S.]. *Ann Intern Med, 94*(5), 661-666.

[29] Sacks, A. H. (1989). Theoretical prediction of a time-at-pressure curve for avoiding pressure sores. *Journal of Rehabilitation Research and Development, 26*(3), 27-34.

[30] Sanders, J. E., Goldstein, B. S., & Leotta, D. F. (1995). Skin response to mechanical stress: Adaptation rather than breakdown - A review of the literature. *Journal of Rehabilitation Research and Development, 32*(3), 214-226.

[31] Stekelenburg, A., Strijkers, G. J., Parusel, H., Bader, D. L., Nicolay, K., & Oomens, C. W. (2007). Role of ischemia and deformation in the onset of compression-induced deep tissue injury: MRI-based studies in a rat model. *J Appl Physiol, 102*(5), 2002-2011. doi: 10.1152/japplphysiol.01115.2006

[32] WIJIT: Move at the Speed of Life. 2012, from http://wiijtcom.ipage.com/index.html